

Supplementary Information of

Systematic Variation of the Optical Bandgap in Titanium Based Isoreticular Metal-Organic Frameworks for Photocatalytic Reduction of CO₂ under Blue Light

Matthew W. Logan,¹ Suliman Ayad,² Jeremy D. Adamson,¹ Tristan Dilbeck,² Kenneth Hanson,² and Fernando J. Uribe-Romo.^{1*}

¹ Department of Chemistry, University of Central Florida, 4111 Libra Dr. Rm. 251 PSB, Orlando, FL 32816-2366, USA.

² Department of Chemistry, Florida State University, 95 Chieftan Way Rm. 118 DLC, Tallahassee, FL 32306-4390, USA.

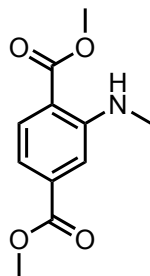
Correspondence Address

*Professor Fernando J. Uribe-Romo
Department of Chemistry
University of Central Florida
Physical Sciences Building Room 255
4111 Libra Drive
Orlando, FL 32816 (USA)
Tel: (+1)-407-823-4876
Fax: (+1)-407-823-2252
Email: *fernando@ucf.edu*

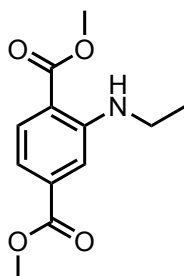
Contents

S1. Characterization Data of Synthesized Linkers	S3
S2. Crystal modeling and Rietveld refinement	S12
S3. Scanning Electron Microscopy	S21
S4. Gas Adsorption	S25
S5. Optical Band Gap Spectra	S45
S6. Transient Absorption spectra	S50
S7. Actinometry	S53
S8. Photocatalysis	S55
S9. NMR Spectra	S62

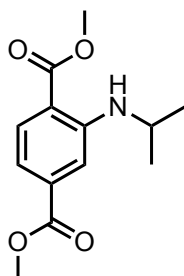
Section S1. Synthesis.



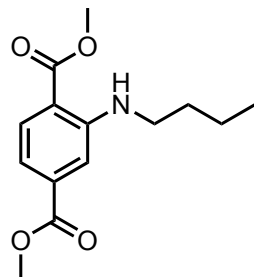
Compound 1a: Yellow solid, yield 0.89 g (45%). ^1H NMR (400 MHz, CDCl_3) δ = 7.84 (dd, J = 8.3, 1.7 Hz, 1H), 7.61 (br, NH), 7.24 (s, br, 1H), 7.11 (d, J = 8.3 Hz, 1H), 3.85 (s, 3H), 3.79 (s, 3H), 2.88 (d, J = 5.2 Hz, 3H). ^{13}C NMR (100 MHz, CDCl_3) δ = 168.34, 166.77, 151.48, 134.99, 131.52, 114.59, 112.87, 111.83, 52.15, 51.58, 29.49. HRMS (ESI-TOF) m/z calculated for $\text{C}_6\text{H}_{13}\text{NO}_3$ $[\text{M}+\text{H}]^+$: 224.0917, found 224.0921.



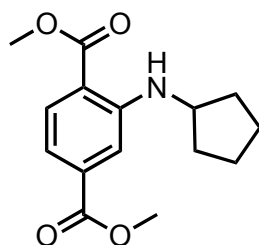
Compound 1b: Yellow solid, yield 0.80 g (40%). ^1H NMR (400 MHz, CDCl_3) δ = 7.89 (d, J = 8.3 Hz, 1H), 7.59 (br, NH), 7.29 (d, J = 1.7 Hz, 1H), 7.13 (dd, J = 8.3, 1.6 Hz, 1H), 3.87 (s, 3H), 3.83 (s, 3H), 3.24 (qd, J = 7.2, 4.9 Hz, 2H), 1.30 (t, J = 7.2 Hz, 3H). ^{13}C NMR (100 MHz, CDCl_3) δ = 168.51, 166.97, 150.74, 135.09, 131.68, 114.54, 112.75, 112.41, 52.26, 51.68, 37.51, 14.47. HRMS (ESI-TOF) m/z calculated for $\text{C}_6\text{H}_{13}\text{NO}_3$ $[\text{M}+\text{H}]^+$: 238.1074, found 238.1055.



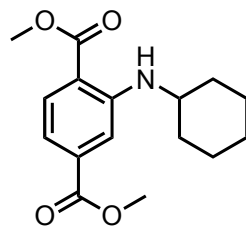
Compound 1c: Yellow solid, yield 0.67 g (34%). ^1H NMR (400 MHz, CDCl_3) δ = 7.91 (d, J = 8.3 Hz, 1H), 7.68 (br, NH), 7.35 (s, 1H), 7.13 (d, J = 8.4 Hz, 1H), 3.89 (s, 3H), 3.84 (s, 3H), 3.79 (m, 1H), 1.27 (d, J = 6.3 Hz, 6H). ^{13}C NMR (100 MHz, CDCl_3) δ = 168.68, 167.04, 150.11, 135.15, 131.98, 114.32, 112.98, 112.74, 52.35, 51.74, 43.50, 22.86. HRMS (ESI-TOF) m/z calculated for $\text{C}_6\text{H}_{13}\text{NO}_3$ $[\text{M}+\text{H}]^+$: 252.1230, found 252.1226.



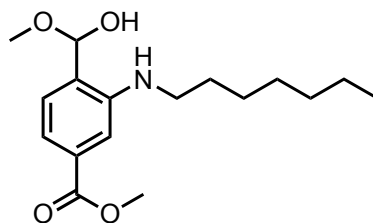
Compound 1d: Yellow solid, yield 0.75 g (38%). $^1\text{H NMR}$ (400 MHz, CDCl_3) δ = 7.87 (d, J = 8.4 Hz, 1H), 7.67 (br, NH), 7.29 (s, 1H), 7.12 (d, J = 8.2 Hz, 1H), 3.87 (s, 3H), 3.83 (s, 3H), 3.23-3.17 (m, 2H), 1.69-1.61 (m, 2H), 1.50-1.40 (m, 3H), 0.97-0.92 (t, J = 7.4, 3H). $^{13}\text{C NMR}$ (100 MHz, CDCl_3) δ = 168.55, 166.92, 150.91, 135.08, 131.70, 114.47, 112.69, 112.44, 52.24, 51.66, 42.62, 31.22, 20.36, 13.87. HRMS (ESI-TOF) m/z calculated for $\text{C}_6\text{H}_{13}\text{NO}_3$ $[\text{M}+\text{H}]^+$: 266.1387, found 266.1364.



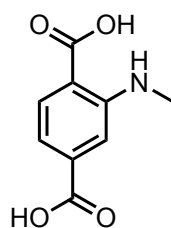
Compound 1e: Yellow liquid, yield 1.20 g (89%). $^1\text{H NMR}$ (400 MHz, CDCl_3) δ = 7.92 (d, J = 8.3 Hz, 1H), 7.79 (br, NH), 7.38 (d, J = 1.6 Hz, 1H), 7.15 (dd, J = 8.3, 1.6 Hz, 1H), 3.95 (dd, J = 9.2, 3.8 Hz, 1H), 3.91 (s, 3H), 3.86 (s, 3H), 2.14 - 2.00 (m, 2H), 1.81 - 1.71 (m, 2H), 1.72 - 1.62 (m, 2H), 1.57 (tdd, J = 12.2, 6.2, 3.2 Hz, 2H). $^{13}\text{C NMR}$ (100 MHz, CDCl_3) δ = 168.73, 167.11, 150.55, 135.09, 131.87, 114.42, 113.41, 112.82, 53.82, 52.42, 51.81, 33.57, 24.16.



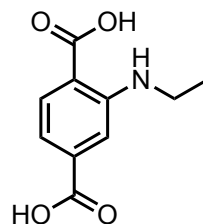
Compound 1f: Yellow liquid, yield 1.24 g (92%). $^1\text{H NMR}$ (400 MHz, Chloroform- d) δ = 7.93 (d, J = 8.3 Hz, 1H), 7.81 (br, NH), 7.12 (dd, J = 8.3, 1.6 Hz, 1H), 3.91 (s, 3H), 3.86 (s, 3H), 3.50 (dtd, J = 12.6, 8.4, 7.9, 3.6 Hz, 1H), 2.02 (td, J = 7.8, 7.3, 3.8 Hz, 2H), 1.77 (dq, J = 13.0, 4.2 Hz, 2H), 1.62 (ddt, J = 14.1, 9.6, 4.5 Hz, 1H), 1.51 - 1.22 (m, 5H). $^{13}\text{C NMR}$ (101 MHz, CDCl_3) δ = 168.79, 167.19, 150.14, 135.18, 132.08, 114.21, 113.06, 112.70, 52.45, 51.82, 50.50, 32.93, 25.96, 24.69.



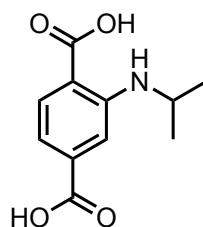
Compound 1g: Yellow liquid, yield 0.53 g (42%). ^1H NMR (400 MHz, Chloroform-*d*) δ = 7.93 (d, J = 8.3 Hz, 1H), 7.70 (br, NH), 7.34 (d, J = 1.6 Hz, 1H), 7.17 (dd, J = 8.3, 1.6 Hz, 1H), 4.12 (t, J = 6.7 Hz, 2H), 3.92 (s, 3H), 3.87 (s, 3H), 1.56 (d, J = 6.4 Hz, 2H), 1.38 - 1.22 (m, 8H), 0.89 (t, J = 3.1 Hz, 3H). ^{13}C NMR (100 MHz, CDCl_3) δ = 168.75, 167.15, 151.07, 135.24, 131.88, 114.61, 112.86, 112.64, 52.45, 51.86, 43.11, 31.91, 29.20, 28.84, 27.29, 22.78, 14.20.



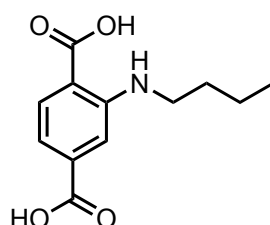
Compound 2a: Yellow solid, yield 0.46 g (92%). ^1H NMR (400 MHz, $\text{DMSO-}d_6$) δ = 7.86 (d, J = 8.2 Hz, 1H), 7.21 (d, J = 1.6 Hz, 1H), 7.09 (dd, J = 8.2, 1.6 Hz, 1H), 2.88 (s, 3H). ^{13}C NMR (100 MHz, $\text{DMSO-}d_6$) δ = 169.37, 167.18, 151.27, 135.78, 131.85, 114.27, 113.09, 111.37, 29.20. HRMS (ESI-TOF) m/z calculated for $\text{C}_6\text{H}_{13}\text{NO}_3$ $[\text{M}+\text{H}]^+$: 196.0604, found 196.0610.



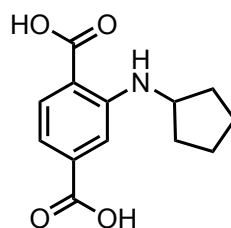
Compound 2b: Yellow solid, yield 0.45 g (90%). ^1H NMR (400 MHz, $\text{DMSO-}d_6$) δ = 7.87 (d, J = 8.2 Hz, 1H), 7.23 (d, J = 1.6 Hz, 1H), 7.08 (dd, J = 8.2, 1.6 Hz, 1H), 3.23 (q, J = 7.2 Hz, 2H), 1.23 (t, J = 7.1 Hz, 3H). ^{13}C NMR (100 MHz, $\text{DMSO-}d_6$) δ = 169.46, 167.15, 150.35, 135.78, 131.96, 114.30, 112.91, 111.71, 36.70, 14.26. HRMS (ESI-TOF) m/z calculated for $\text{C}_6\text{H}_{13}\text{NO}_3$ $[\text{M}+\text{H}]^+$: 210.0761, found 210.0746.



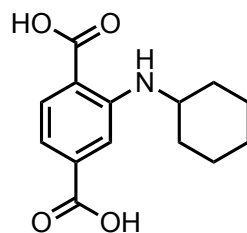
Compound 2c: Yellow solid, yield 0.47 g (94%). $^1\text{H NMR}$ (400 MHz, $\text{DMSO-}d_6$) δ = 7.87 (d, J = 8.2 Hz, 1H), 7.25 (d, J = 1.6 Hz, 1H), 7.05 (dd, J = 8.2, 1.6 Hz, 1H), 3.74 (hept, J = 6.4 Hz, 1H), 1.21 (d, J = 6.3 Hz, 6H). $^{13}\text{C NMR}$ (100 MHz, $\text{DMSO-}d_6$) δ = 169.57, 167.19, 149.58, 135.75, 132.11, 114.08, 113.04, 112.14, 42.74, , 22.46. HRMS (ESI-TOF) m/z calculated for $\text{C}_6\text{H}_{13}\text{NO}_3$ $[\text{M}+\text{H}]^+$: 224.0917, found 224.0924.



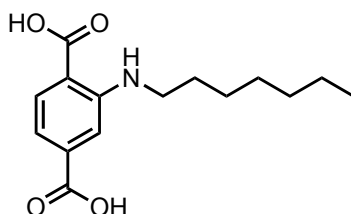
Compound 2d: Yellow solid, yield 0.48 g (96%). $^1\text{H NMR}$ (400 MHz, $\text{DMSO-}d_6$) δ = 7.85 (d, J = 8.2 Hz, 1H), 7.24 (d, J = 1.5 Hz, 1H), 7.07 (dd, J = 8.2, 1.6 Hz, 1H), 3.20 (t, J = 7.0 Hz, 2H), 1.60 (m, 2H), 1.40 (m, 2H), 0.93 (t, J = 7.1 Hz, 3H). $^{13}\text{C NMR}$ (100 MHz, $\text{DMSO-}d_6$) δ = 169.52, 167.15, 150.51, 135.77, 131.96, 114.25, 112.90, 111.74, 41.72, 30.58, 19.71, 13.68. HRMS (ESI-TOF) m/z calculated for $\text{C}_6\text{H}_{13}\text{NO}_3$ $[\text{M}+\text{H}]^+$: 238.1074, found 238.1058.



Compound 2e: Yellow solid, yield 0.47 g (93%). $^1\text{H NMR}$ (400 MHz, $\text{DMSO-}d_6$) δ = 7.86 (d, J = 8.2 Hz, 1H), 7.27 (d, J = 1.5 Hz, 1H), 7.07 (dd, J = 8.2, 1.5 Hz, 1H), 3.88 (p, J = 6.1 Hz, 1H), 2.02 (dq, J = 12.1, 6.0, 5.1 Hz, 2H), 1.65 (dq, J = 22.4, 7.8, 3.7 Hz, 4H), 1.45 (dq, J = 11.6, 5.5 Hz, 2H). $^{13}\text{C NMR}$ (100 MHz, DMSO) δ = 169.60, 167.21, 150.05, 135.72, 132.05, 114.28, 112.99, 112.58, 53.08, 32.92, 23.57. HRMS (ESI-TOF) m/z calculated for $\text{C}_{13}\text{H}_{16}\text{NO}_4$ $[\text{M}+\text{H}]^+$: 250.1079, found 250.1041.

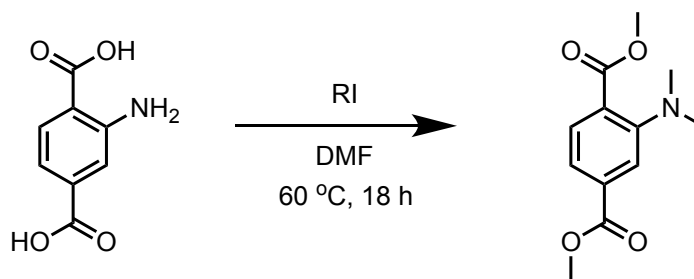


Compound 2f: Yellow solid, yield 0.46 g (92%). ^1H NMR (400 MHz, $\text{DMSO-}d_6$) δ = 7.98 (br, NH), 7.86 (d, J = 8.2 Hz, 1H), 7.25 (s, 1H), 7.04 (dd, J = 8.3, 1.4 Hz, 1H), 3.45 (d, J = 8.9 Hz, 2H), 1.93 (dt, J = 12.6, 3.9 Hz, 2H), 1.68 (dt, J = 13.3, 4.3 Hz, 2H), 1.58 (dt, J = 10.0, 4.3 Hz, 1H), 1.49 - 1.34 (m, 2H), 1.34 - 1.19 (m, 3H). ^{13}C NMR (100 MHz, DMSO) δ = 169.67, 167.23, 149.54, 135.74, 132.15, 114.02, 112.11, 49.54, 32.23, 25.33, 23.97. HRMS (ESI-TOF) m/z calculated for $\text{C}_{14}\text{H}_{18}\text{NO}_4$ $[\text{M}+\text{H}]^+$: 264.1235, found 264.1189.



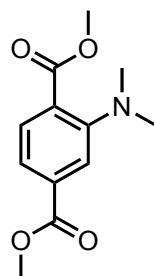
Compound 2g: Yellow solid, yield 0.48 g (96%). ^1H NMR (400 MHz, $\text{DMSO-}d_6$) δ = 7.86 (d, J = 8.2 Hz, 1H), 7.23 (d, J = 1.6 Hz, 1H), 7.07 (dd, J = 8.2, 1.5 Hz, 1H), 3.19 (t, J = 7.0 Hz, 2H), 1.61 (p, J = 7.0 Hz, 2H), 1.44 - 1.20 (m, 8H), 0.92 - 0.80 (m, 3H). ^{13}C NMR (100 MHz, DMSO) δ = 169.54, 167.16, 150.52, 135.77, 131.97, 114.25, 112.89, 111.75, 42.02, 31.20, 28.41, 28.36, 26.45, 22.01, 13.94. HRMS (ESI-TOF) m/z calculated for $\text{C}_{15}\text{H}_{22}\text{NO}_4$ $[\text{M}+\text{H}]^+$: 280.1548, found 280.1500

Scheme S1: Synthesis of *N,N*-2-dimethyl amino-terephthalate dimethyl ester

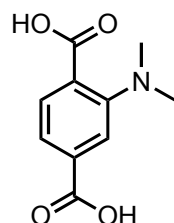


N,N-2-dimethyl amino- terephthalic acid (2.00 g, 9.56 mmol) was suspended in anhydrous DMF (20 mL) and stirred until fully dissolved. K_2CO_3 (5.30 g, 38.2 mmol) was added, followed by dropwise addition of methyl iodide (7.66 g, 54.0 mmol), and the mixture was stirred for 18 h at 60 °C. The reaction mixture was then cooled to room temperature and quenched with 2 M HCl (aq) to a pH = 3.

The mixture was extracted with EtOAc (3 × 50 mL), the combined organic extracts were washed with brine (3 × 50 mL), dried over anhydrous MgSO₄, filtered through celite and the solvent was removed using a rotary evaporator. The obtained crude was purified using flash chromatography (SiO₂, 15% v/v EtOAc:hexanes, dry loading).



Compound S1: Yellow solid, yield 0.69 g (31%). ¹H NMR (400 MHz, CDCl₃) δ = 7.65(d, *J* = 5.9 Hz, 1H), 7.60 (s, 1H), 7.45 (d, *J* = 7.5 Hz, 1H), 3.91 (d, *J* = 3.8 Hz, 6H), 2.89 (d, *J* = 3.1 Hz, 6H). ¹³C NMR (100 MHz, CDCl₃) δ = 168.69, 166.90, 151.95, 133.26, 131.59, 124.43, 119.19, 117.73, 52.44, 43.57.



Compound 3: Protocol: The alkylated diester (0.50 g) was dissolved in THF (25 mL), followed by addition of 1 M NaOH (*aq*, 12.8 mL). The solution was heated to 70 °C and stirred for 8 h. The mixture was concentrated in a rotary evaporator at 45 °C to remove the excess THF. The mixture was cooled to room temperature followed by addition of 1 M HCl (*aq*) until a pH = 3. The observed precipitate was isolated by filtration, rinsed with water, and dried in air at room temperature for 6 h. Yellow solid, yield 0.45 g (90%). ¹H NMR (400 MHz, DMSO-*d*₆) δ = 7.99 (d, *J* = 1.8 Hz, 1H), 7.95 - 7.89 (m, 1H), 7.76 - 7.71 (m, 1H), 2.86 (s, 6H). ¹³C NMR (100 MHz, DMSO) δ = 167.11, 166.43, 150.74, 134.69, 130.85, 127.29, 124.41, 120.82, 43.85.

General procedure for solvothermal MOF crystallization in flame-sealed glass tube vessel. A meter-long borosilicate glass tube measuring 10 × 8 mm (o.d × i.d), was divided into six equal portions with a marker. Using a glass cutter, the long tube was cut into three shorter tubes by only cutting every other mark.

The cut ends of the tube were etched using an oxygen-propane torch. The final glass tubes were made by melting the intermediate glass tubes at the mark with the torch. After the reactants and solvents were loaded into the glass tubes, a hose adaptor was used to connect the glass tube to a high vacuum (10 mtorr) using a Schlenk line constructed by fitting the open end of the tube inside a short length of standard rubber hose that was further affixed to a ground glass tap which could be closed to insulate this assembly from dynamic vacuum. The mixture was flash frozen at 77 K (liquid N₂), evacuated to an internal pressure of 150 mtorr (\pm 10 mtorr), and sealed under static vacuum. Upon sealing, the length of the tube was reduced to 18-20 cm; the reactant mixture was allowed to thaw and placed in an isothermal oven inside a sand bath. After the reaction was complete, the tube was allowed to cool to room temperature, the tube was opened using a glass cutter, and the solids were isolated by filtration.

MIL-125-NHMe. Yellow solid. Yield: 0.015 g [66% yield based on Ti₈O₁₂(C₉H₇NO₄)₆]. FTIR (ATR, cm⁻¹) 3388.88, 2923.01, 1717.1, 1538.36, 1505.04, 1484.73, 1456.67, 1408.86, 1384.32, 1311.53, 1278.29, 1163.53, 1080.44, 1062.15, 1036.26, 950.04, 882.39, 768.58, 632.14, 583.12, 553.84, 507.68, 460.66

MIL-125-NHEt. Yellow solid. Yield: 0.015 g [63% yield based on Ti₈O₁₂(C₁₀H₉NO₄)₆]. FTIR (ATR, cm⁻¹) 3364.35, 2969.06, 2927.83, 2871.17, 1622.55, 1574.24, 1538.33, 1504.43, 1480.27, 1454.32, 1385.56, 1304.75, 1279.43, 1269.21, 1157.09, 1081.55, 1058.47, 983.03, 950.64, 886.9, 768.8, 665.76, 630.17, 585.19, 512.73

MIL-125-NHⁱPr. Yellow solid. Yield: 0.014 g [56% yield based on Ti₈O₁₂(C₁₁H₁₁NO₄)₆]. FTIR (ATR, cm⁻¹) 3354.94, 2965.73, 2927.26, 1622.02, 1573.66, 1538.12, 1503.89, 1454.54, 1445.82, 1410.07, 1384.84, 1279.16, 1246.65, 1117.76, 1006.2, 951.41, 888.56, 850.56, 768.24, 665.95, 636.51, 613.79, 600.93, 538.98, 482.13

MIL-125-NHBu. Yellow solid. Yield: 0.015 g [57% yield based on Ti₈O₁₂(C₁₂H₁₃NO₄)₆]. FTIR (ATR, cm⁻¹) 3362.48, 2955.93, 2927.6, 2870.25, 1622.53, 1573.94, 1537.91, 1503.55, 1451.88, 1386.73, 1314.03, 1304.04, 1280.91, 1259.32, 1115.87, 970.85, 951.52, 906.68, 885.87, 837.9, 769.03, 731, 633.97, 616.57, 583.52, 534.70, 503.04

MIL-125-NHCyp. Yellow solid. Yield: 0.010 g [39% yield based on Ti₈O₁₂(C₁₃H₁₃NO₄)₆]. FTIR (ATR, cm⁻¹) 3365.09, 2956.52, 2870.11, 1622.59, 1572.58, 1533.02, 1499.83, 1453.63, 1409.16, 1385.58, 1323.65, 1276.65, 1184.97, 1115.98, 1060.09, 980.45, 951.9, 886.01, 768.43, 620.1, 597.1, 523.84, 470.79

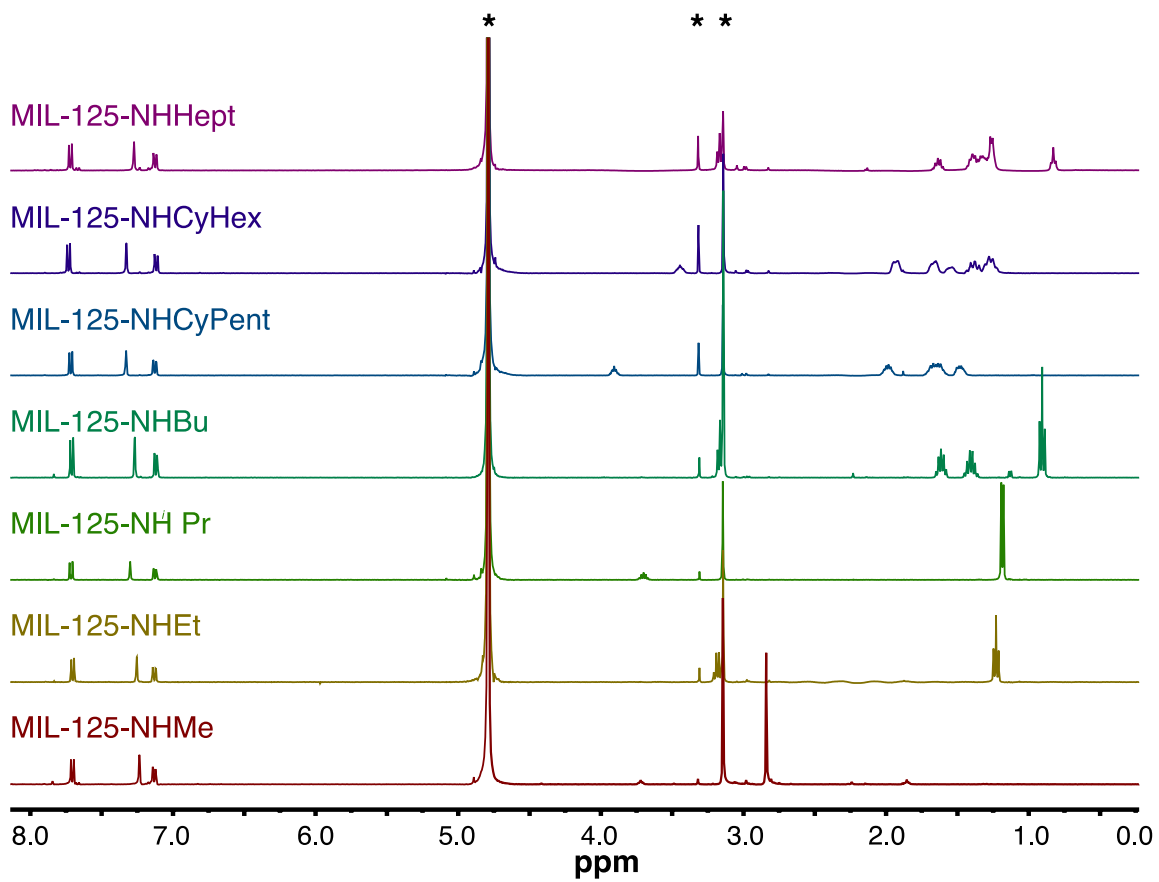
MIL-125-NHCy. Yellow solid. Yield: 0.011 g [42% yield based on Ti₈O₁₂(C₁₄H₁₅NO₄)₆]. FTIR (ATR, cm⁻¹) 3352.11, 2927.79, 2853.15, 1620.61,

1571.39, 1532.66, 1501.01, 1453.71, 1383.93, 1322.94, 1281.56, 1248.78, 1187.03, 1150.25, 1073.88, 994.46, 959.79, 887.69, 767.44, 664.76, 631.11, 602.49, 526.78, 479.16

MIL-125-NHhept. Yellow solid. Yield: 0.015 g [52% yield based on $\text{Ti}_8\text{O}_{12}(\text{C}_{15}\text{H}_{19}\text{NO}_4)_6$]. FTIR (ATR, cm^{-1}) 3373.41, 2953.73, 2926, 2854.98, 1622.82, 1573.83, 1537.73, 1532.36, 1504.52, 1454.97, 1403.36, 1385.54, 1311.73, 1278.64, 1123.5, 1063.3, 982.81, 954.74, 884.31, 768.1, 665.83, 617.89, 582.38, 548.52, 505.48

Activation procedure for gas adsorption. The dried MOF powder was placed in a sample tube for gas adsorption, evacuated to ~ 5 mtorr at room temperature and then heated up to 120 °C under dynamic vacuum for 18 h.

Figure S1. ^1H NMR spectra (400 MHz, 0.1 M NaOD/D₂O, 25 °C) of NaOD/D₂O digested MOFs (0.1M NaOD in D₂O). * = Residual solvent signals.



Section S2. Crystal modeling and Rietveld refinements.

Rietveld refinements were performed in GSAS-II with the experimental diffractograms, and the respective crystal model generated in Materials Studio. Refinements were performed using a Thomson-Cox-Hasting modified pseudo-Voigt function with 6 terms, and Finger-Cox-Jephcoat peak asymmetry with 1 parameter. The background was initially hand fit to a 6th order Shifted Chebyshev polynomial. The profile was initially calculated using the LeBail routine (Peakfit) with manually picked peaks, refining first the Gaussian and then the Lorentzian components, followed by asymmetry and background, observing convergent refinements. Following LeBail fit, Rietveld routine with extraction of the structure factors (F_{obs}) was then used refining the scale factor, unit cell parameters, zero shift and LP function, followed by the background function, the crystallite size and strain broadening, transparency and extinction. Oxygen atoms were included inside the pores to partially correct for the influence of water guest molecules (likely present from the interaction with ambient surroundings over the course of the data collection), and their occupancy factors and positions were refined with convergent results. The atom positions of the alkyl chains were not refined and assumed highly disordered. A preferred orientation correction was added to the refinements using a 2nd order spherical harmonic function. Isotropic atomic displacement parameters (U_{iso}) of all non-hydrogen atoms were refined with constraints (constraining all the chemically equivalent atoms). Final refinements included all parameters, which were refined iteratively until convergent refinements were obtained. F_{obs} were extracted, bond distances and angles were calculated and a crystallographic information file (CIF) was generated.

Note: MIL-125-NHⁱPr, MIL-125-NHBu, and MIL-125-NHCyp exhibit three unindexed peaks at 32.3, 34.0, and 38.8 2-theta degrees. Those peaks do not correspond to starting materials or titanium dioxide polymorphs.

Figure S2. Rietveld plot of MIL-125-NHMe. Blue marks = observed, green trace = refined, teal = difference, red trace = background.

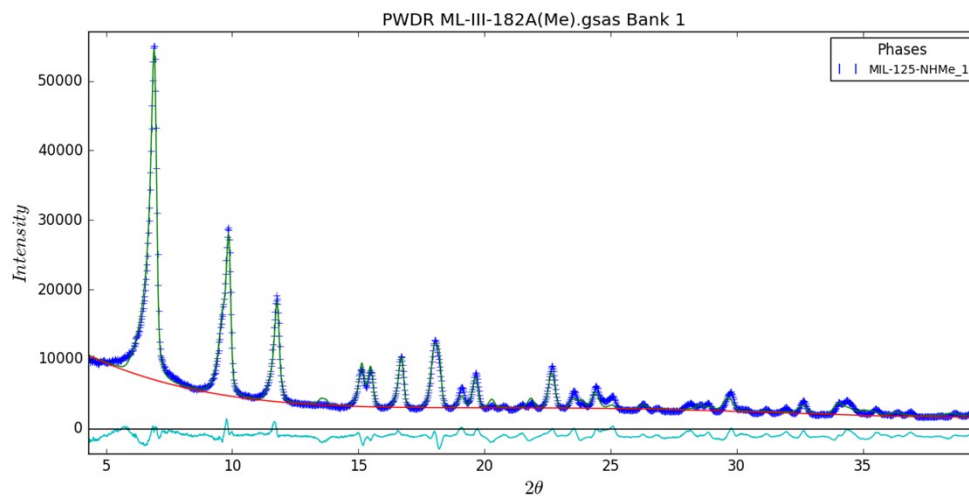


Figure S3. Rietveld plot of MIL-125-NHEt. Blue marks = observed, green trace = refined, teal = difference, red trace = background.

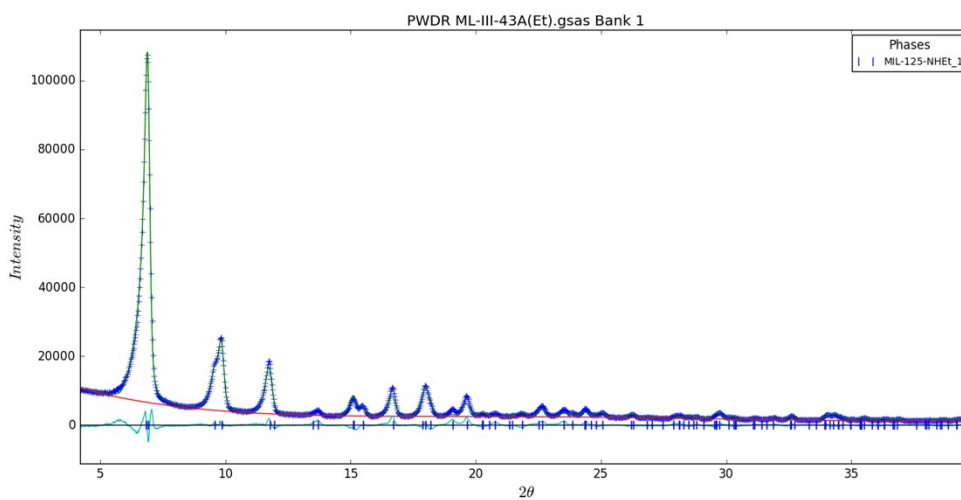


Figure S4. Rietveld plot of MIL-125-NH/Pr. Blue marks = observed, green trace = refined, teal = difference, red trace = background.

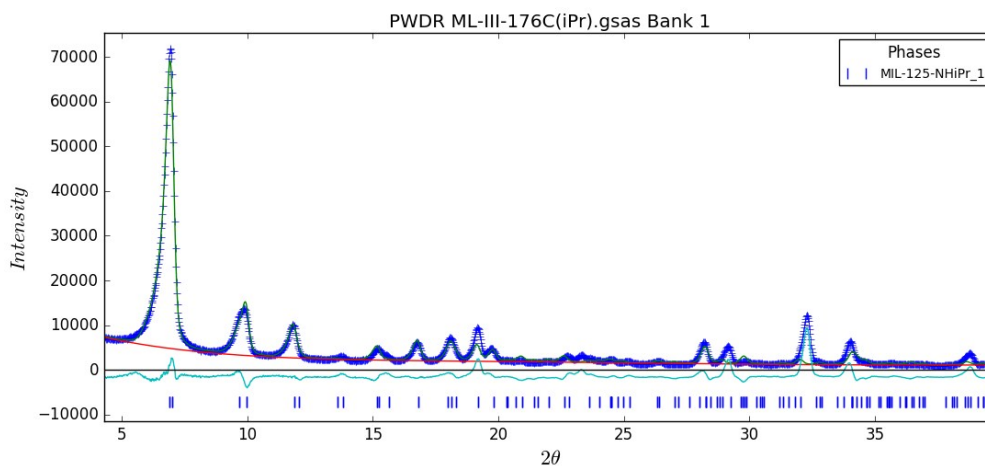


Figure S5. Rietveld plot of MIL-125-NHBu. Blue marks = observed, green trace = refined, teal = difference, red trace = background.

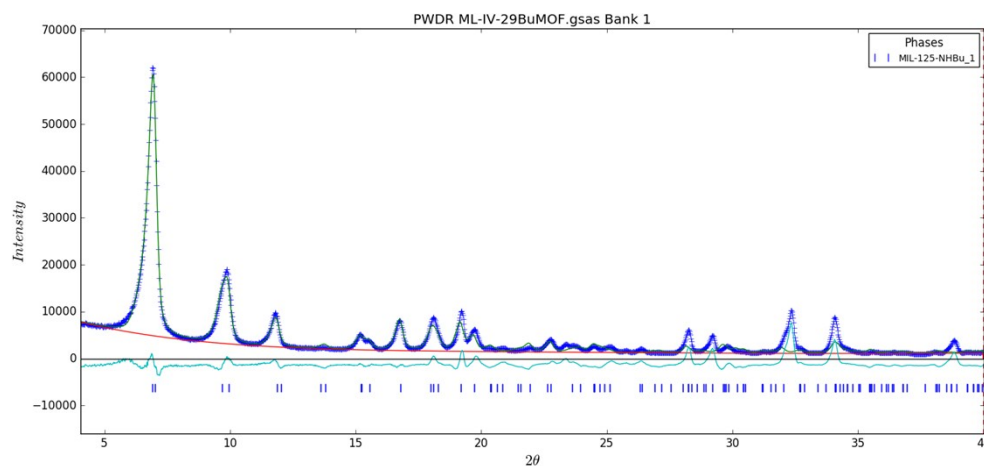


Figure S6. Rietveld plot of MIL-125-NHCyp. Blue marks = observed, green trace = refined, teal = difference, red trace = background.

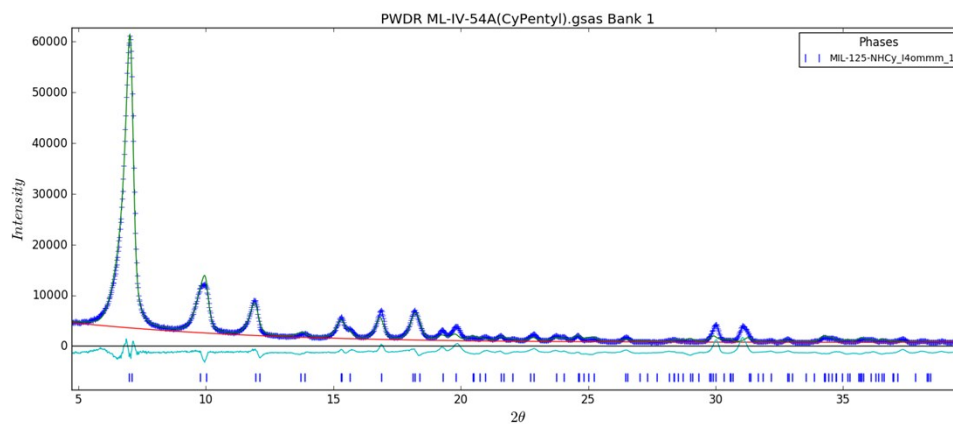


Figure S7. Rietveld plot of MIL-125-NHCy. Blue marks = observed, green trace = refined, teal = difference, red trace = background.

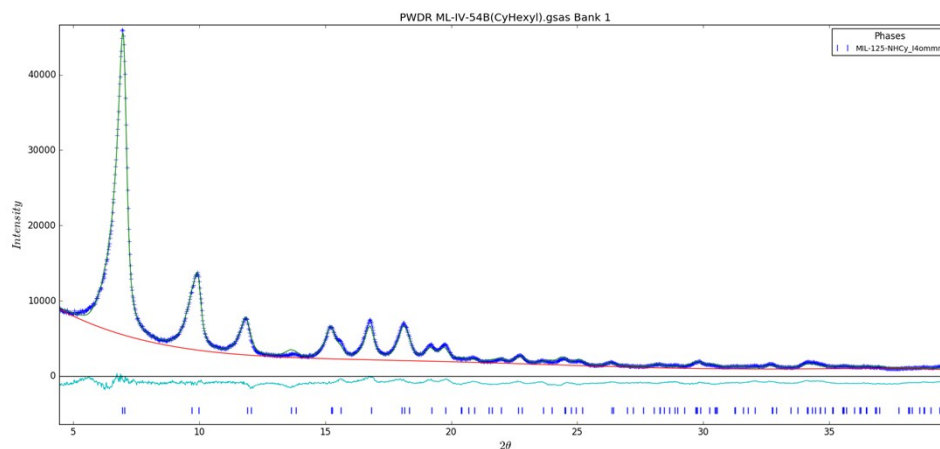


Figure S8. Rietveld plot of MIL-125-NHhep. Blue marks = observed, green trace = refined, teal = difference, red trace = background.

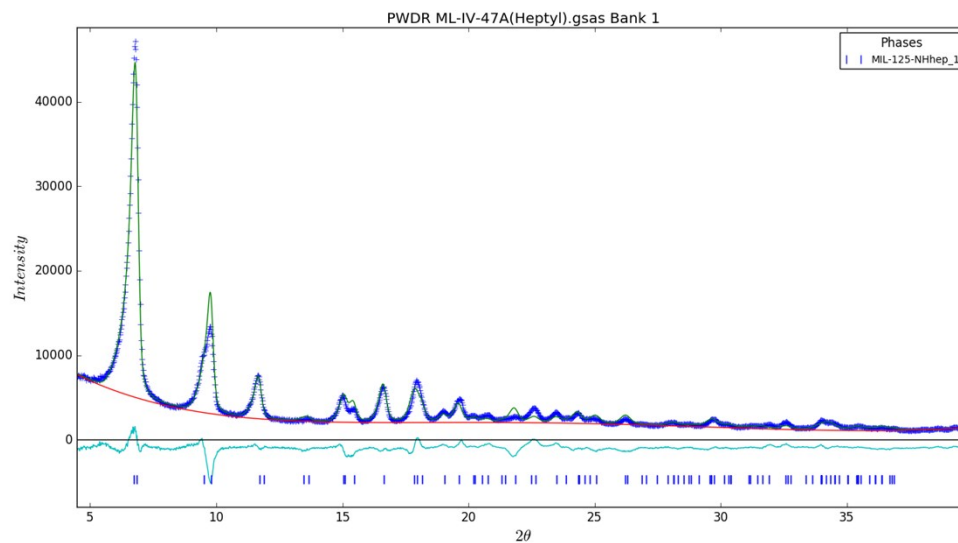


Table S1. Crystallographic information from Rietveld Refinement.

Name	MIL-125-NHMe	MIL-125-NHMEt	MIL-125-NHⁱPr
Assymmetric unit composition	C _{1.395} N _{0.315} O _{2.415} Ti _{0.25}	C _{1.785} N _{0.315} O _{2.148} Ti _{0.25}	C _{2.175} N _{0.315} O _{3.017} Ti _{0.25}
Formula weight (g mol ⁻¹)	71.78	72.19	90.78
Temperature (K)	300	300	300
Z	32	32	32
Crystal system	tetragonal	tetragonal	tetragonal
Space Group	<i>I4/mmm</i> (No. 123)	<i>I4/mmm</i> (No. 123)	<i>I4/mmm</i> (No. 123)
<i>a</i> (Å)	18.635(16)	18.626(20)	18.70(5)
<i>c</i> (Å)	18.131(14)	18.088(18)	18.11(5)
<i>V</i> (Å ³)	6296(15)	6275(20)	6330(50)
Number of independent atoms	23	27	29
Observed reflections	104	103	104
Number of data points	1900	1850	1850
Max <i>d</i> -spacing resolution (Å)	13.177	13.171	13.226
Min <i>d</i> -spacing resolution (Å)	2.256	2.259	2.263
Refined parameters (total)	53	66	97
<i>R_p</i> (%)	6.478	6.175	12.331
<i>wR_p</i> (%)	8.686	8.551	21.211
<i>R_B</i> (%)	5.966	5.884	13.300
GOF (χ ²)	6.26	6.35	14.27

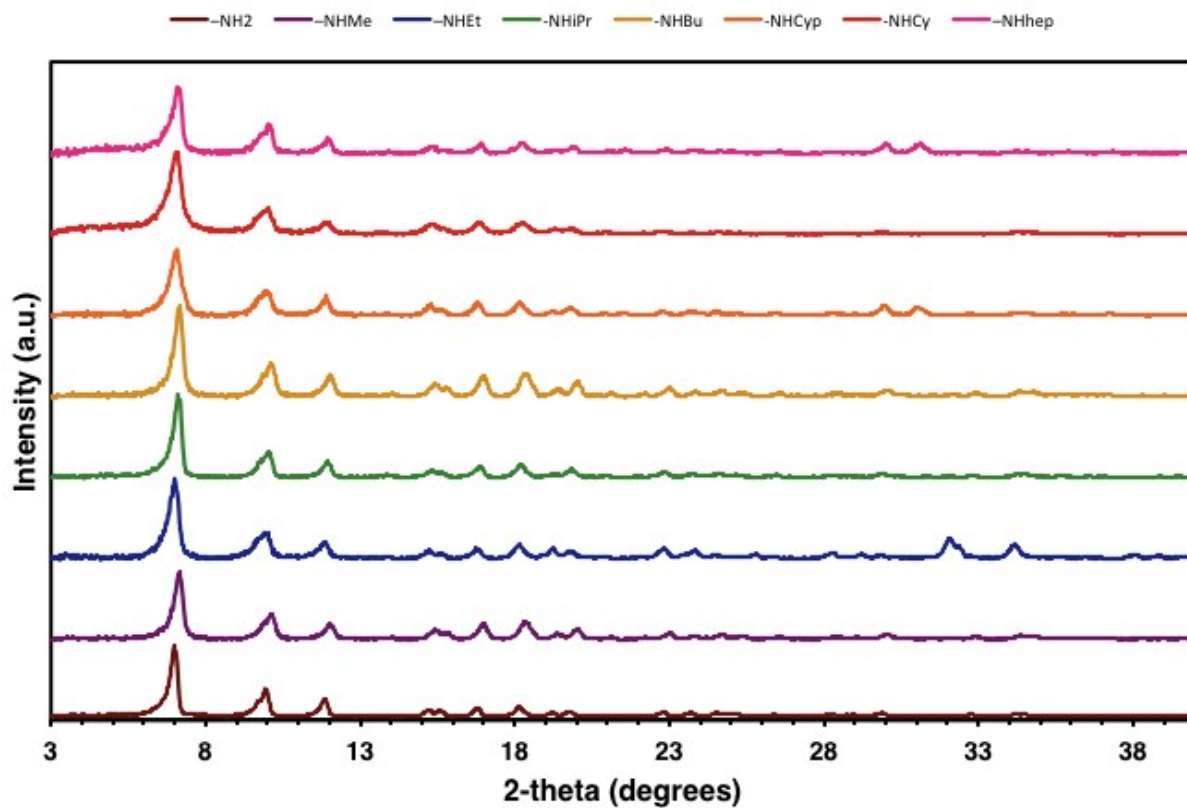
Table S2. Crystallographic information from Rietveld Refinement.

Name	MIL-125-NHBu	MIL-125-NHCyp	MIL-125-NHCy
Assymmetric unit composition	C _{2.995} N _{0.315} O _{2.833} Ti _{0.25}	C _{2.955} N _{0.315} O _{2.149} Ti _{0.25}	C _{3.345} N _{0.315} O _{2.019} Ti _{0.25}
Formula weight (g mol ⁻¹)	97.68	86.26	88.86
Temperature (K)	300	300	300
Z	32	32	32
Crystal system	tetragonal	tetragonal	tetragonal
Space Group	<i>I4/mmm</i> (No. 123)	<i>I4/mmm</i> (No. 123)	<i>I4/mmm</i> (No. 123)
<i>a</i> (Å)	18.70(4)	18.682(29)	18.675(23)
<i>c</i> (Å)	18.21(4)	18.204(28)	18.147(22)
<i>V</i> (Å ³)	6370(40)	6354(29)	6329(23)
Number of independent atoms	27	34	35
Observed reflections	104	92	100
Number of data points	1850	1850	1850
Max <i>d</i> -spacing resolution (Å)	13.225	13.210	13.205
Min <i>d</i> -spacing resolution (Å)	2.264	2.364	2.282
Refined parameters (total)	69	61	70
<i>R_p</i> (%)	12.135	7.869	3.969
<i>wR_p</i> (%)	20.323	13306	5.597
<i>R_B</i> (%)	13.303	7.777	3.445
GOF (χ ²)	13.18	7.60	3.502

Table S3. Crystallographic information from Rietveld Refinement.

Name	MIL-125-NHhep
Assymmetric unit composition	$C_{3.735}N_{0.315}O_{2.361}Ti_{0.25}$
Formula weight (g mol ⁻¹)	99.02
Temperature (K)	300
Z	32
Crystal system	tetragonal
Space Group	<i>I4/mmm</i> (No. 123)
<i>a</i> (Å)	18.854(27)
<i>c</i> (Å)	18.292(23)
<i>V</i> (Å ³)	6502(27)
Number of independent atoms	36
Observed reflections	88
Number of data points	1850
Max <i>d</i> -spacing resolution (Å)	13.332
Min <i>d</i> -spacing resolution (Å)	2.464
Refined parameters (total)	63
<i>R_p</i> (%)	6.291
<i>wR_p</i> (%)	9.196
<i>R_B</i> (%)	7.049
GOF (χ ²)	5.62

Figure S9. Powder X-ray diffraction patterns of the isorecticular family of MIL-125-NHR post photocatalysis showing no significant degradation in crystallinity.



Section S3. Scanning Electron Microscopy

Figure S10. Scanning electron micrograph images of MIL-125-NHMe prepared in glass vessel. Scale is indicated.

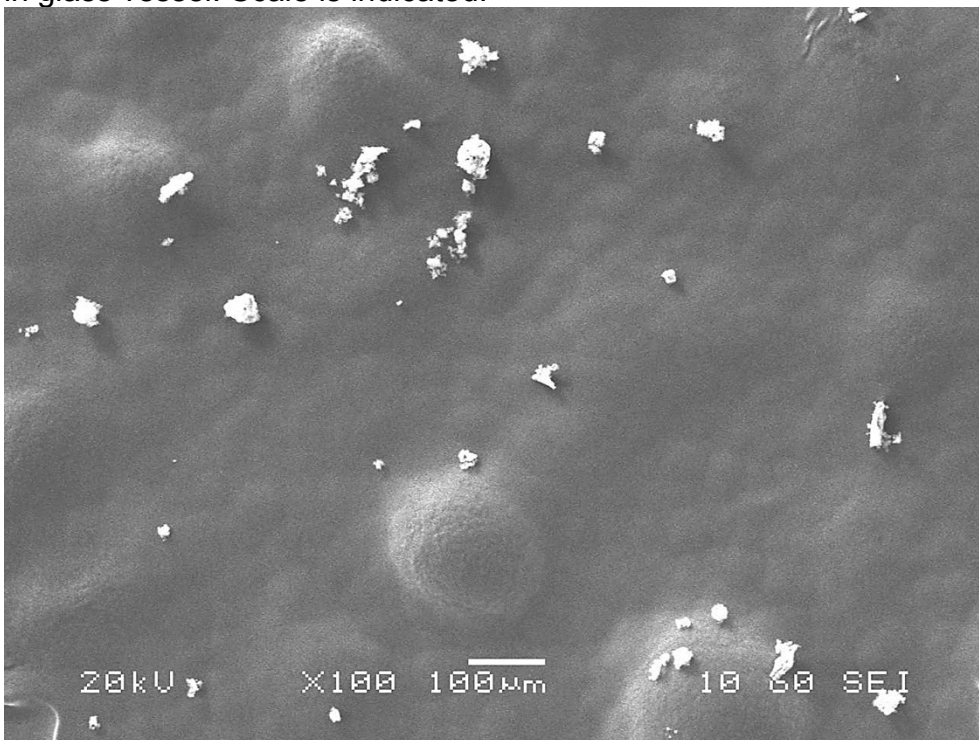


Figure S11. Scanning electron micrograph images of MIL-125-NHMe prepared in glass vessel. Scale is indicated.

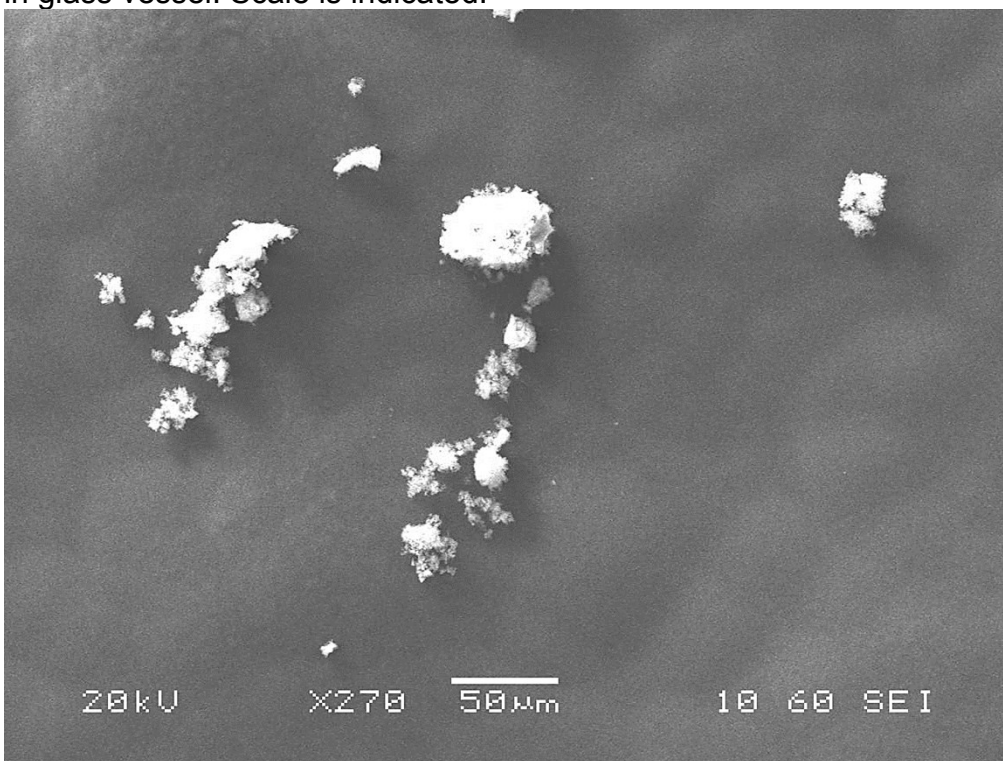


Figure S12. Scanning electron micrograph images of MIL-125-NH₂ prepared in glass vessel. Scale is indicated.

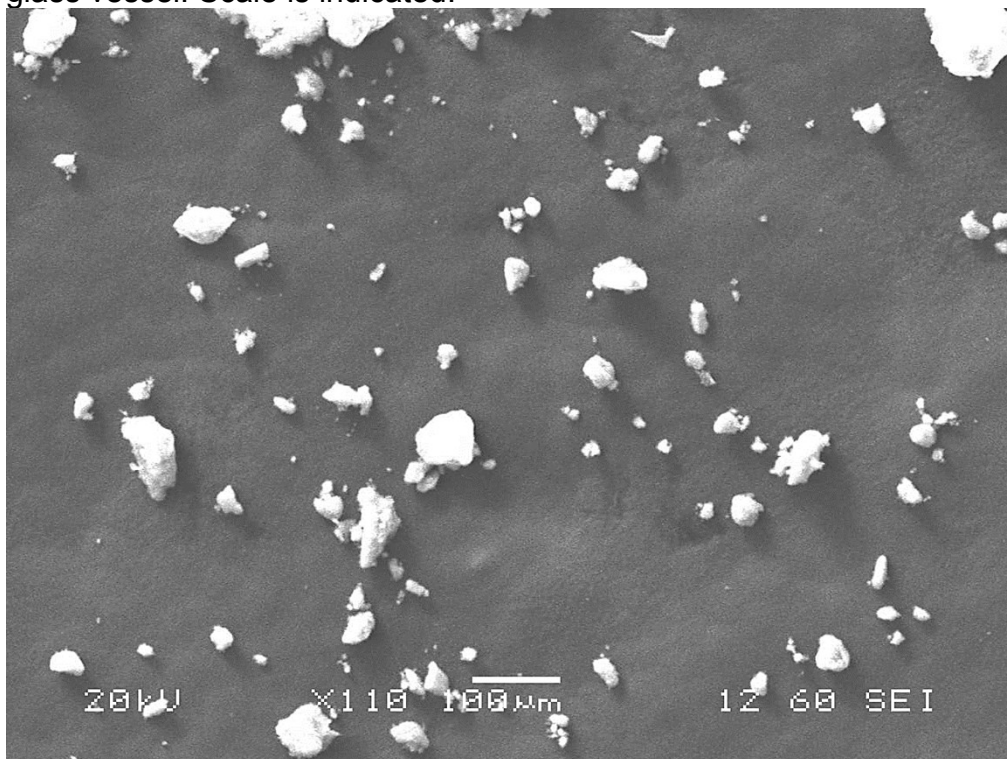


Figure S13. Scanning electron micrograph images of MIL-125-NH₂ prepared in glass vessel. Scale is indicated.

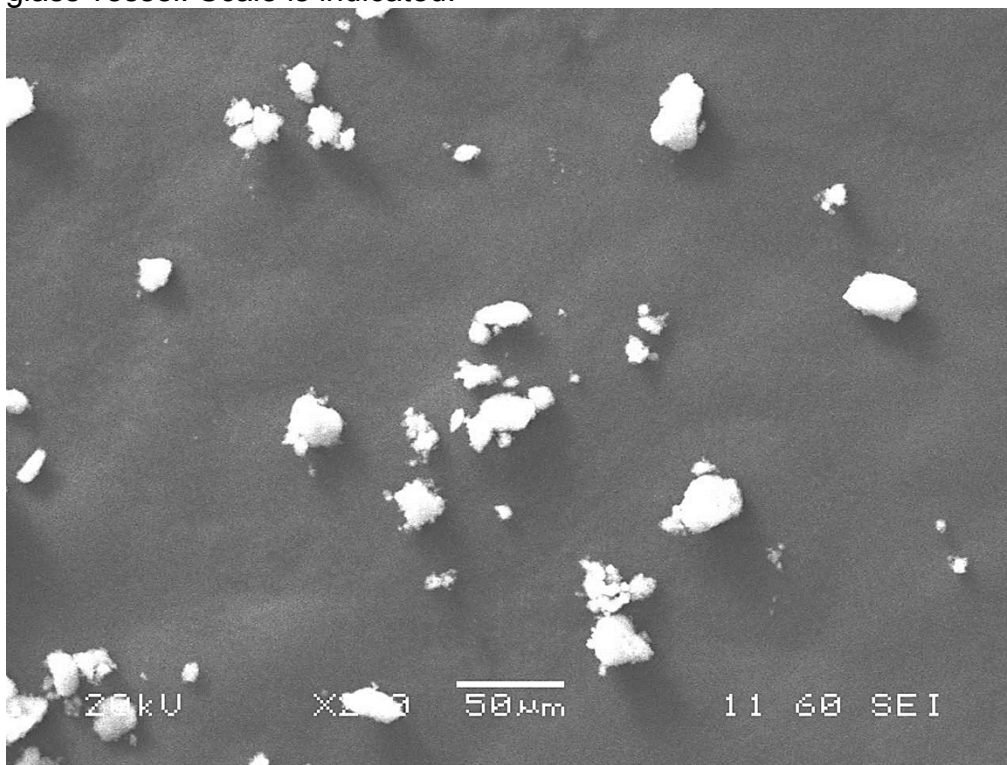


Figure S14. Scanning electron micrograph images of MIL-125-NH/Pr prepared in glass vessel. Scale is indicated.

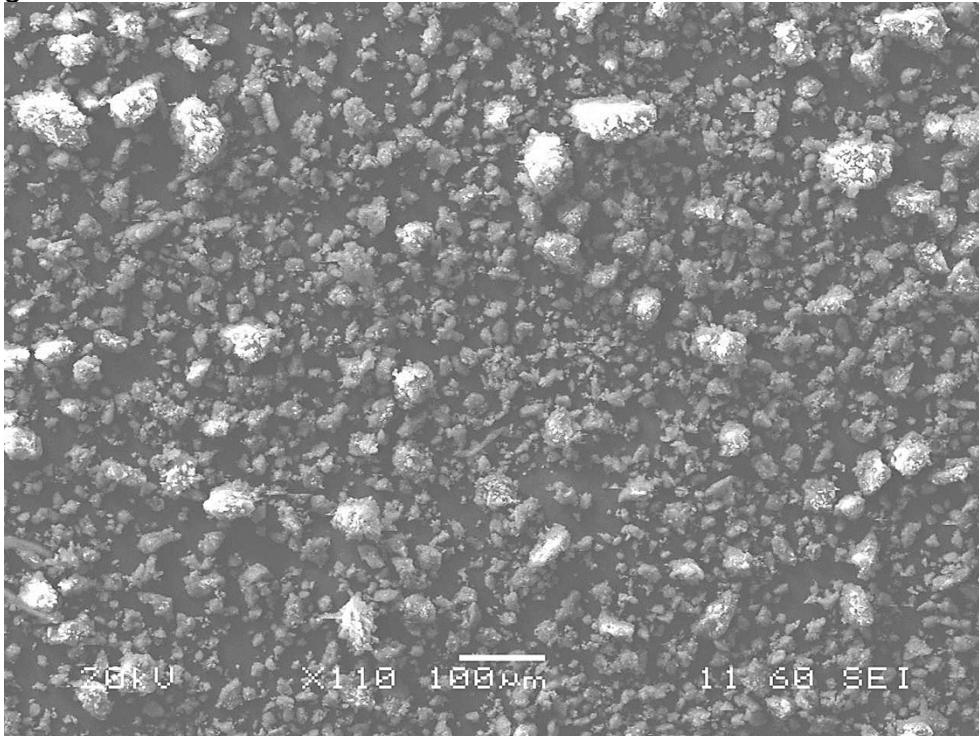


Figure S15. Scanning electron micrograph images of MIL-125-NH/Pr prepared in glass vessel. Scale is indicated.

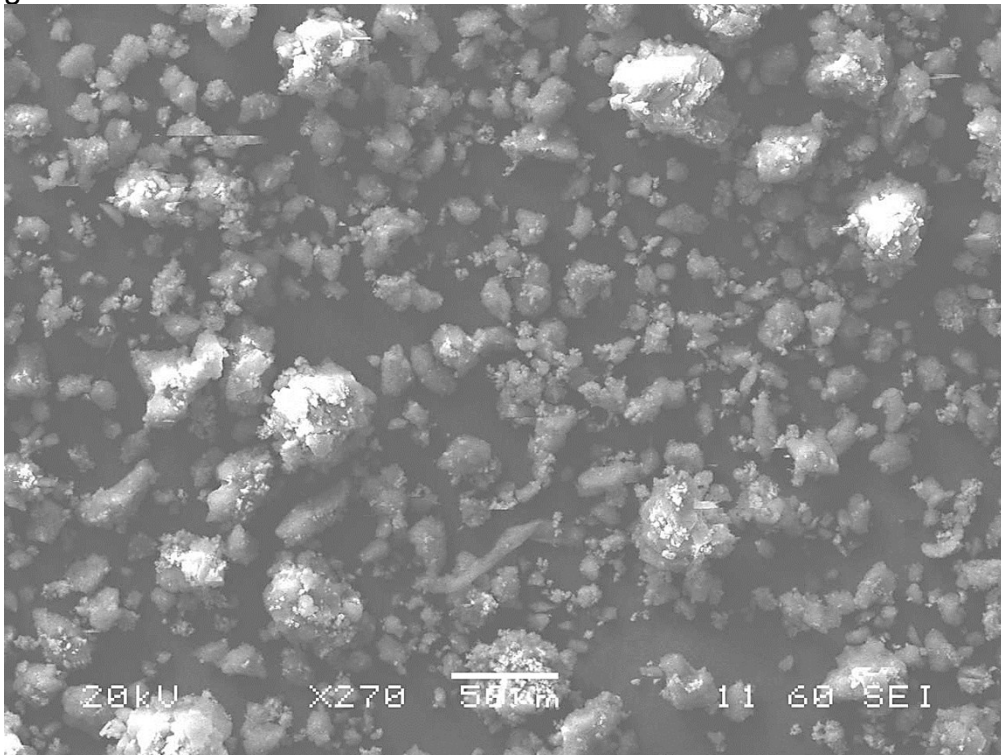


Figure S16. Scanning electron micrograph images of MIL-125-NHBu prepared in glass vessel. Scale is indicated.

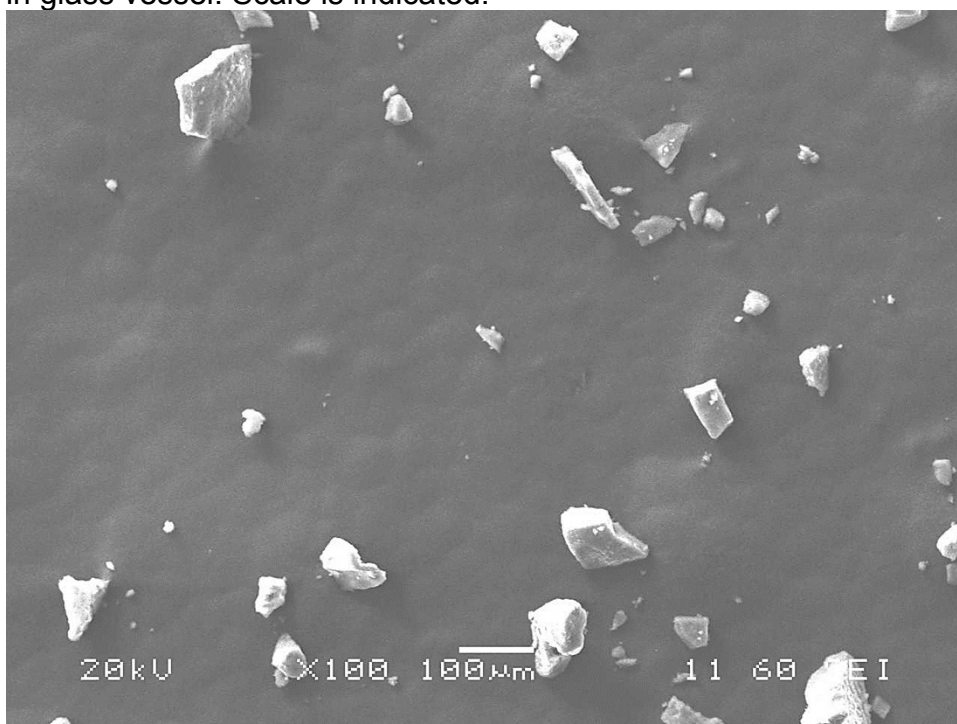
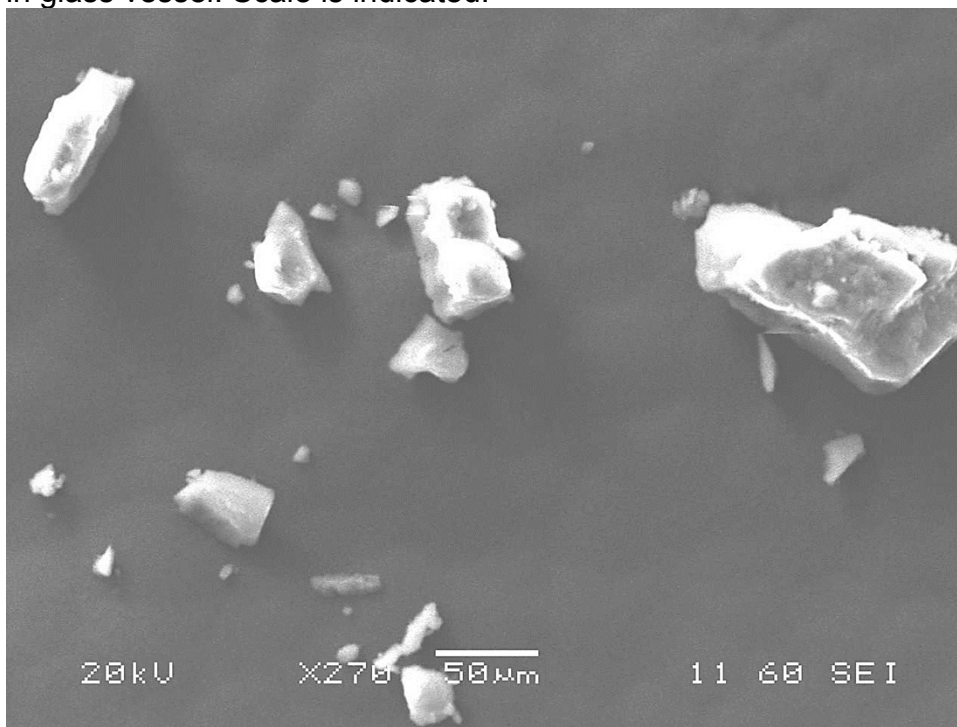


Figure S17. Scanning electron micrograph images of MIL-125-NHBu prepared in glass vessel. Scale is indicated.



Section S4. Gas Adsorption

Figure S18. Nitrogen Gas adsorption isotherm (77 K) of MIL-125-NH₂.

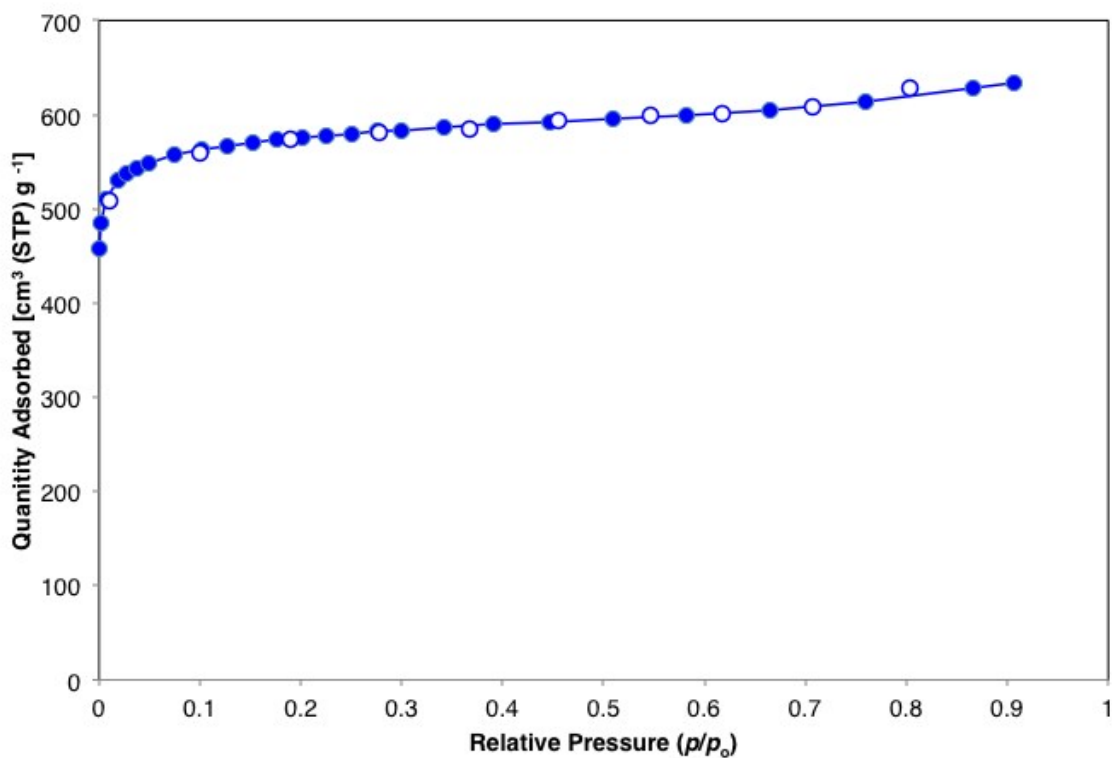


Figure S19. NLDFT pore size distribution of MIL-125-NH₂ using data measured from N₂ gas isotherm at 77 K.

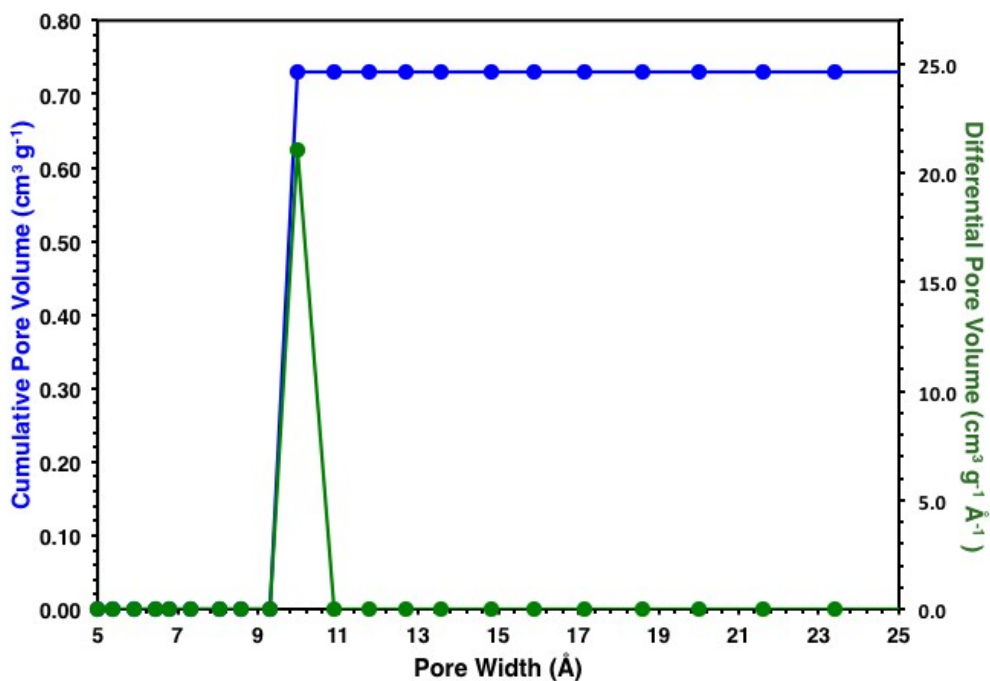


Figure S20. Nitrogen Gas adsorption isotherm (77 K) of MIL-125-NHMe.

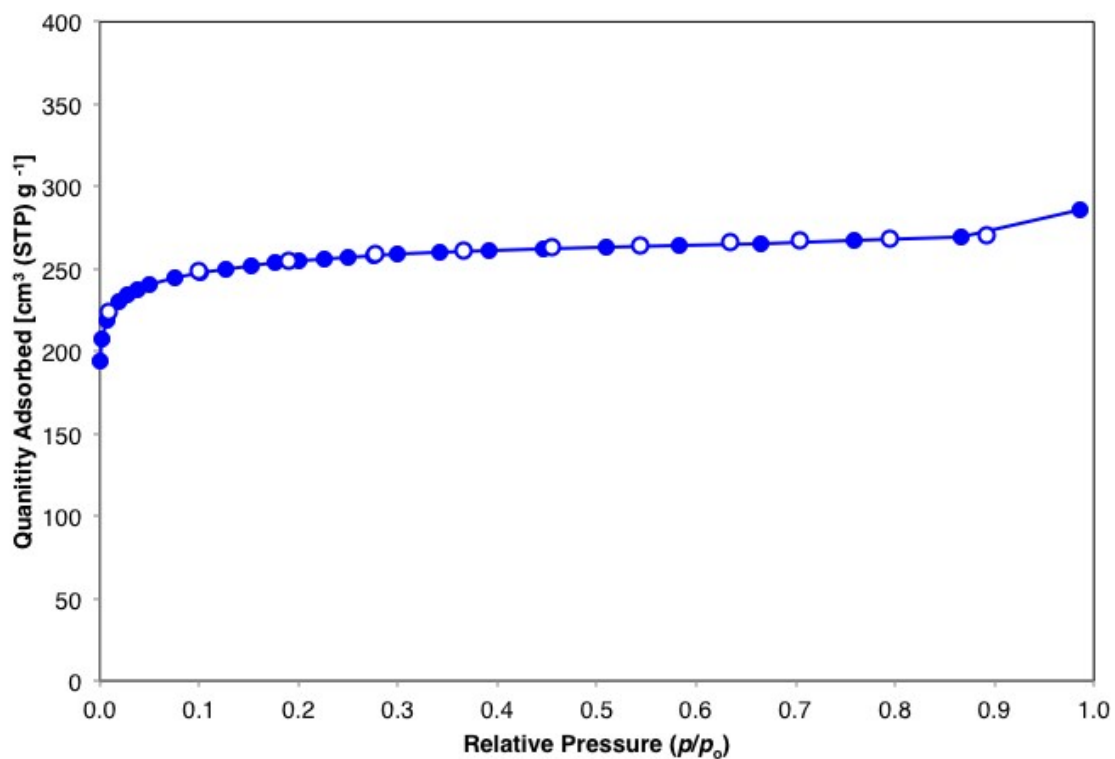


Figure S21. Rouquerol plot MIL-125-NHMe.

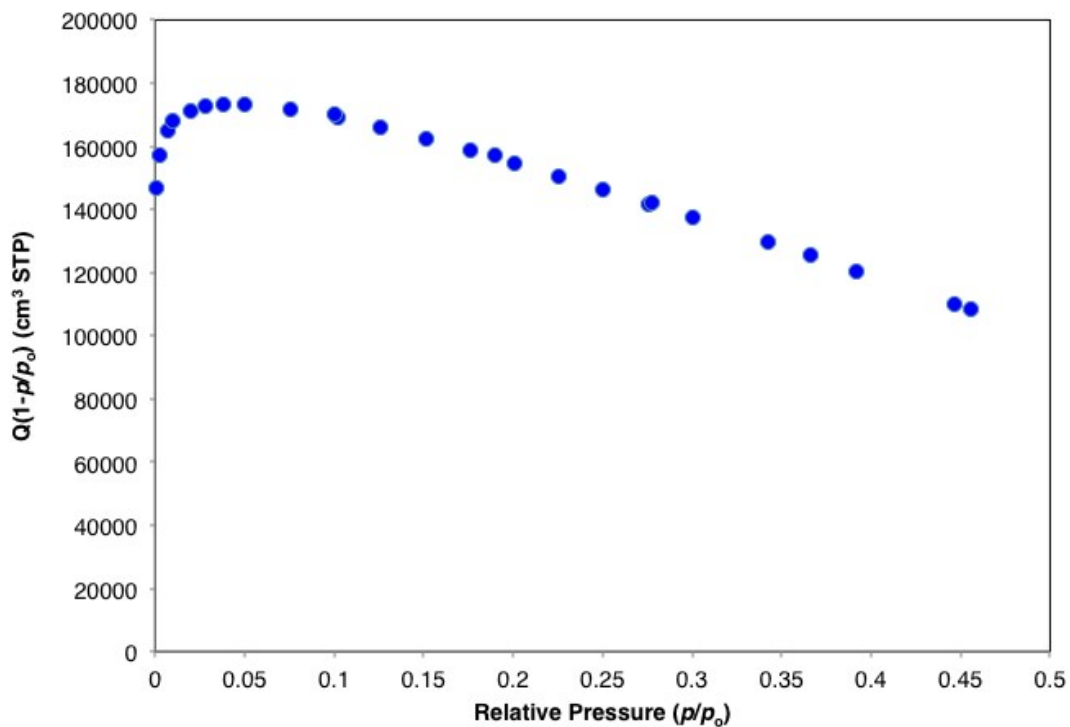


Figure S22. Linear BET plot MIL-125-NHMe.

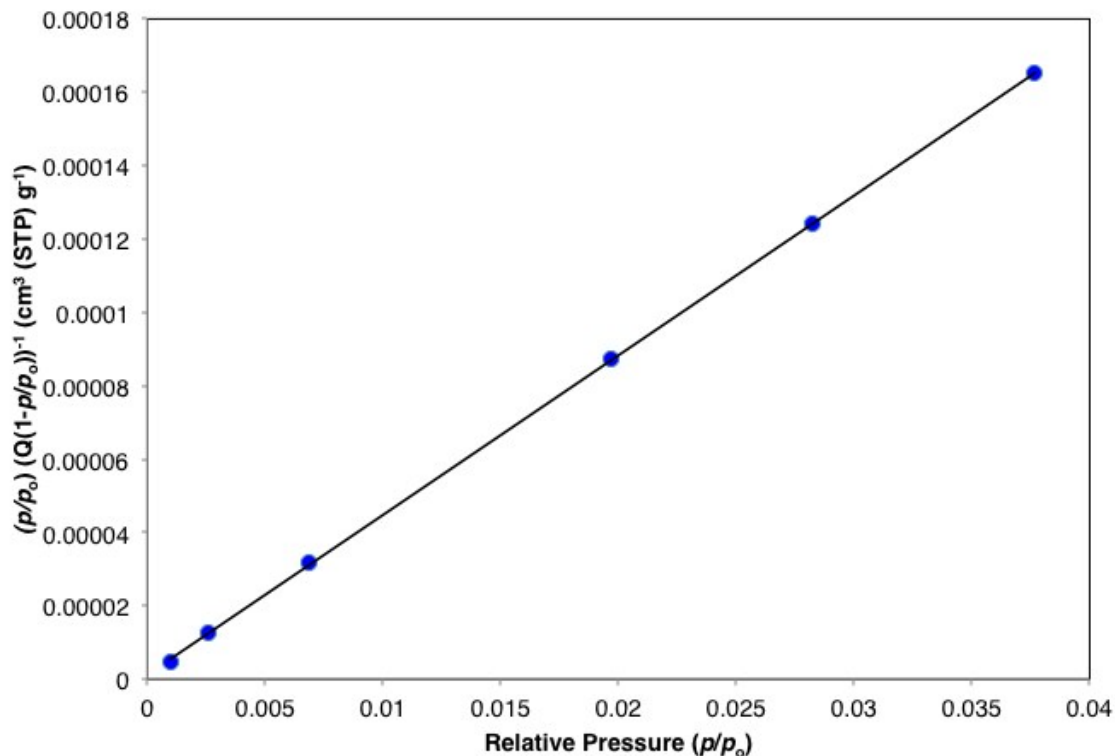


Figure S23. NLDFT pore size distribution of MIL-125-NHMe using data measured from N₂ gas isotherm at 77 K.

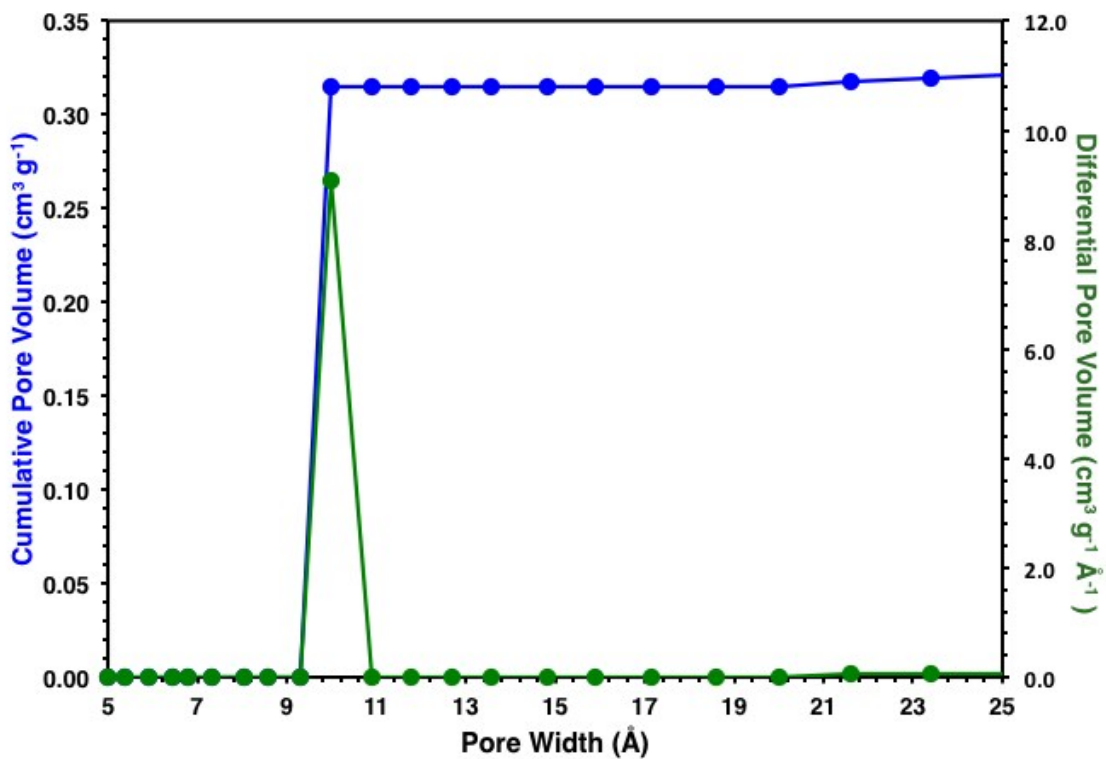


Figure S24. Gas adsorption isotherm (77 K) of MIL-125-NH₂.

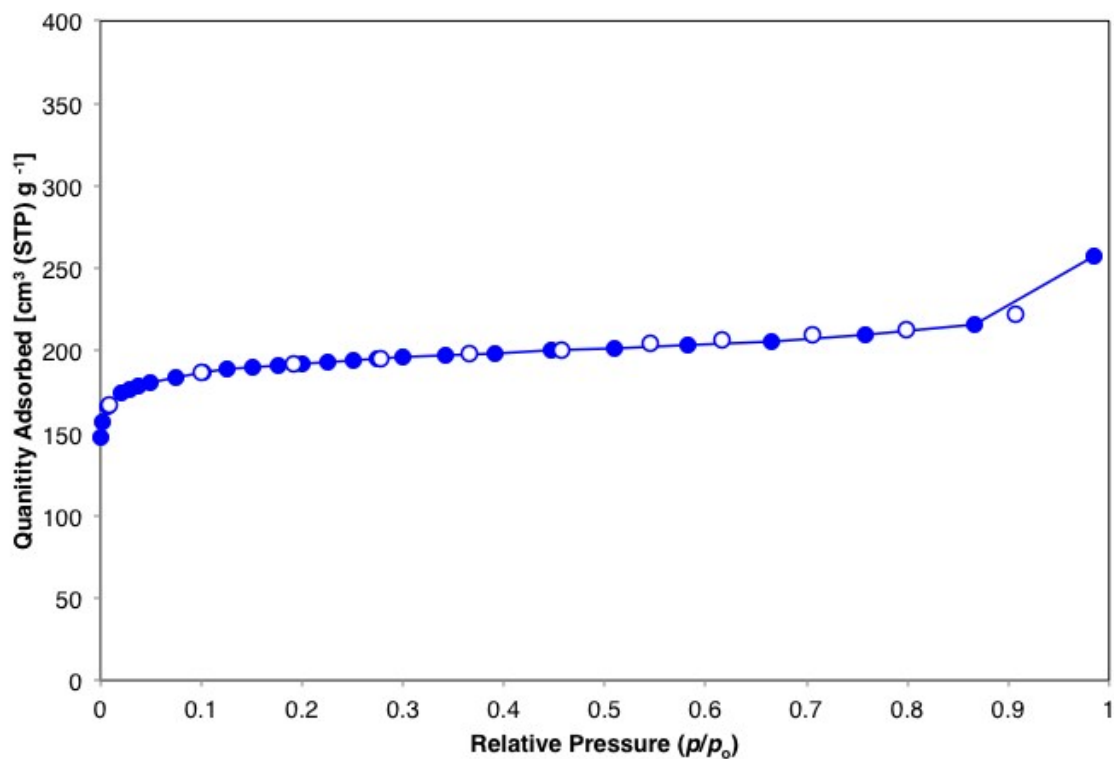


Figure S25. Rouquerol plot MIL-125-NH₂.

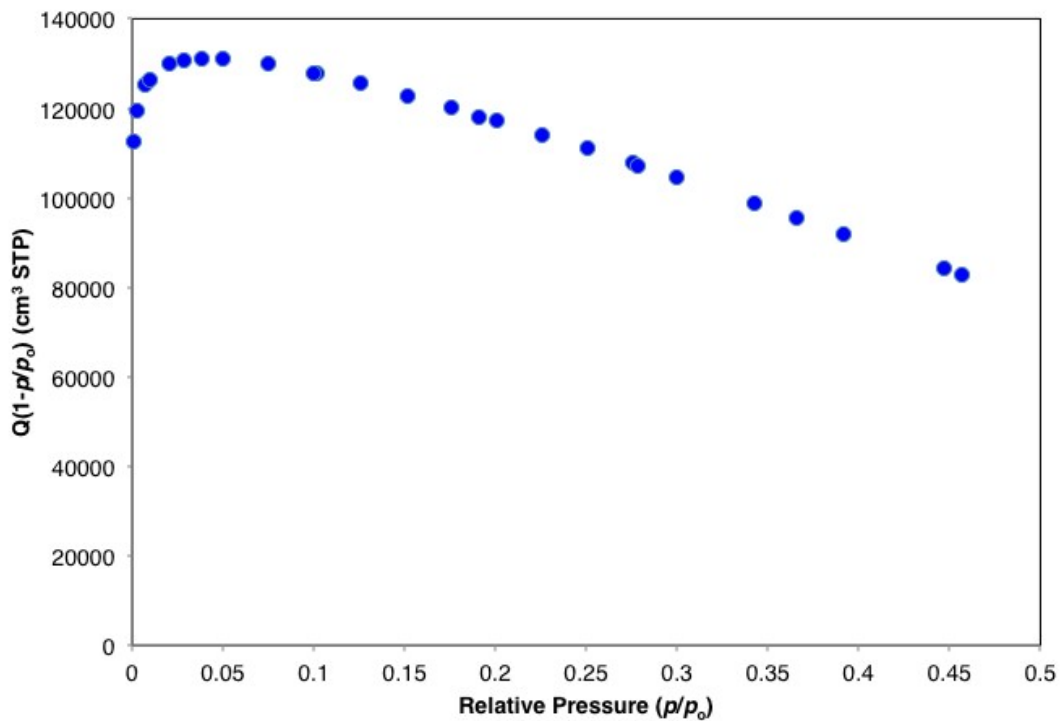


Figure S26. Linear BET plot MIL-125-NHET

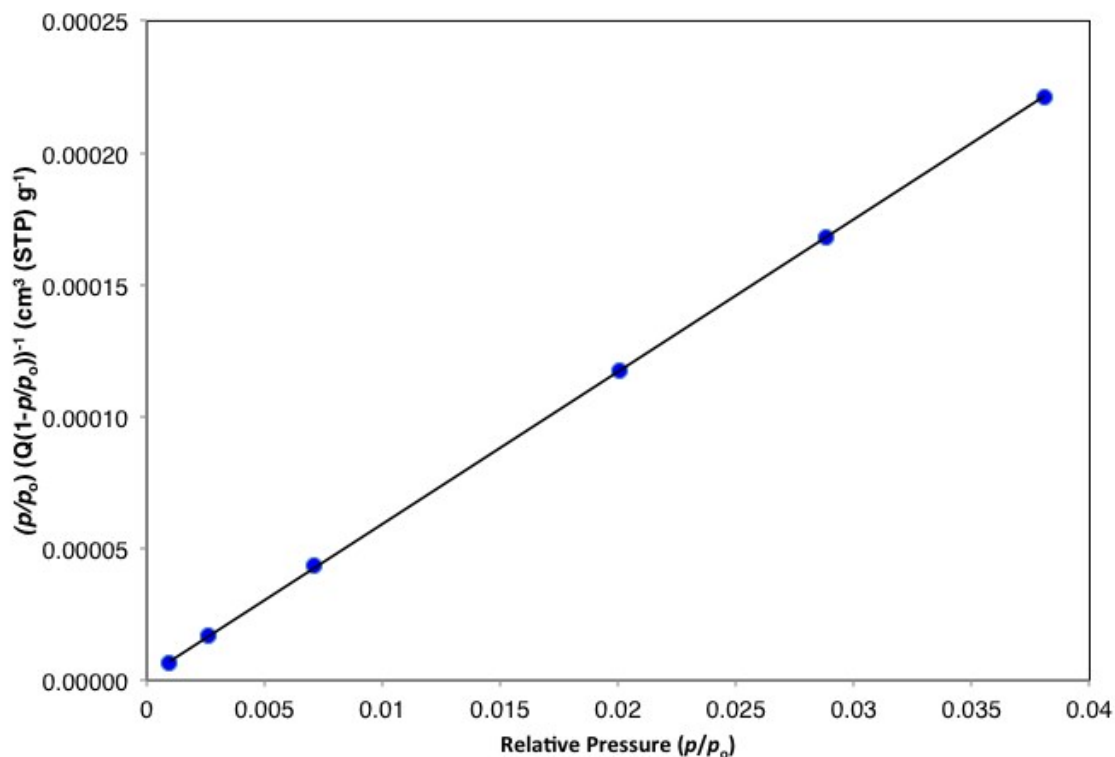


Figure S27. NLDFT pore size distribution of MIL-125-NHET using data measured from N₂ gas isotherm at 77 K.

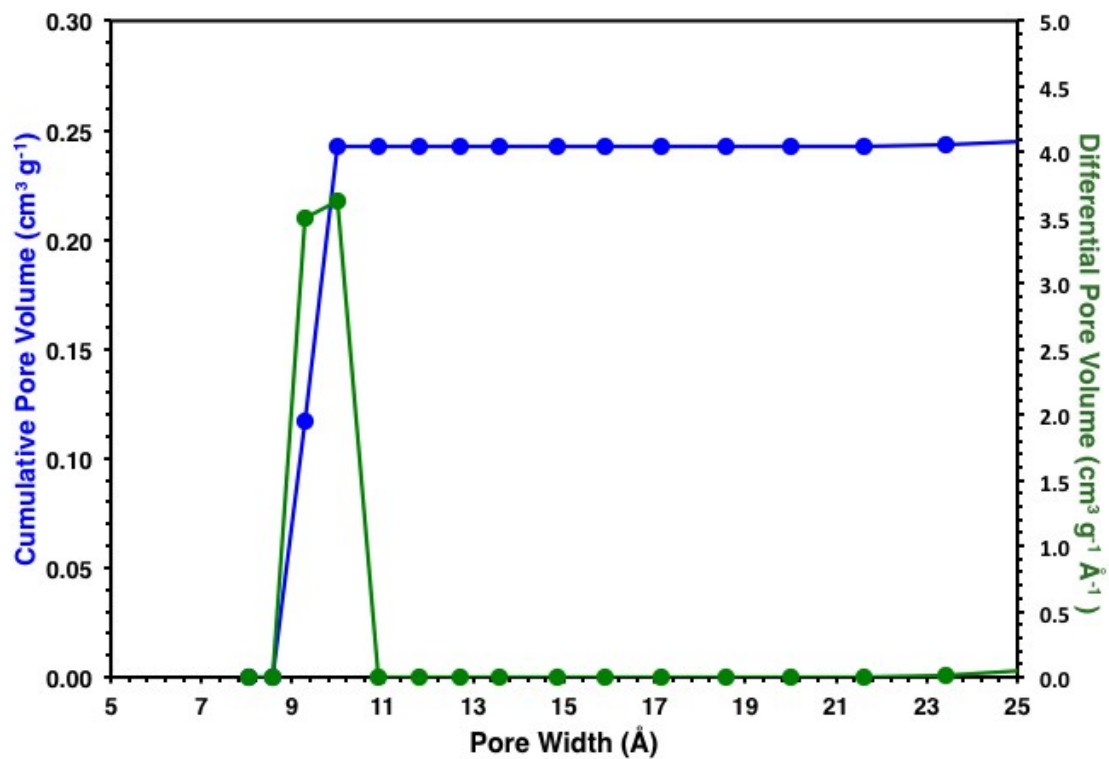


Figure S28. Gas adsorption isotherm (77 K) of MIL-125-NHⁱPr.

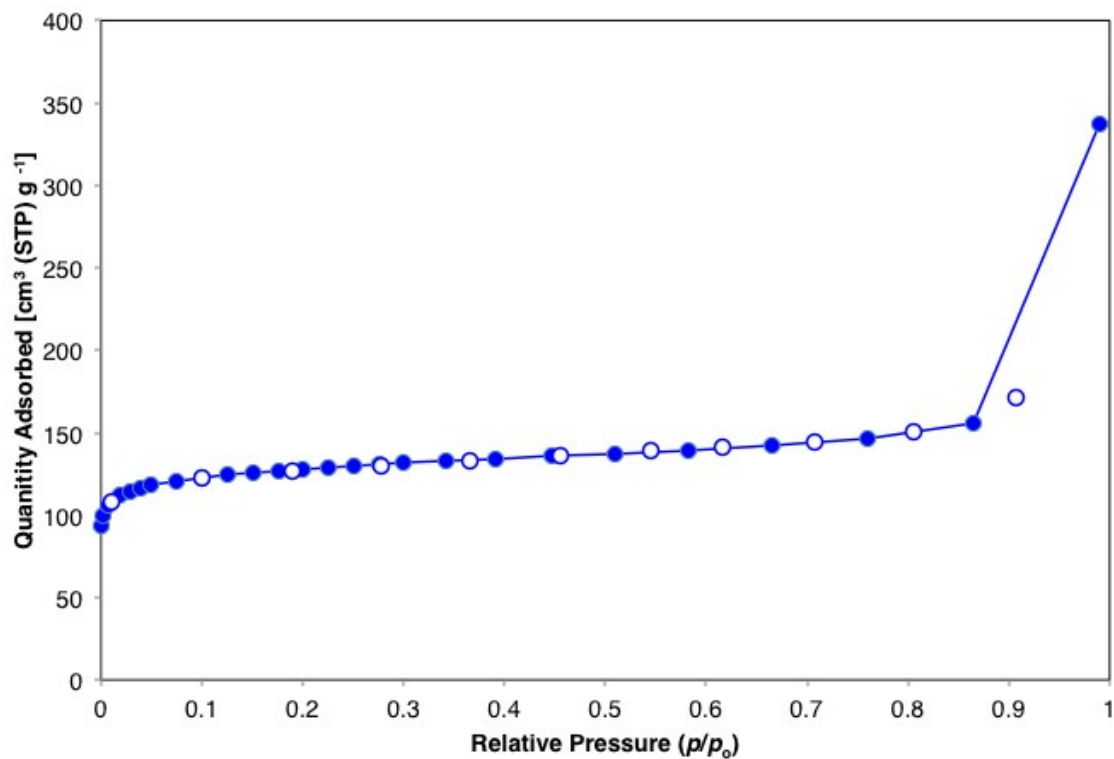


Figure S29. Rouquerol plot MIL-125-NHⁱPr

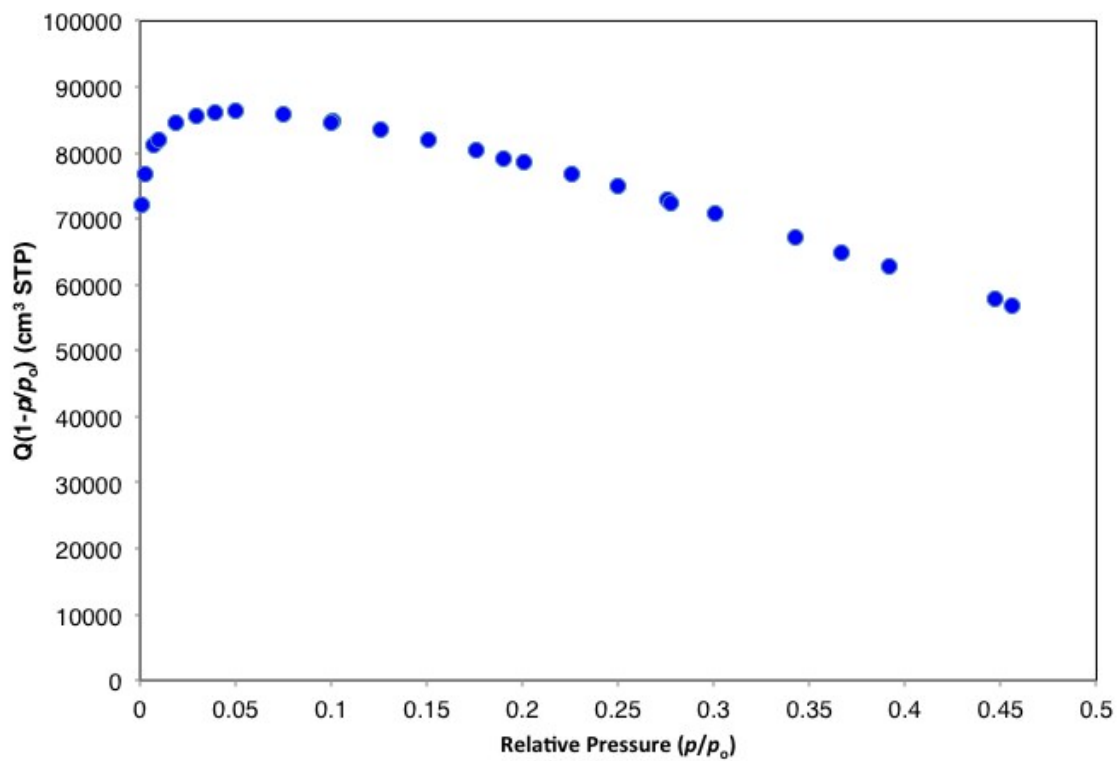


Figure S30. Linear BET plot MIL-125-NHⁱPr.

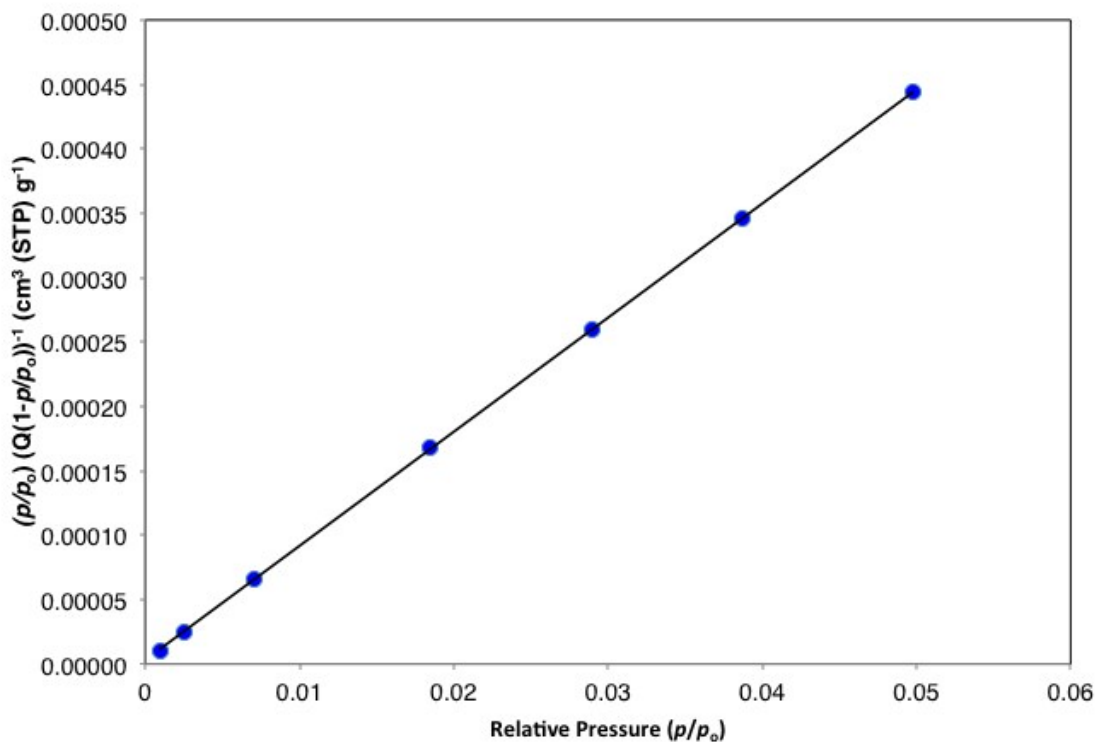


Figure S31. DFT pore size distribution of MIL-125-NHⁱPr using data measured from N₂ gas isotherm at 77 K.

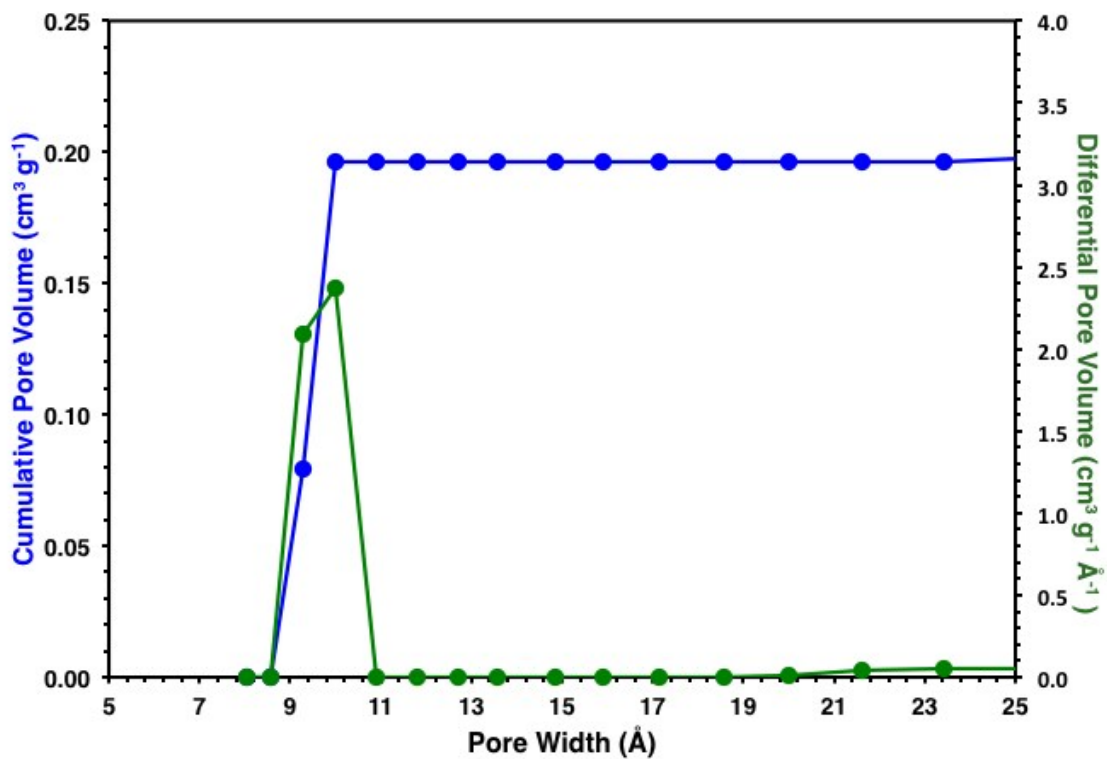


Figure S32. Gas adsorption isotherm (77 K) of MIL-125-NHBu.

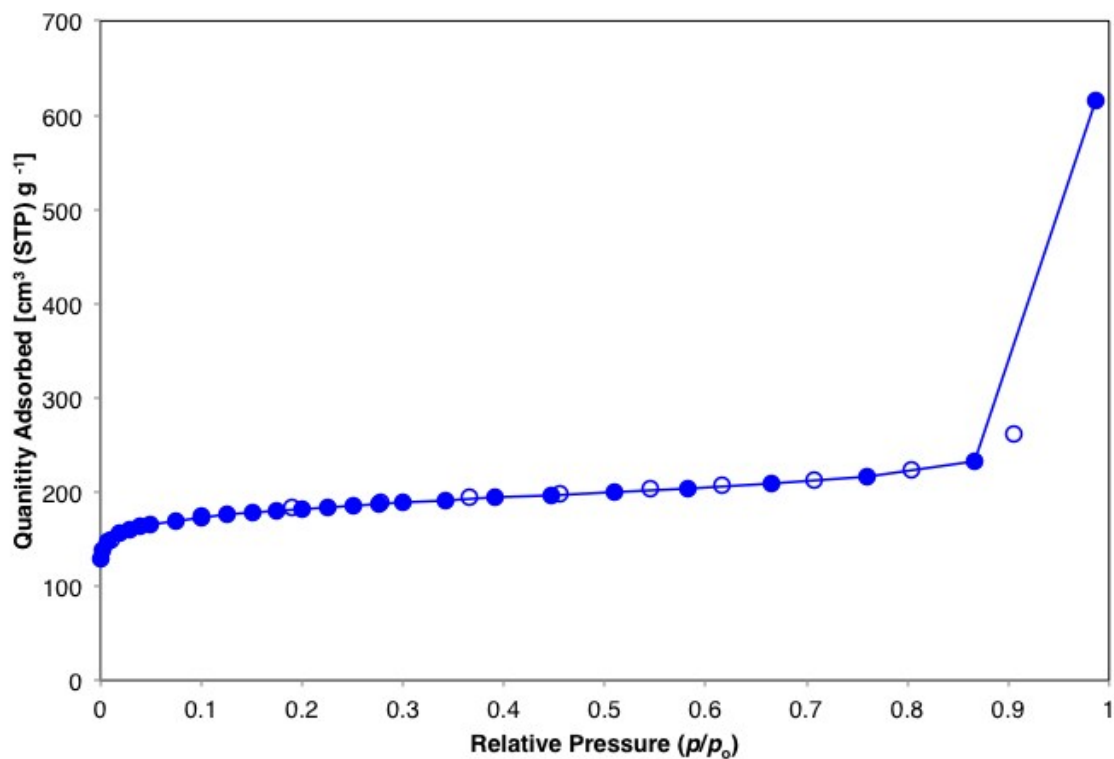


Figure S33. Rouquerol plot MIL-125-NHBu.

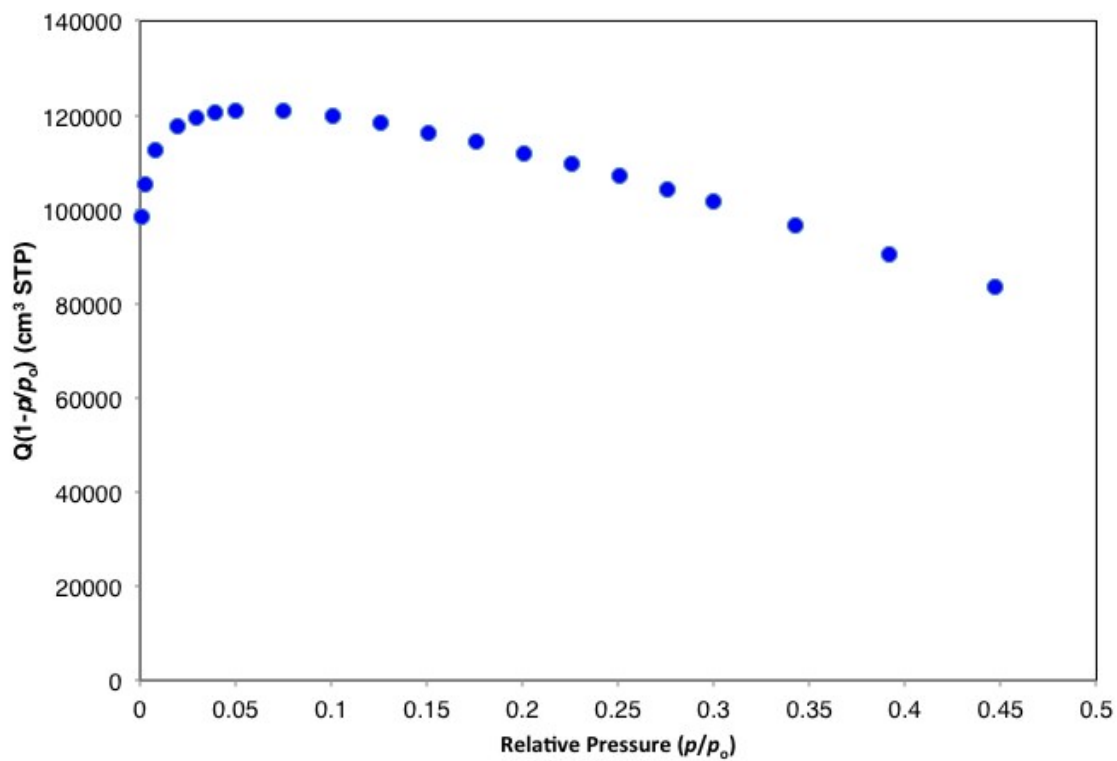


Figure S34. Linear BET plot MIL-125-NHBu.

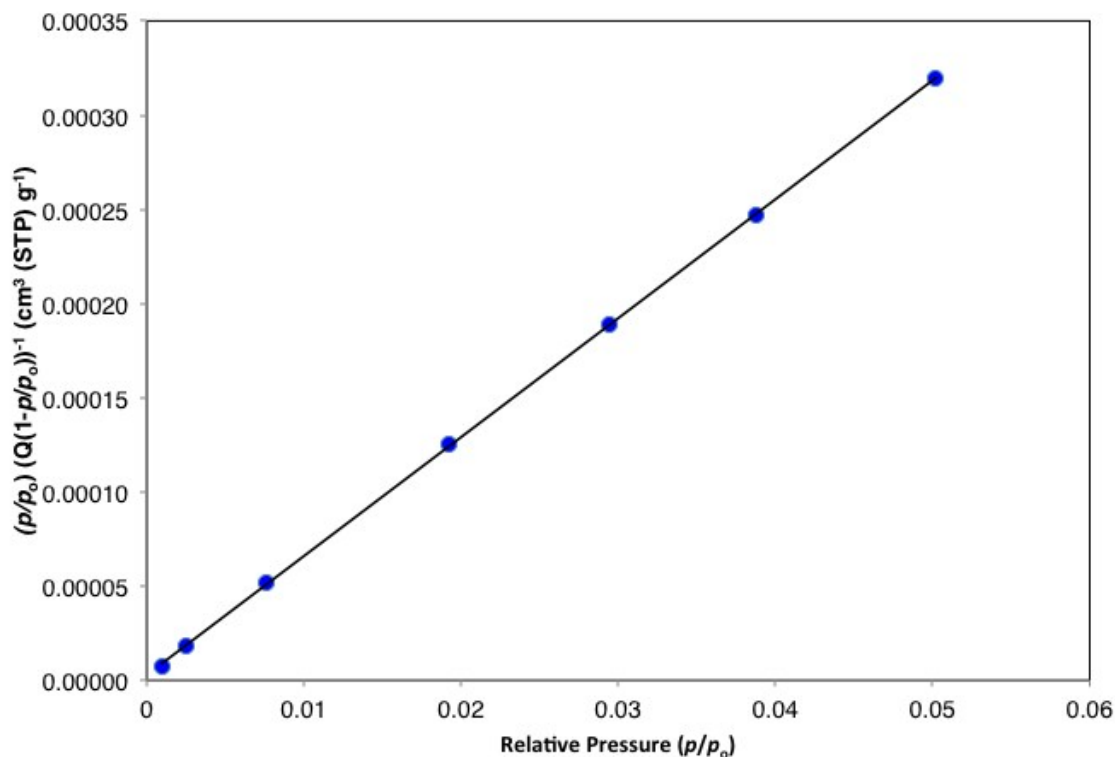


Figure S35. DFT pore size distribution of MIL-125-NHBu using data measured from N₂ gas isotherm at 77 K.

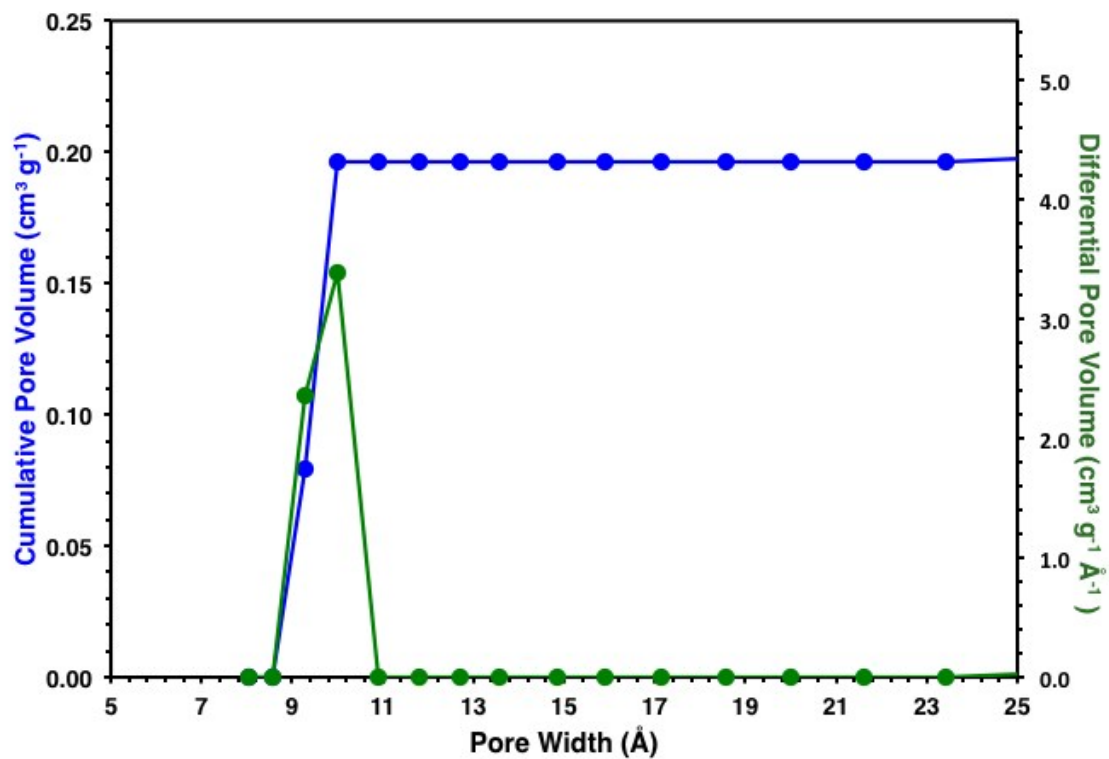


Figure S36. Gas adsorption isotherm (77 K) of MIL-125-NHCyp

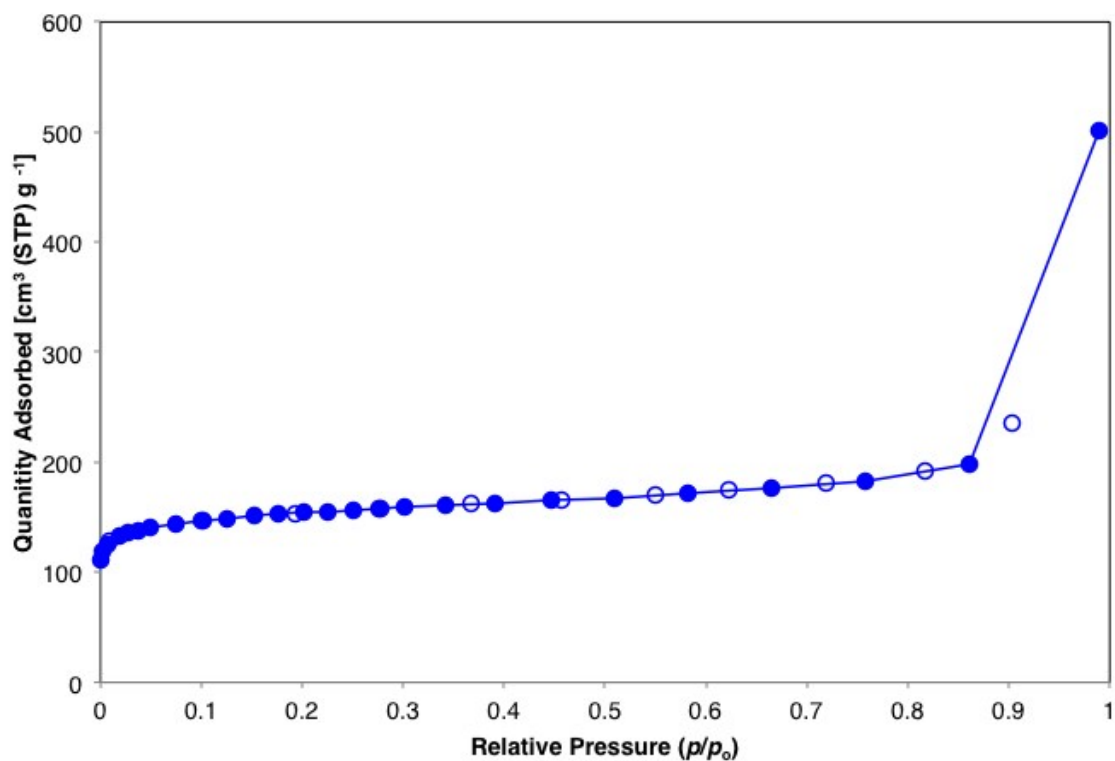


Figure S37. Rouquerol plot MIL-125-NHCyp

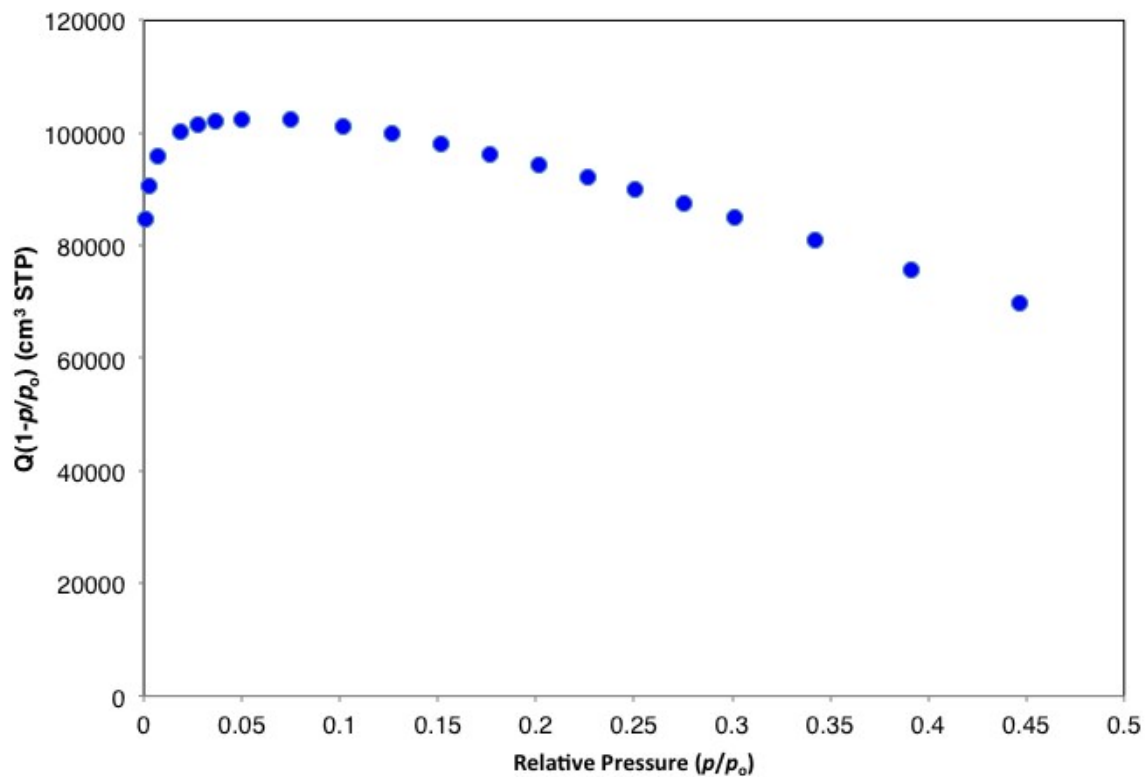


Figure S38. Linear BET plot MIL-125-Cyp

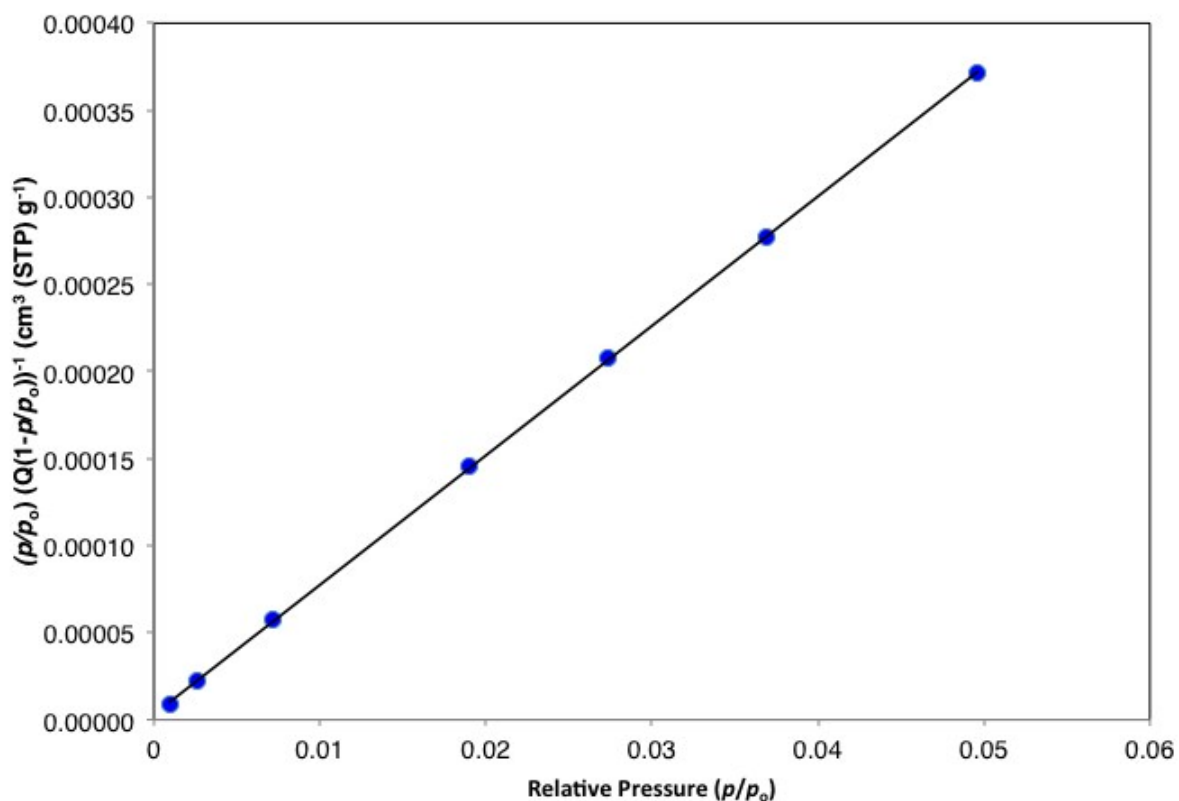


Figure S39. DFT pore size distribution of MIL-125-NHCyp using data measured from N_2 gas isotherm at 77 K.

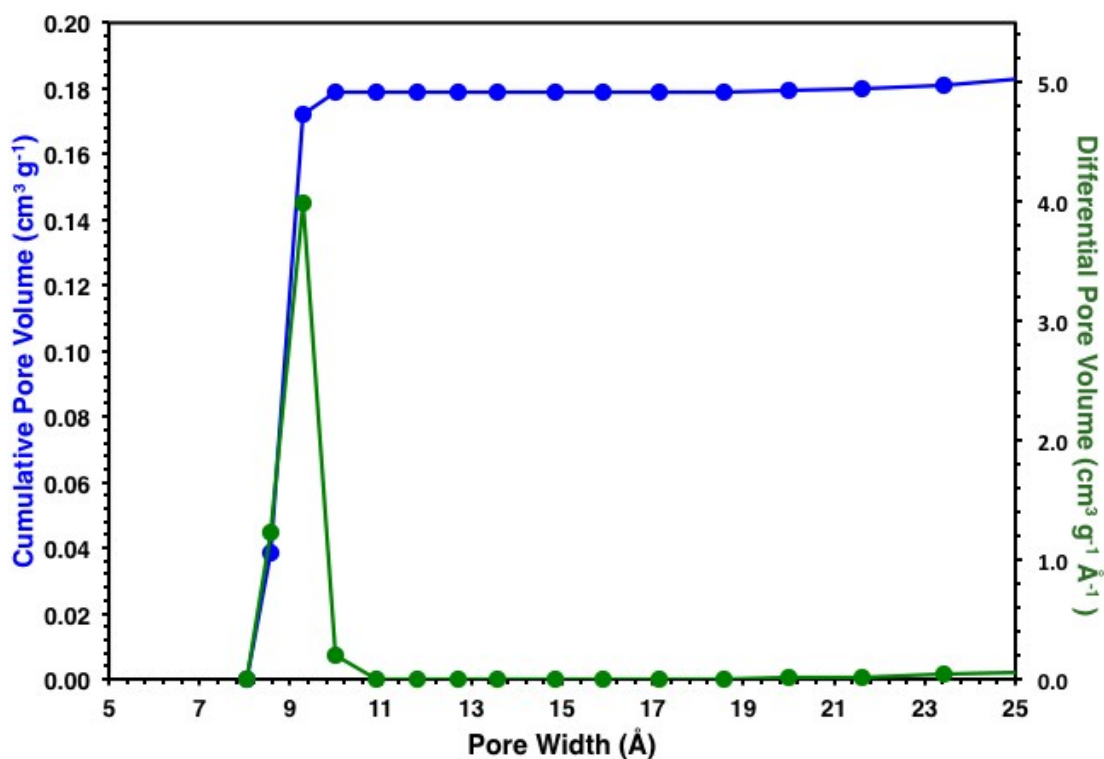


Figure S40. Gas adsorption isotherm (77 K) of MIL-125-NHCy

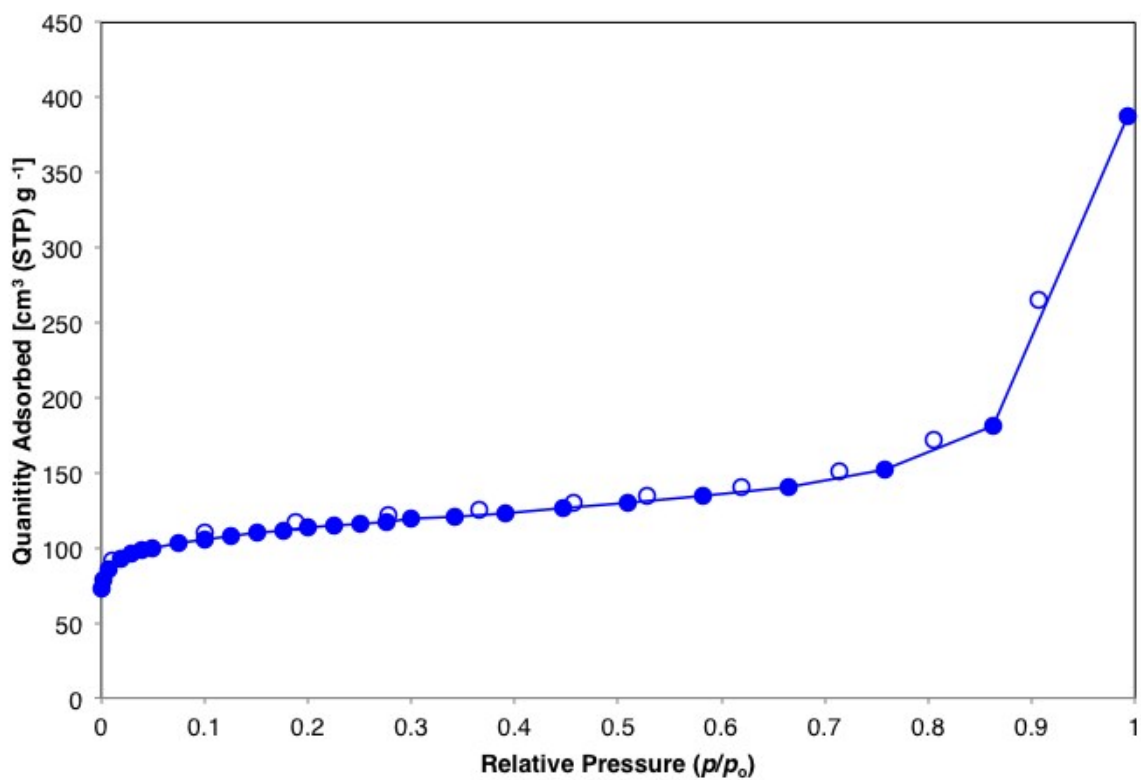


Figure S41. Rouquerol plot MIL-125-NHCy

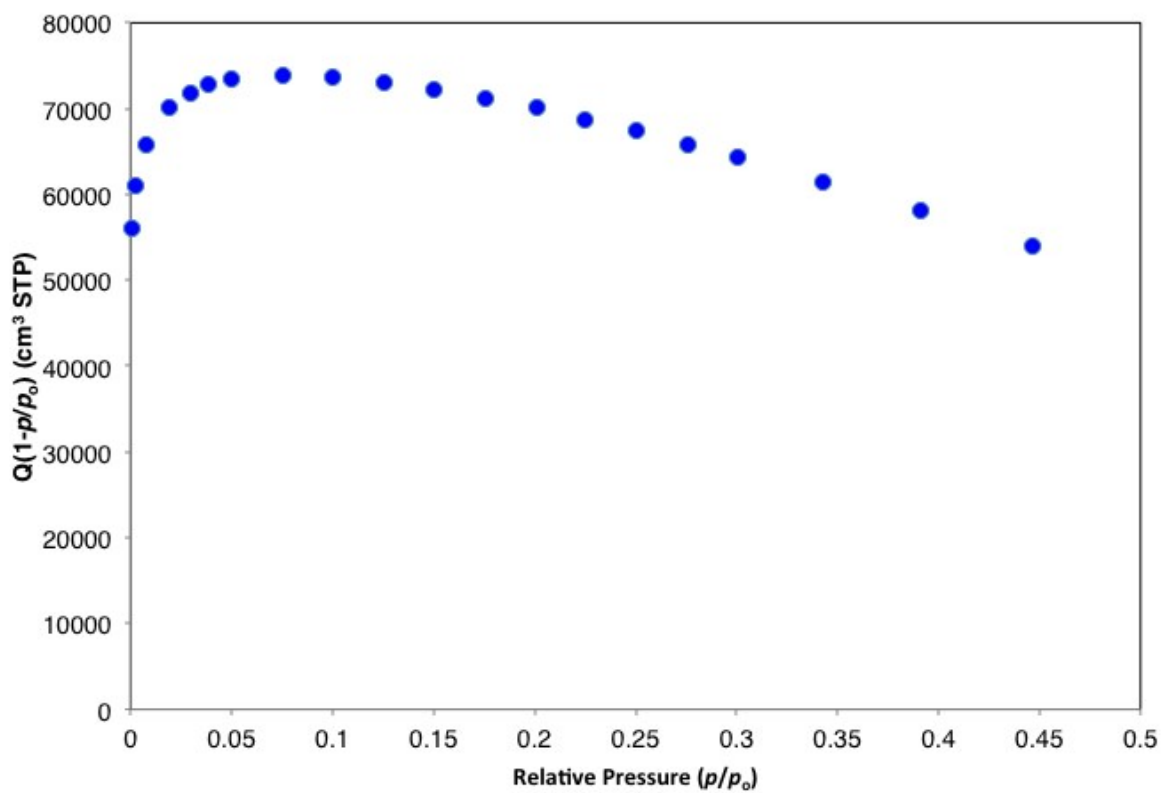


Figure S42. Linear BET plot MIL-125-NHCy.

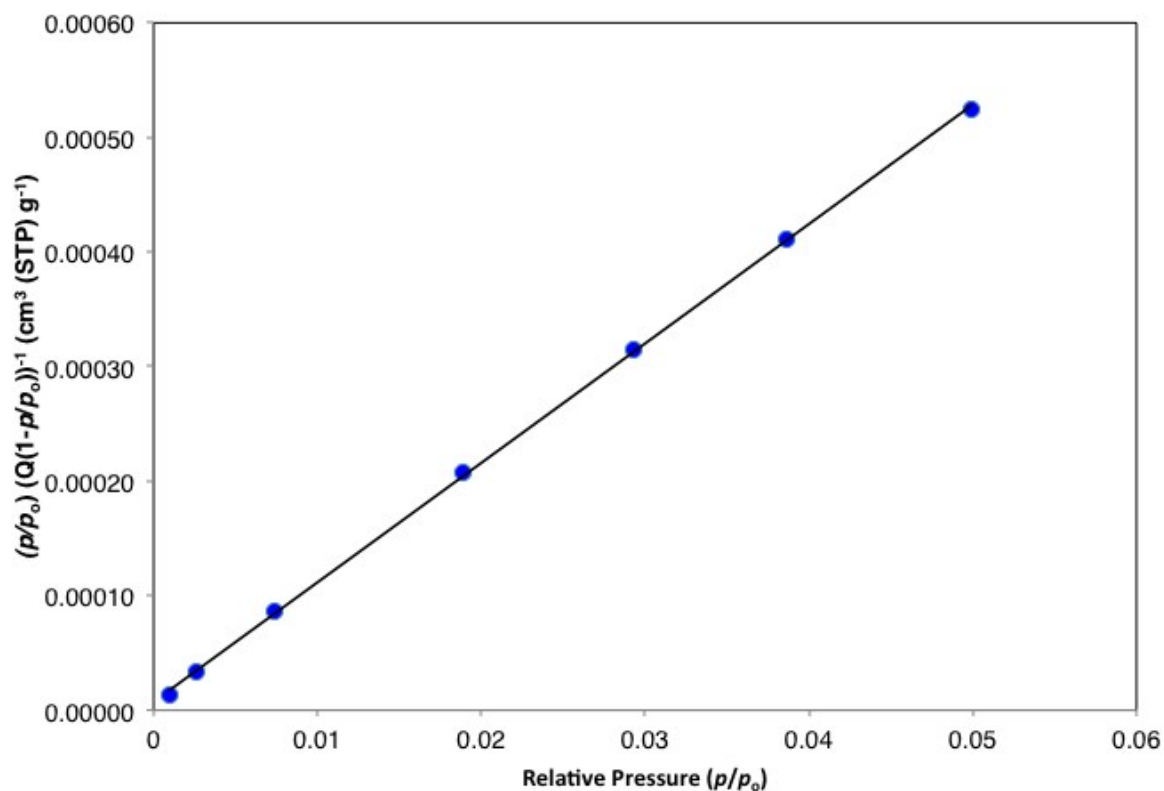


Figure S43. DFT pore size distribution of MIL-125-NHCy using data measured from N_2 gas isotherm at 77 K.

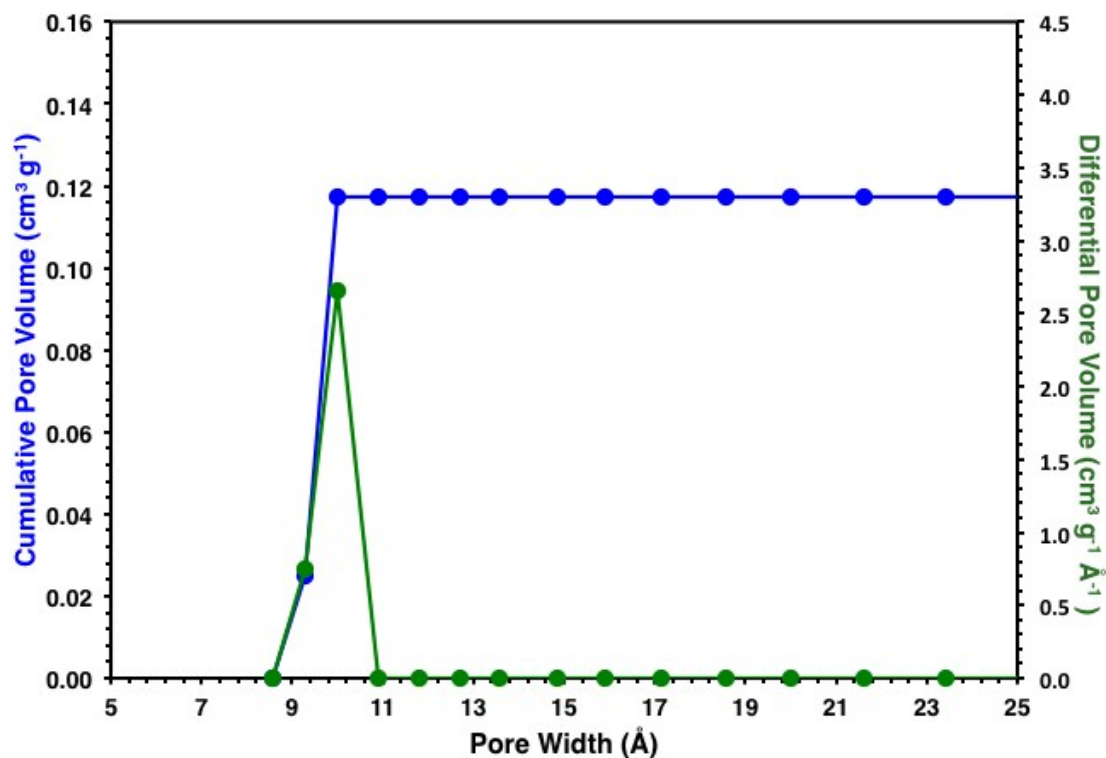


Figure S44. Gas adsorption isotherm (77 K) of MIL-125-NHhep.

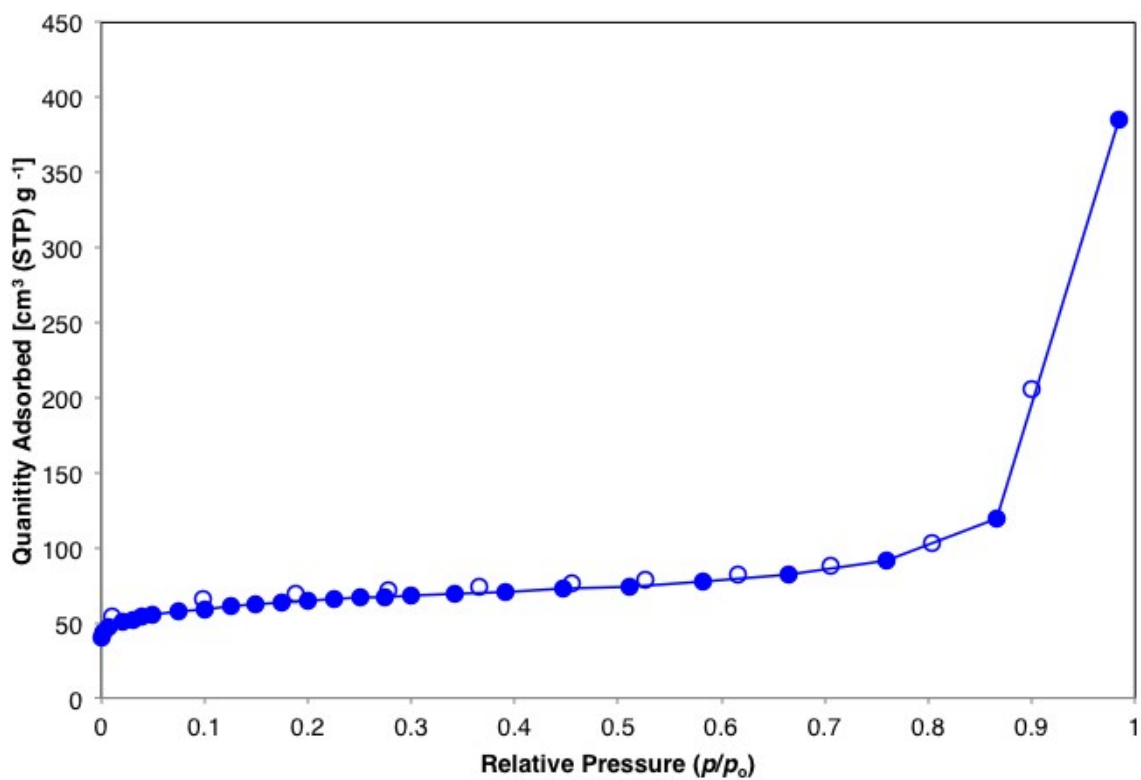


Figure S45. Rouquerol plot MIL-125-NHhep

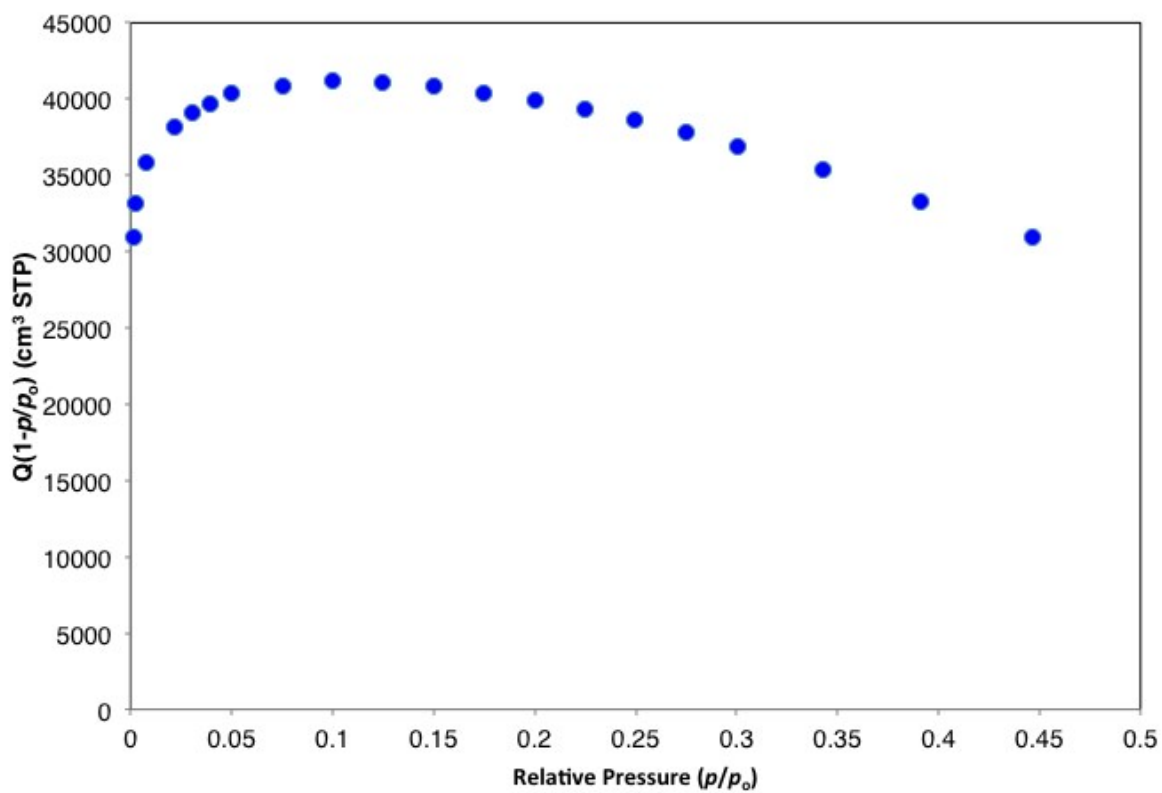


Figure S46. Linear BET plot MIL-125-NHhep

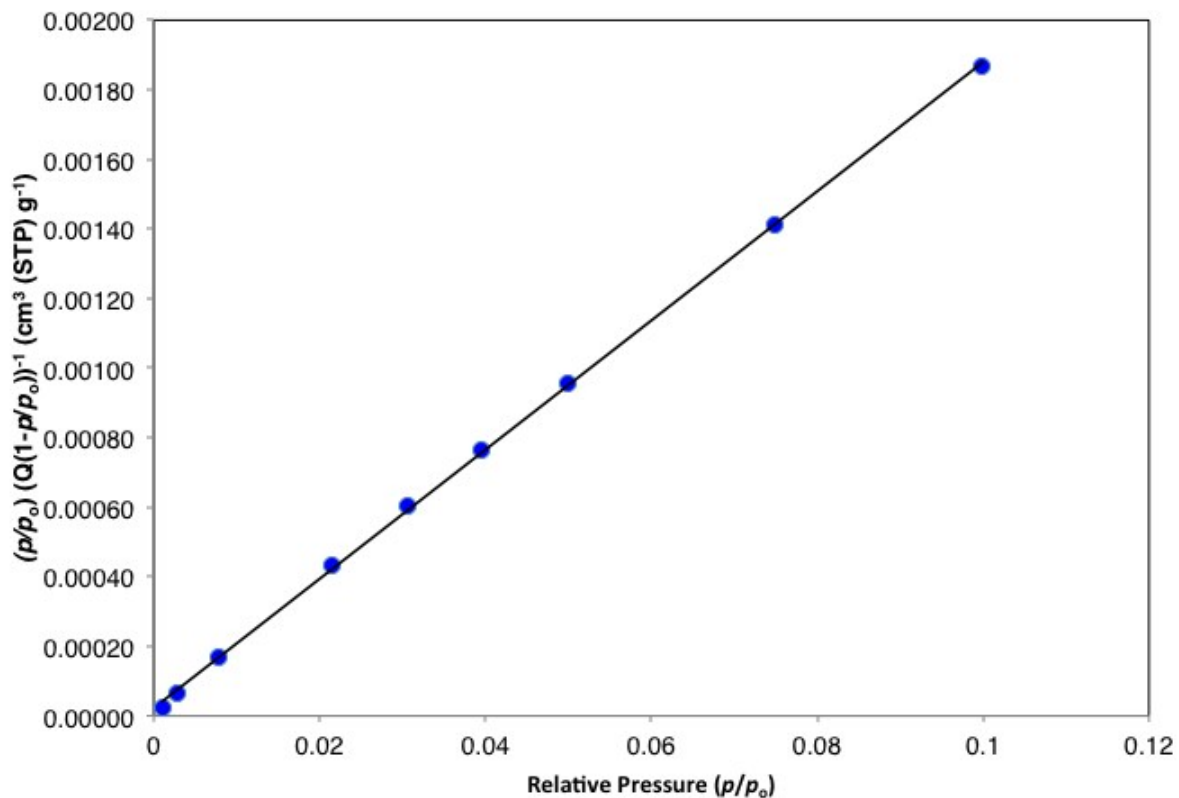


Figure S47. DFT pore size distribution of MIL-125-NHhep using data measured from N_2 gas isotherm at 77 K.

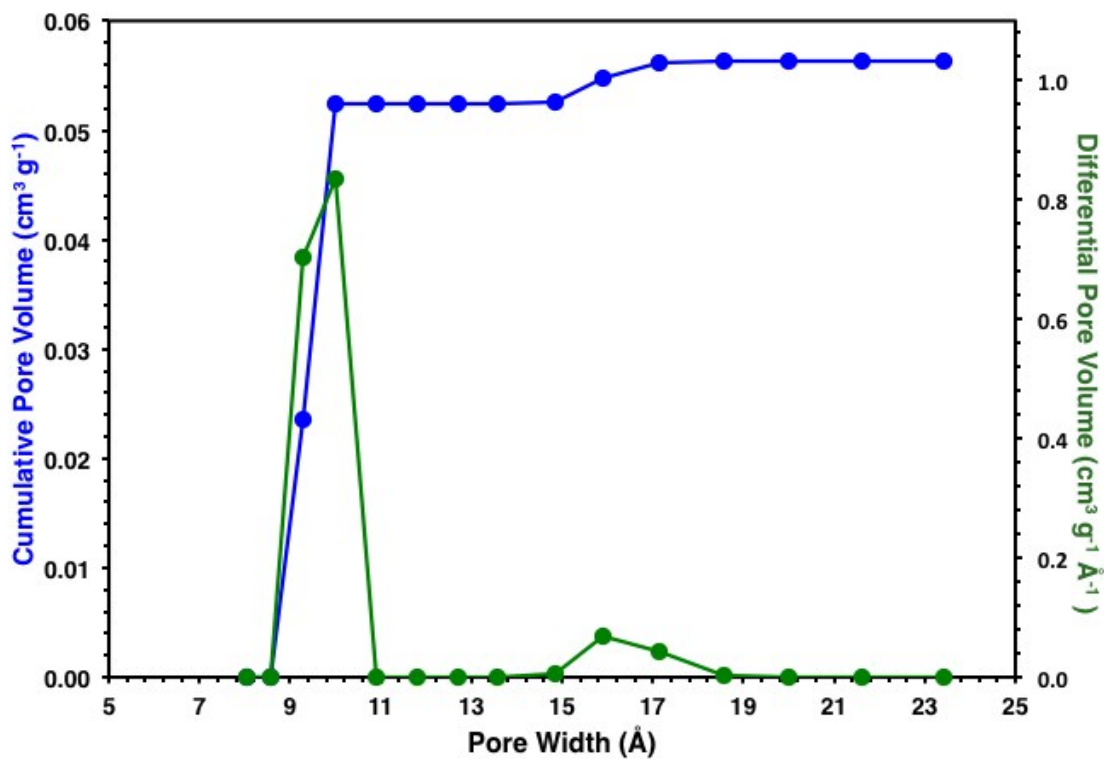


Table S4. N₂ BET Surface area parameters.

MIL-125-NHR	Me	Et	<i>i</i> Pr	Bu
V_m (cm ³ (STP) g ⁻¹)	229.64	173.09	112.86	158.38
σ_{V_m}	0.62	0.42	0.28	0.61
S_{BET} (m² g⁻¹)	998.9	752.9	491.0	689.0
$\sigma_{S_{BET}}$	2.7	1.8	1.2	2.6
C_{BET}	3382	3663	2800	2159
$\sigma_{C_{BET}}$	640	676	521	481

Table S5. N₂ BET Surface area parameters.

MIL-125-NHR	Cyp	Cy	hep
V_m (cm ³ (STP) g ⁻¹)	134.41	96.37	53.79
σ_{V_m}	0.44	0.46	0.35
S_{BET} (m² g⁻¹)	584.7	419.2	234.0
$\sigma_{S_{BET}}$	1.9	2.0	1.5
C_{BET}	2424	1262	822
$\sigma_{C_{BET}}$	505	274	205

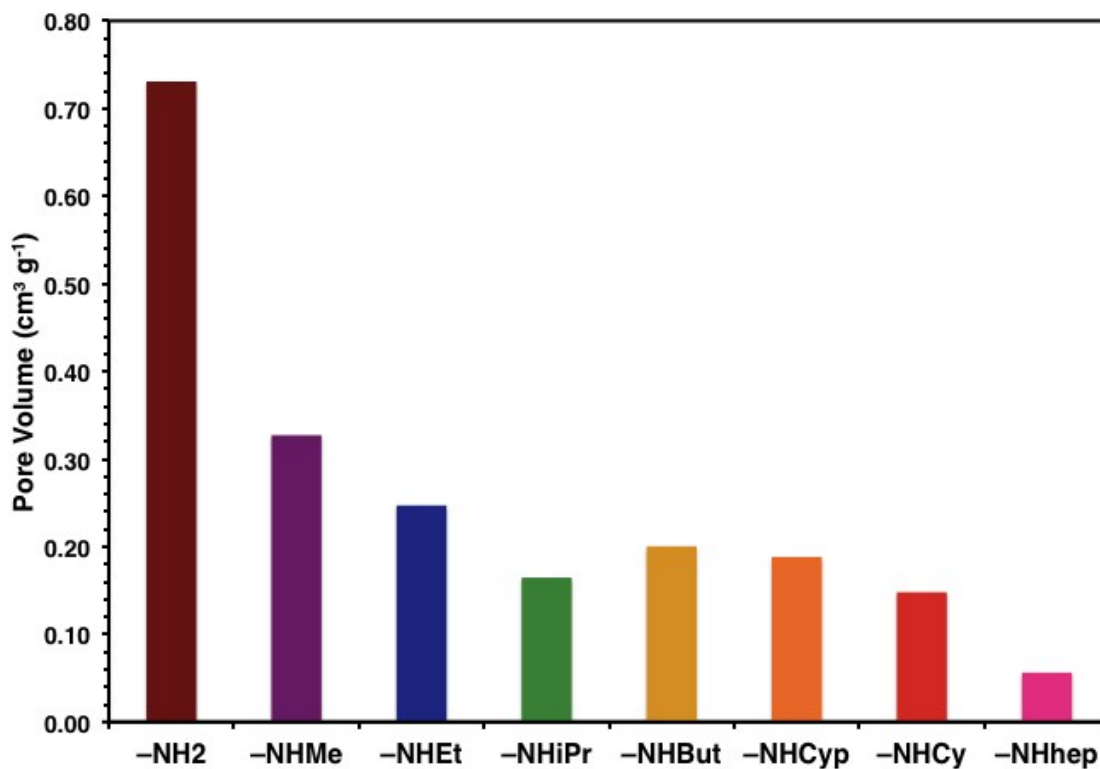
Figure S48. Pore volume of as prepared MOFs calculated from NLDFT using data measured from N₂ gas isotherm at 77 K.

Figure S49. CO₂ Gas adsorption isotherm of MIL-125-NH₂ at 273 K (blue), 283 K (red), and 298 K (green).

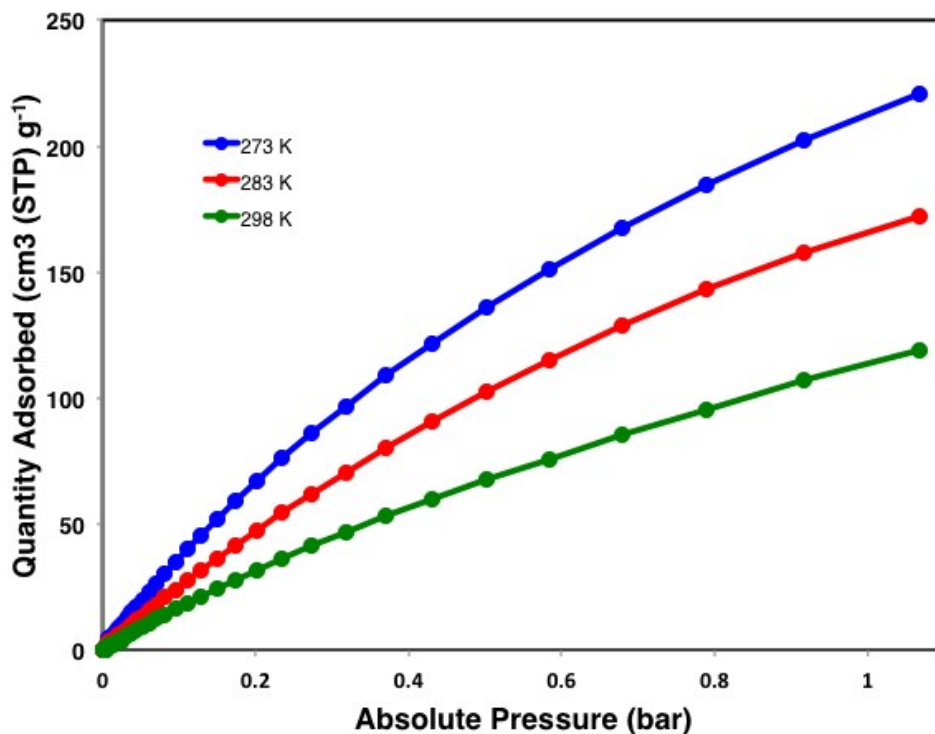


Figure S50. CO₂ Gas adsorption isotherm of MIL-125-NHMe at 273 K (blue), 283 K (red), and 298 K (green).

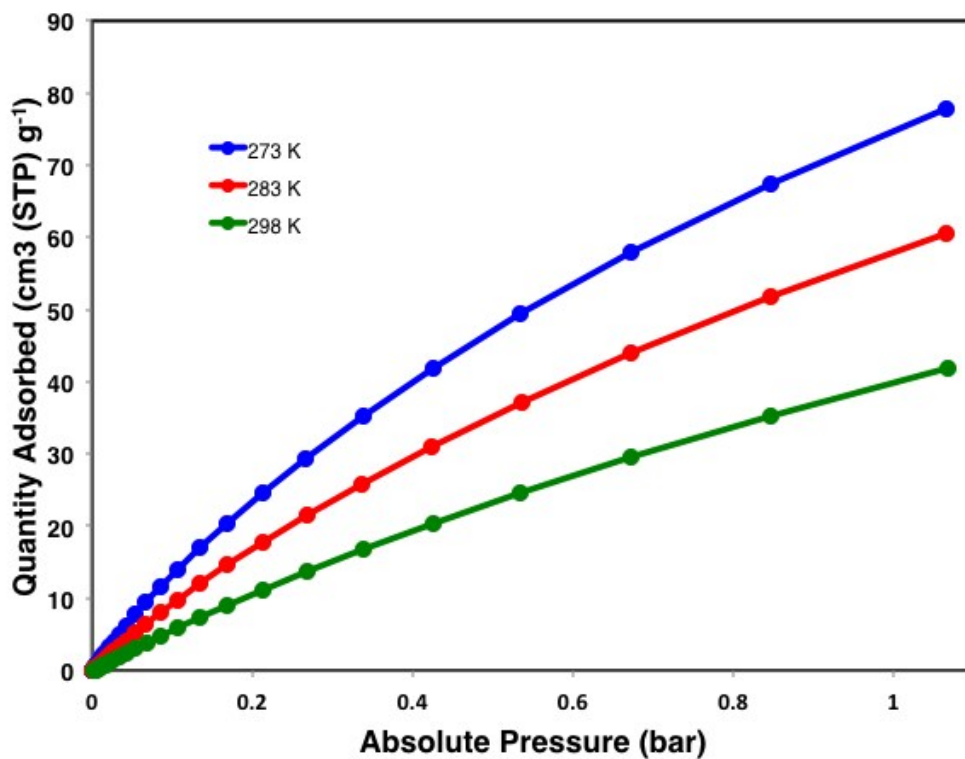


Figure S51. CO₂ Gas adsorption isotherm of MIL-125-NHEt at 273 K (blue), 283 K (red), and 298 K (green).

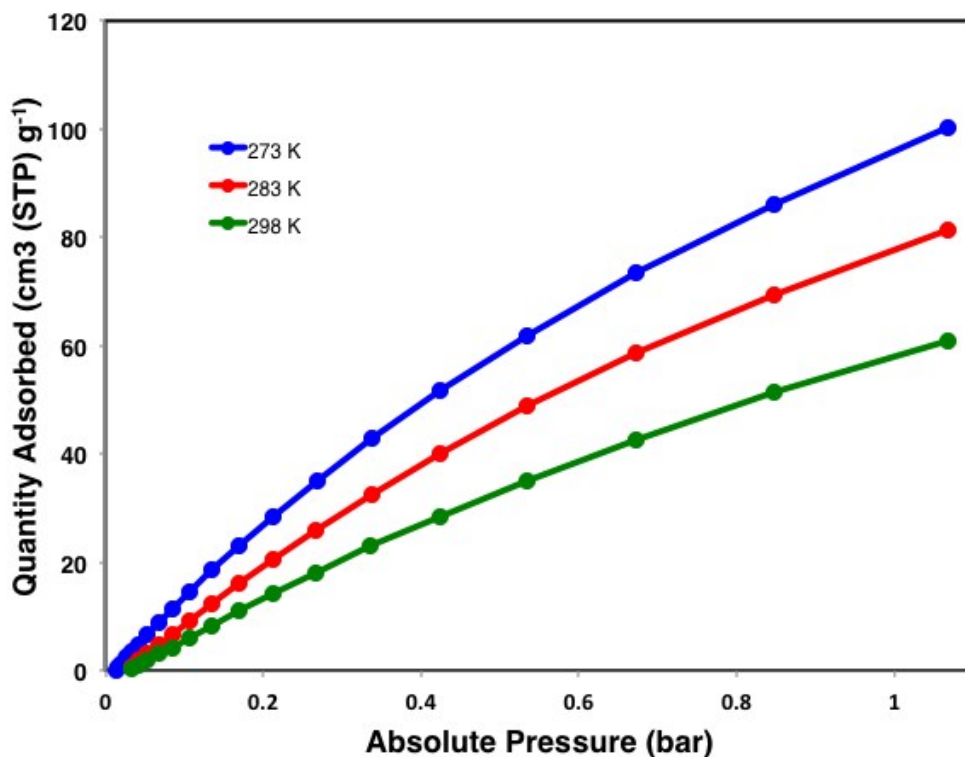


Figure S52. CO₂ Gas adsorption isotherm of MIL-125-NHⁱPr at 273 K (blue), 283 K (red), and 298 K (green).

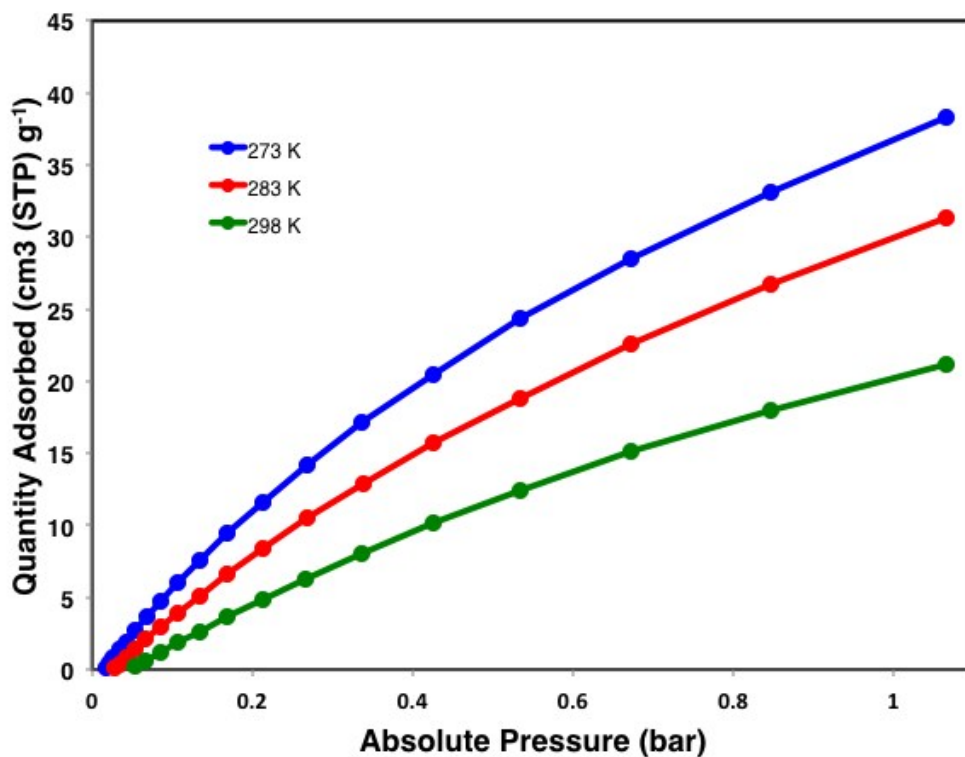


Figure S53. CO₂ Gas adsorption isotherm of **MIL-125-NHBu** at 273 K (blue), 283 K (red), and 298 K (green).

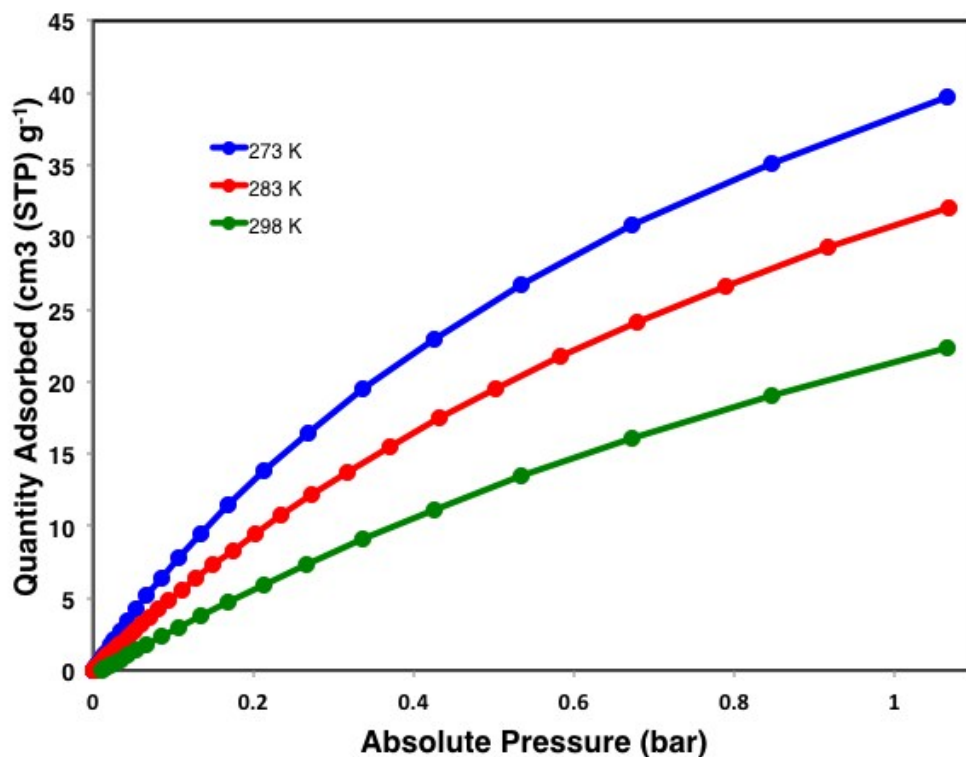


Figure S54. CO₂ Gas adsorption isotherm of **MIL-125-NHCyp** at 273 K (blue), 283 K (red), and 298 K (green).

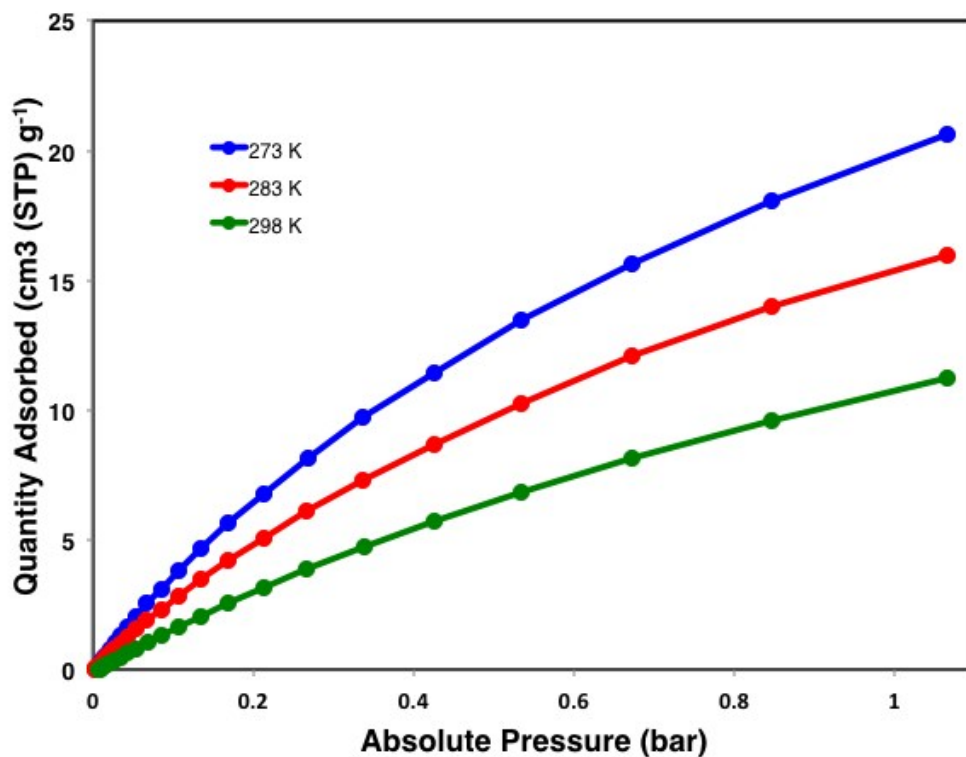


Figure S55. CO₂ Gas adsorption isotherm of **MIL-125-NHCy** at 273 K (blue), 283 K (red), and 298 K (green).

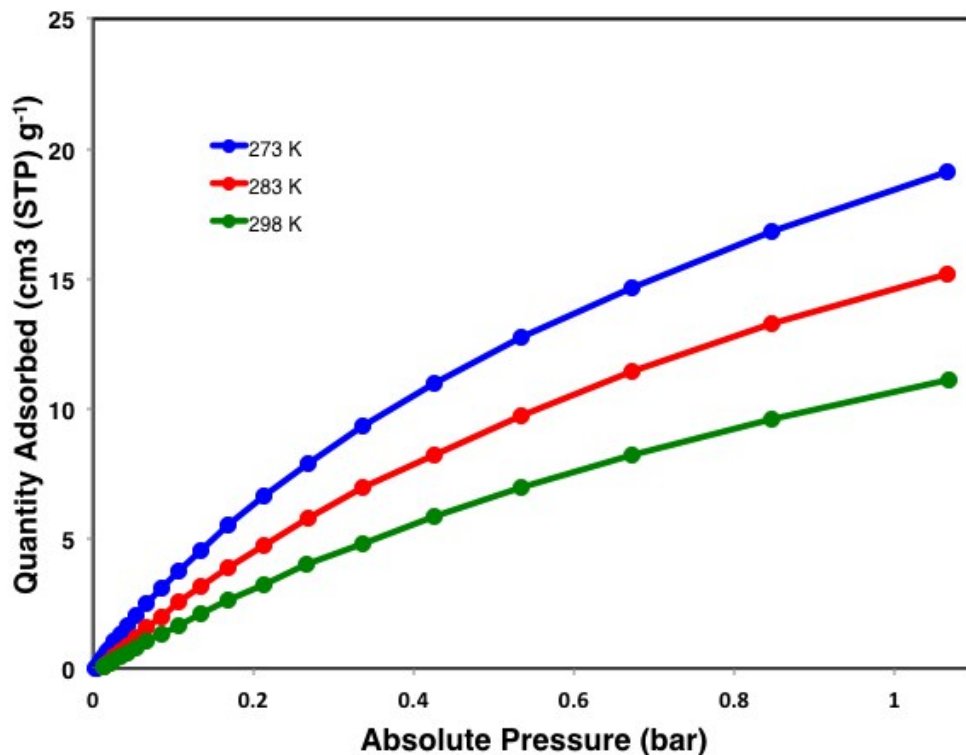
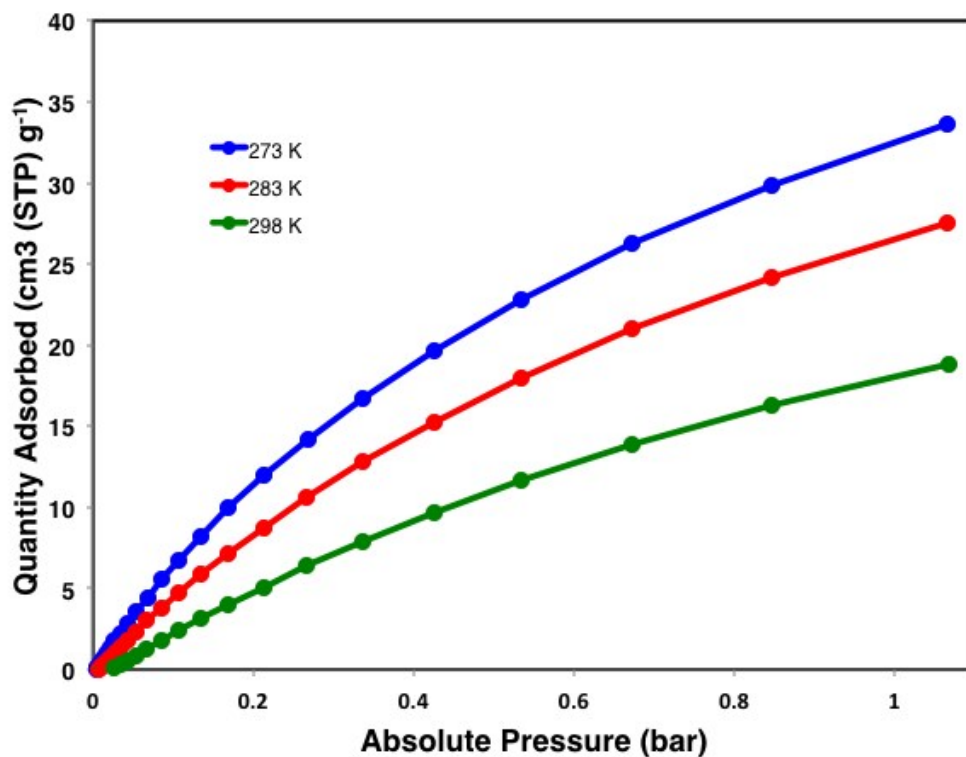


Figure S56. CO₂ Gas adsorption isotherm of **MIL-125-NHhep** at 273 K (blue), 283 K (red), and 298 K (green).



Section S5. Optical Band Gap Spectra

Figure S57. Tauc plot for MIL-125-NH₂. Linear region is indicated.

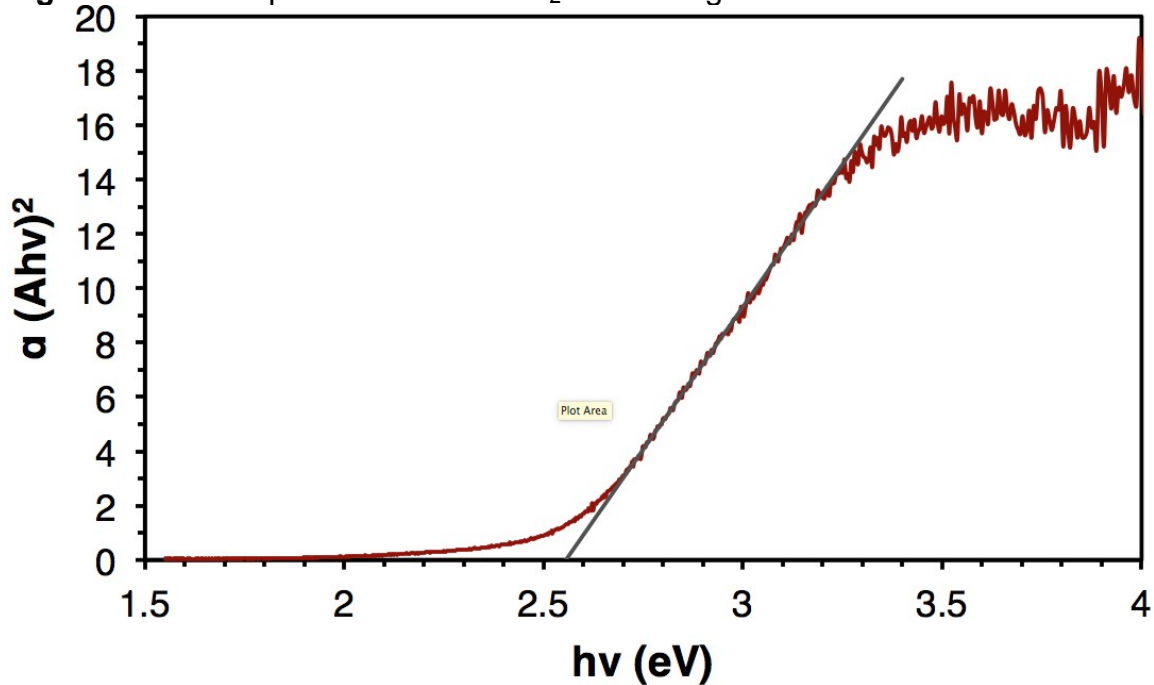


Figure S58. Tauc plot for MIL-125-NHMe. Linear region is indicated.

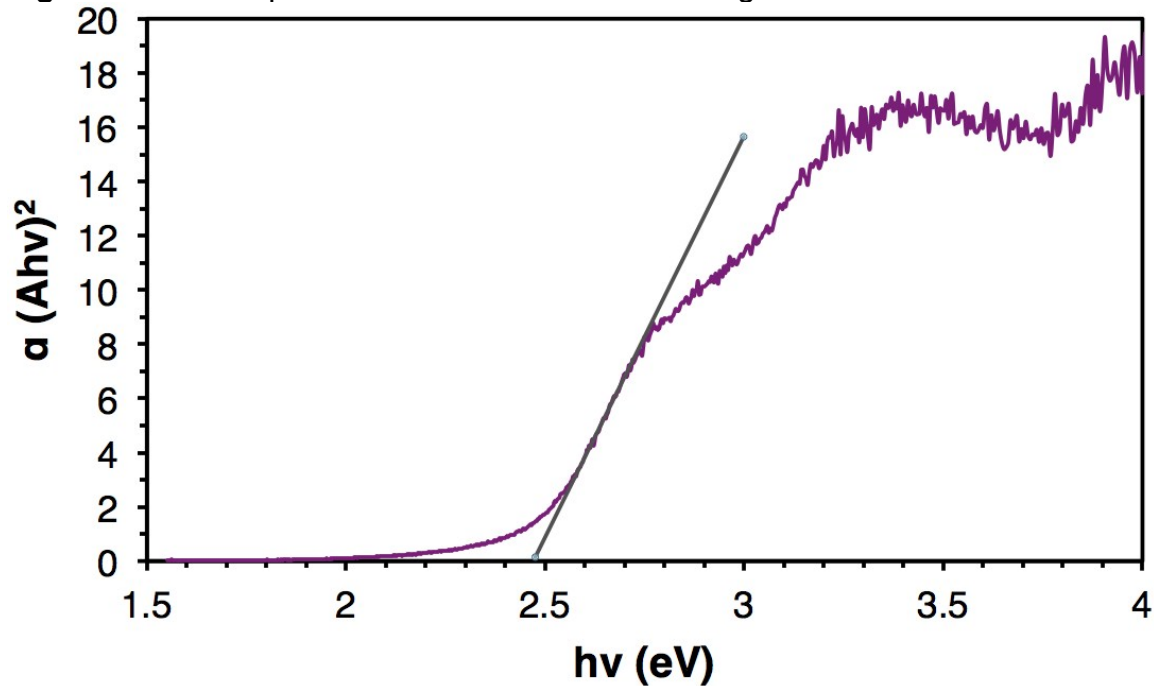


Figure S59. Tauc plot for MIL-125-NHEt. Linear region is indicated.

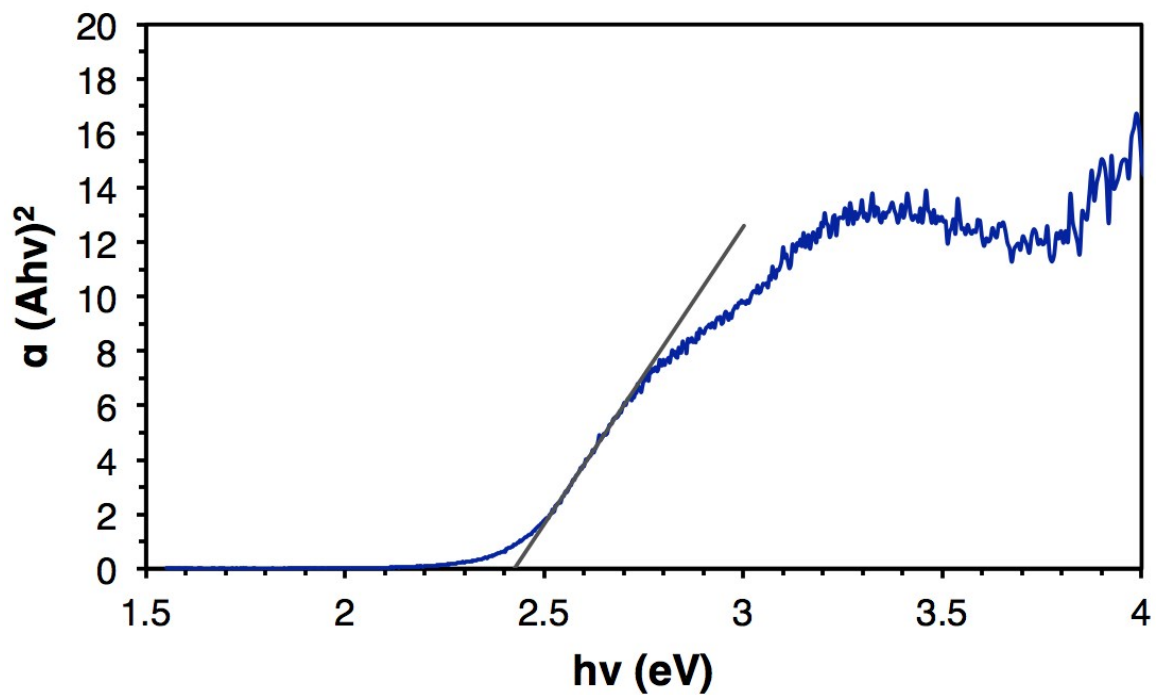


Figure S60. Tauc plot for MIL-125-NH/Pr. Linear region is indicated.

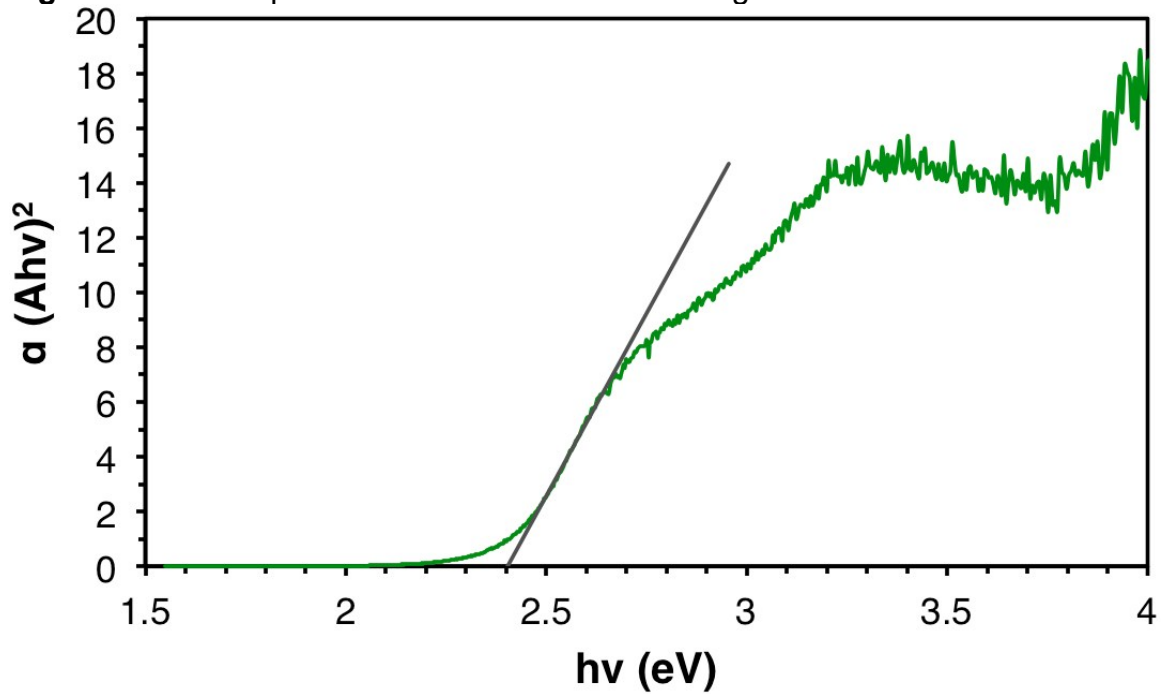


Figure S61. Tauc plot for MIL-125-NHBu. Linear region is indicated.

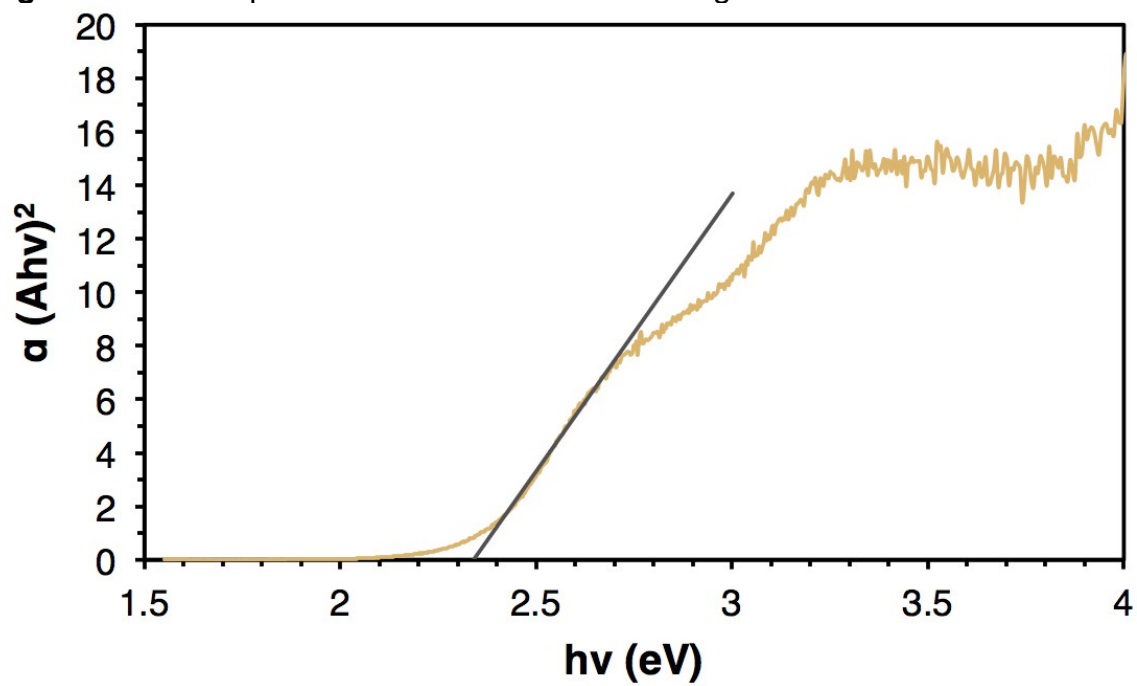


Figure S62. Tauc plot for MIL-125-NHCyp. Linear region is indicated.

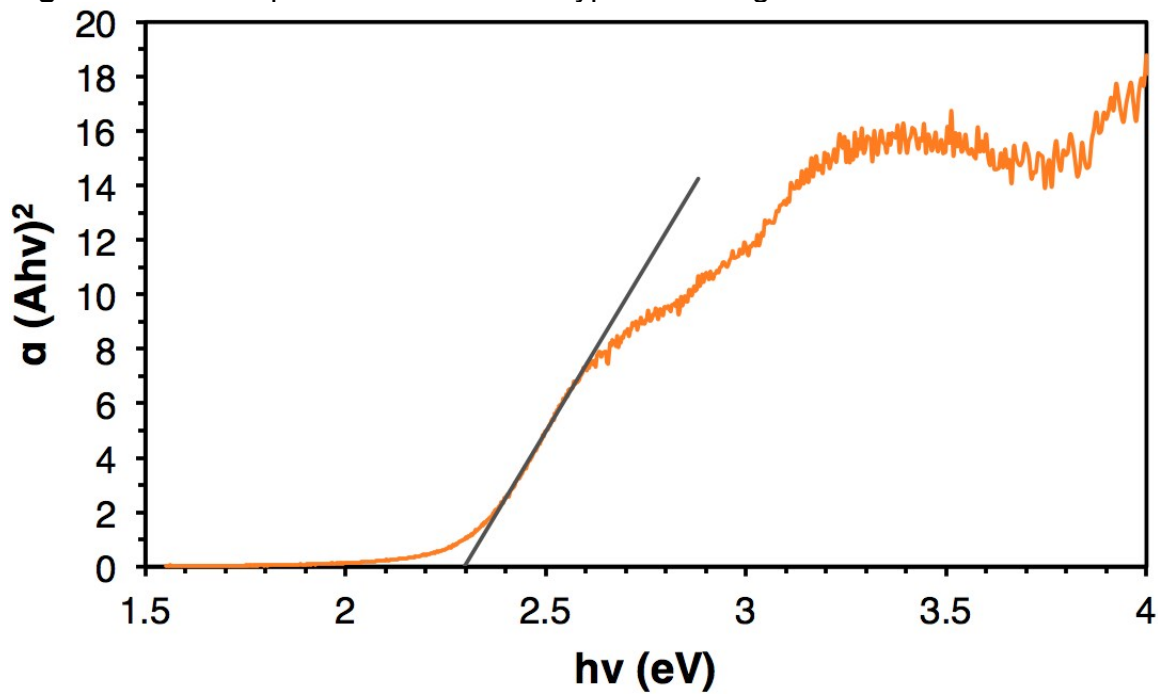


Figure S63. Tauc plot for MIL-125-NHCy. Linear region is indicated.

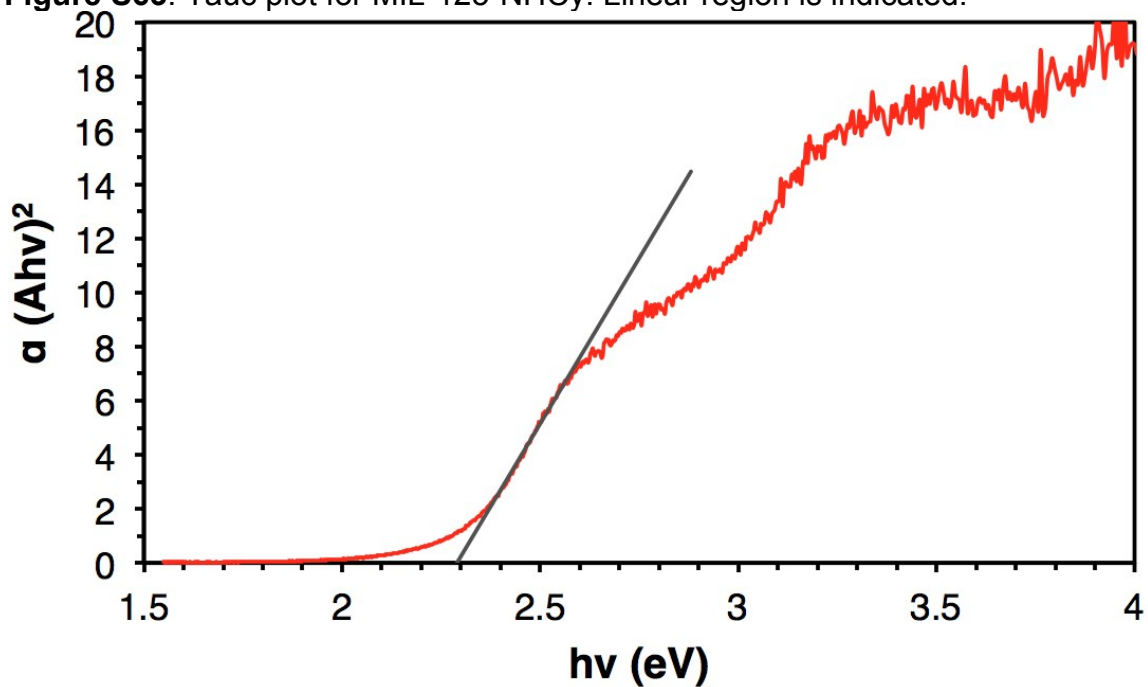


Figure S64. Tauc plot for MIL-125-NHhep. Linear region is indicated.

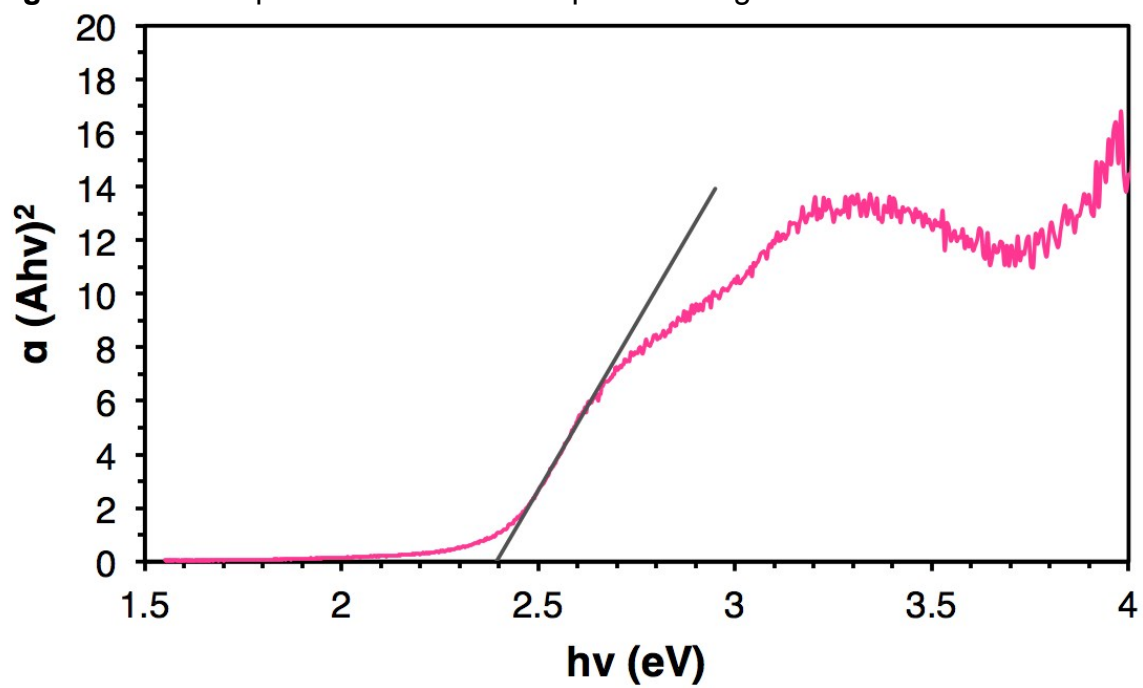


Table S6. Optical bandgap of the prepared MOFs.

MIL-125-NHR	E_g (eV)	Std. Dev. (eV)
-NH ₂	2.56	0.02
-NHMe	2.46	0.03
-NEt	2.42	0.02
-NH ⁱ Pr	2.40	0.03
-NHBu	2.35	0.04
-NHCyp	2.30	0.02
-NHCy	2.29	0.02
-NHhep	2.39	0.02

Section S6. Transient absorption spectra

Figure S65. Transient absorption spectra for a) MIL-125-NH₂, suspended in MeCN ($\lambda_{\text{ex}} = 405 \text{ nm}$).

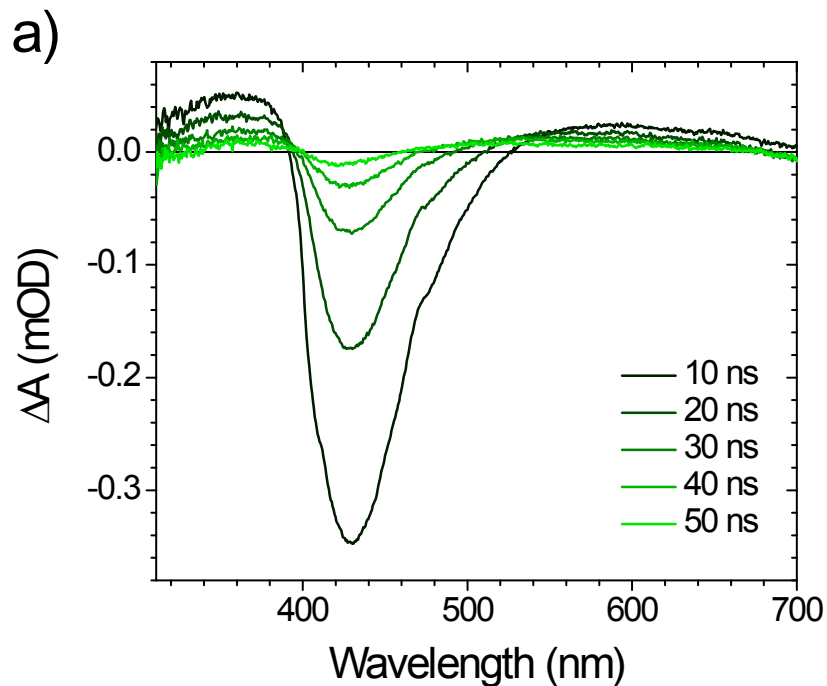


Figure S66. Transient absorption spectra for b) MIL-125-NHMe, suspended in MeCN ($\lambda_{\text{ex}} = 405 \text{ nm}$).

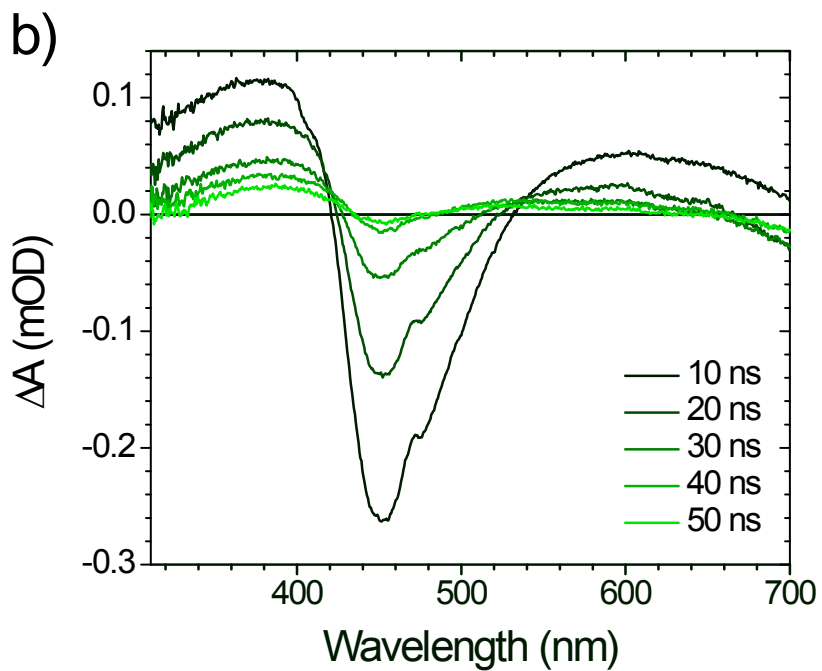


Figure S67. Transient absorption spectra for c) MIL-125-NHEt, suspended in MeCN ($\lambda_{\text{ex}} = 405 \text{ nm}$).

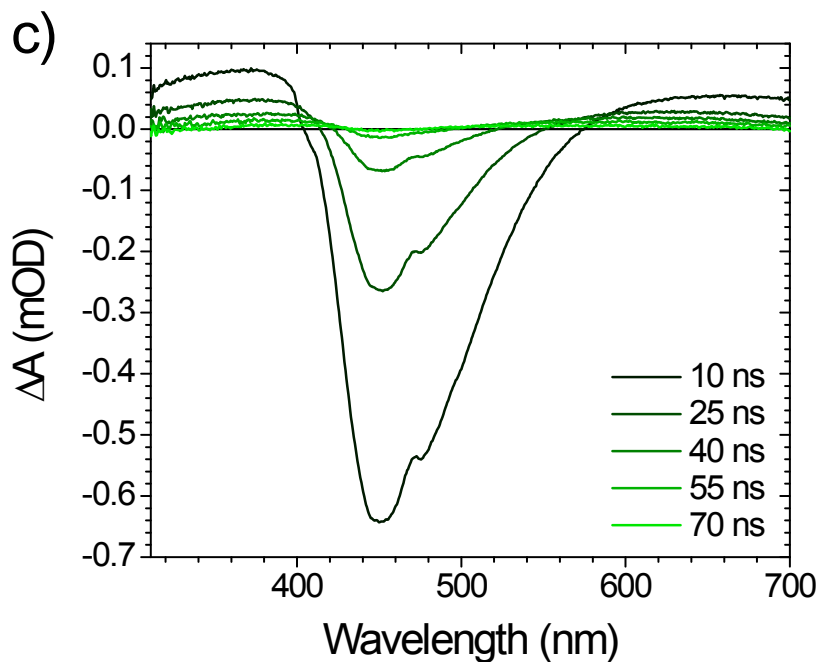


Figure S68. Transient absorption spectra for d) MIL-125-NHBu suspended in MeCN ($\lambda_{\text{ex}} = 405 \text{ nm}$).

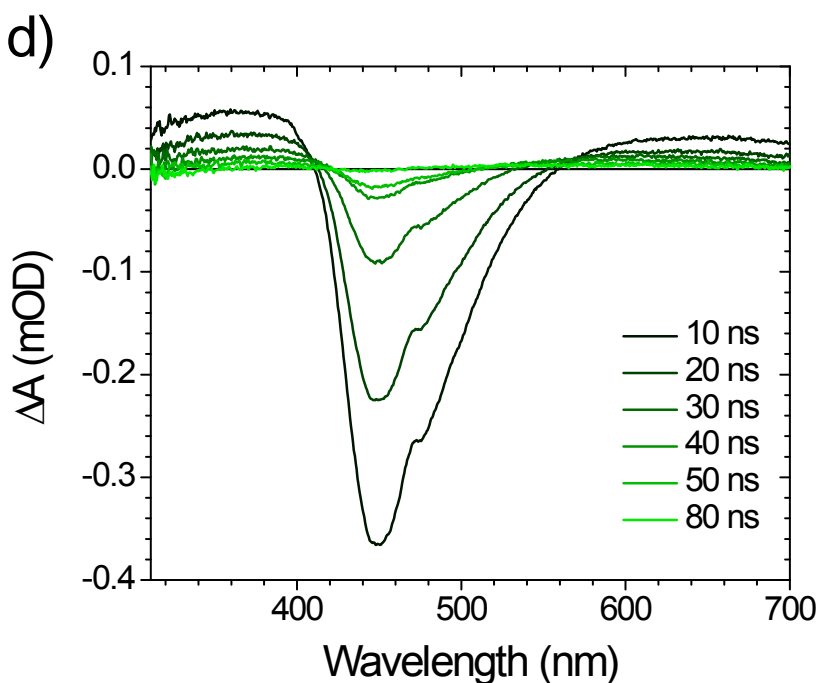


Figure S69. Transient absorption spectra for e) MIL-125-NHⁱPr suspended in MeCN ($\lambda_{\text{ex}} = 405 \text{ nm}$).

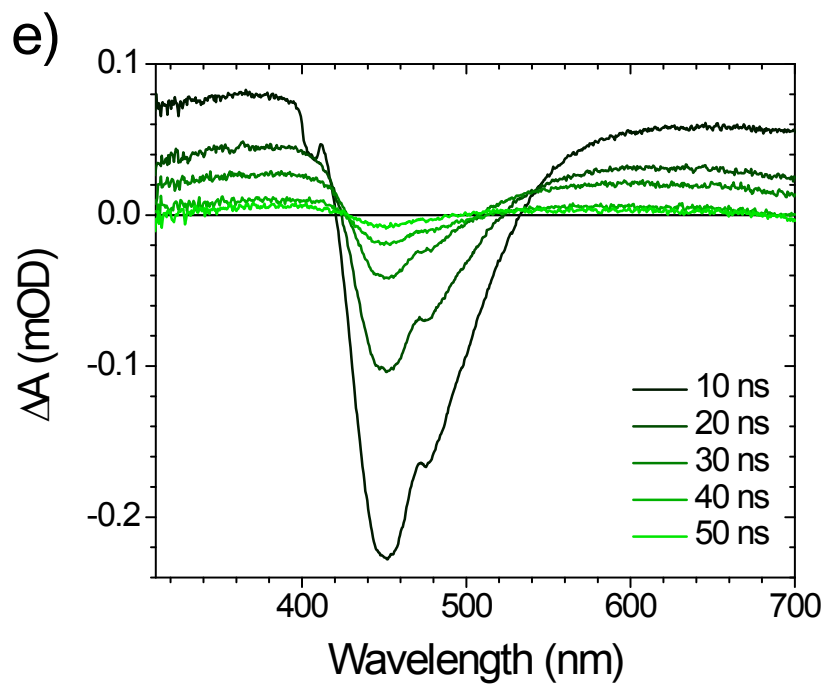


Table S7. Lifetime constant from time-resolved absorption spectra of the prepared MOFs.

MIL-125-NHR	τ (ns)
-NH ₂	12.77
-NHMe	38.19
-NHEt	60.63
-NH ⁱ Pr	75.11
-NHBu	52.13
-NHCyp	68.88
-NHCy	91.35
-NHhep	69.17

Section S7. Actinometry

Calibration of the LED photoreactor was performed by chemical actinometry through standard photoreduction of $K_3[Fe(C_2O_4)_3]$ to $Fe((C_2O_4)_2)^{2-}$ as described by Parker *et al.*²⁴ After the preparation of a calibration curve of ferrous iron (Figure S51), the photoreduction of $K_3[Fe(C_2O_4)_3]$ is irradiated over 360 seconds. The absorbance at 510 nm as converted to concentration of ferrous iron using the calibration curve. The radiation dose of a photoreactor using blue LED can be obtained by using the recommended quantum efficiency of 0.925 in the following equation:

$$\Phi_{\lambda} = \frac{R^{in}}{R_{o,\lambda}} \quad \text{eq. (2)}$$

Where Φ_{λ} is the photochemical quantum yield, R^{in} is the initial rate of the photochemical reaction, and $R_{o,\lambda}$ is the incident volumetric photon flux.

The obtained photon flux in the photoreactor is $R_{o,\lambda} = 1.92 \times 10^{-3} \text{ mol (photons) L}^{-1} \text{ h}^{-1}$.

Figure S70. Calibration curve showing the concentration of Fe(II) vs. absorbance at 510 nm. Plotted with linear regression line and R^2 value.

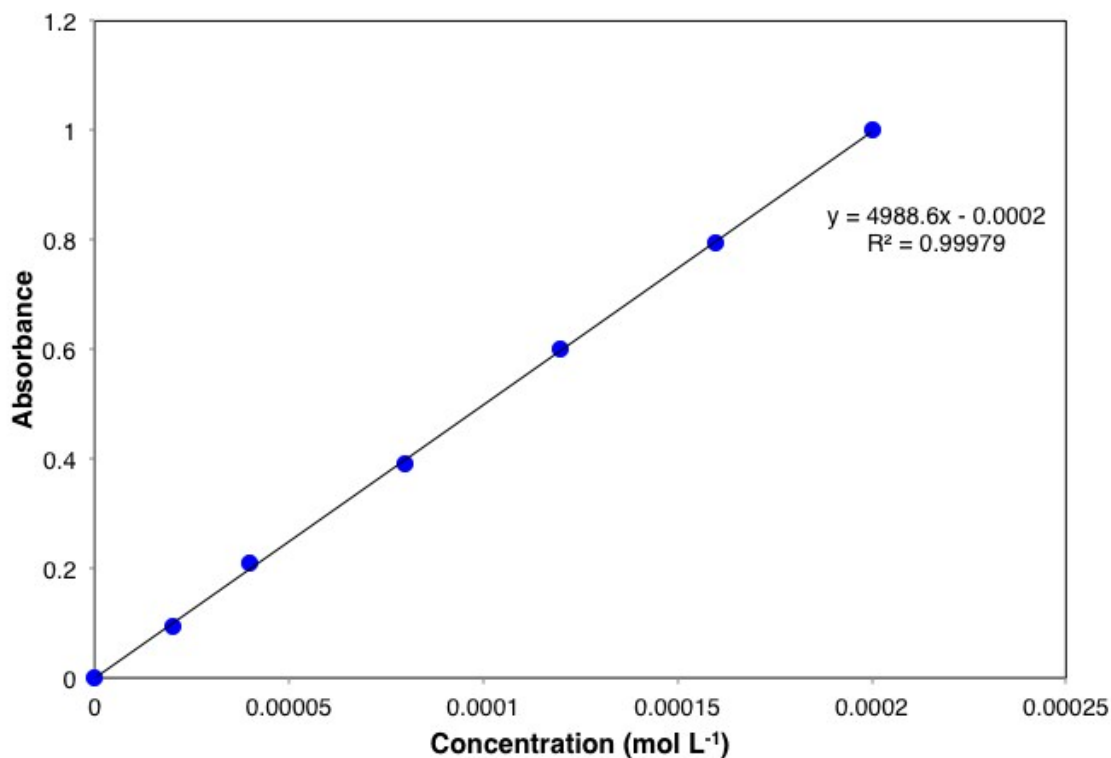


Figure S71. Emission spectrum of blue LED photoreactor.

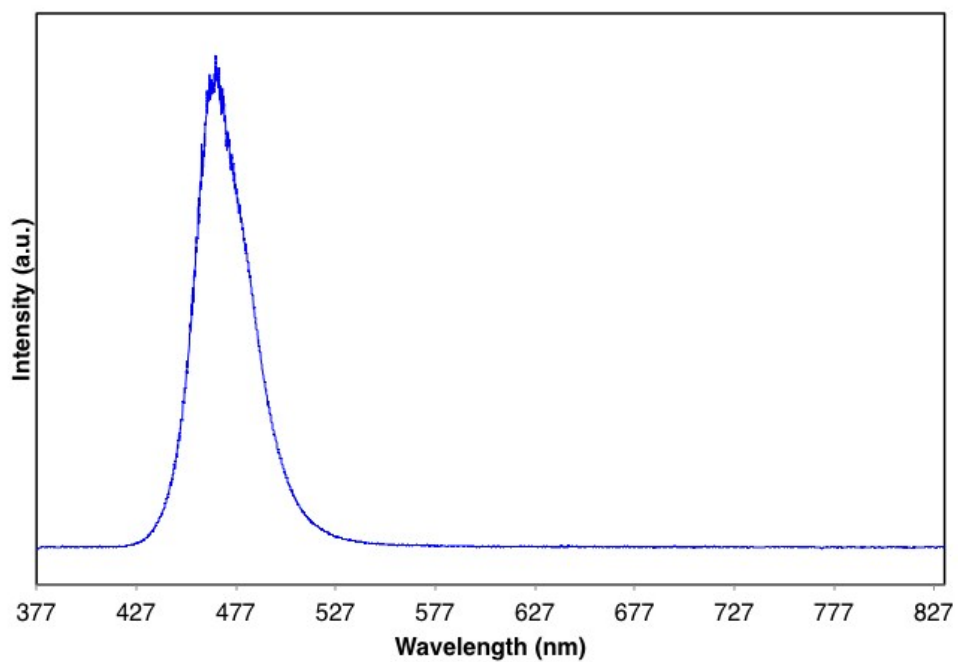
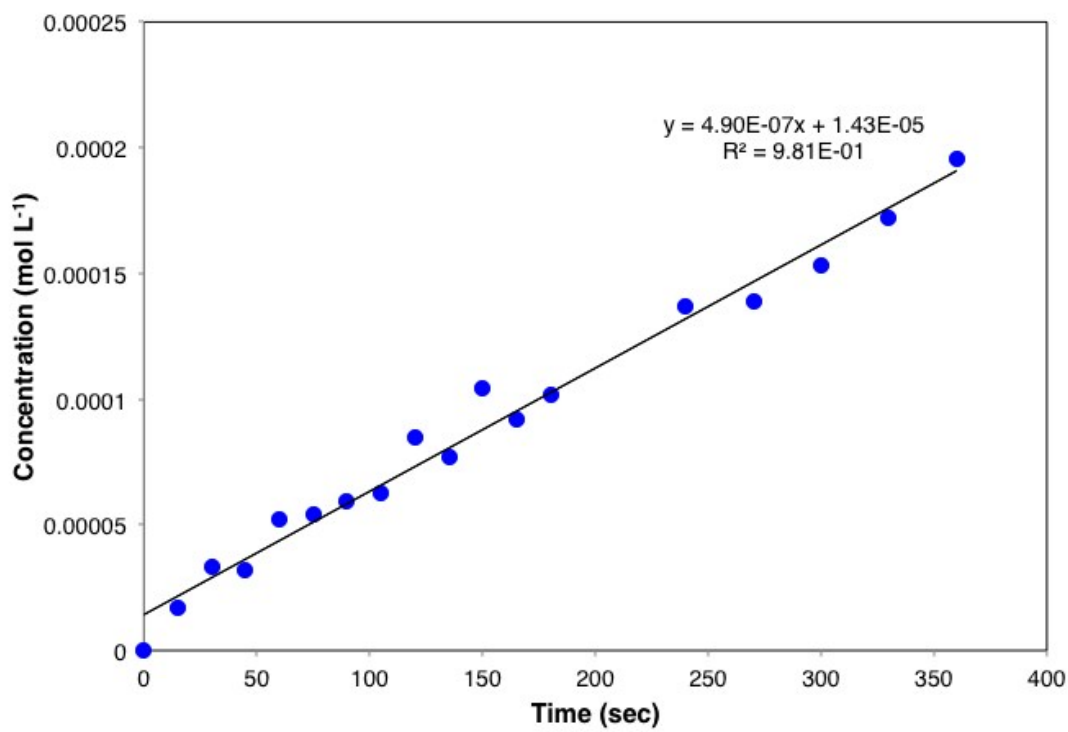


Figure S72. Photoreduction of $K_3[Fe(C_2O_4)_3]$ to $Fe((C_2O_4)_2)^{2-}$ vs. time in blue LED reactor. Plotted with linear regression line and R^2 value.



Section S8. Photocatalysis

Figure S73. ^1H NMR (CDCl_3 , 400 MHz, 25 $^\circ\text{C}$) of HEF and BHEF compared to CO_2 -photoreduced products using MIL-125-NHCy. Signal at 7.26 ppm is residual solvent and its corresponding satellite peaks.

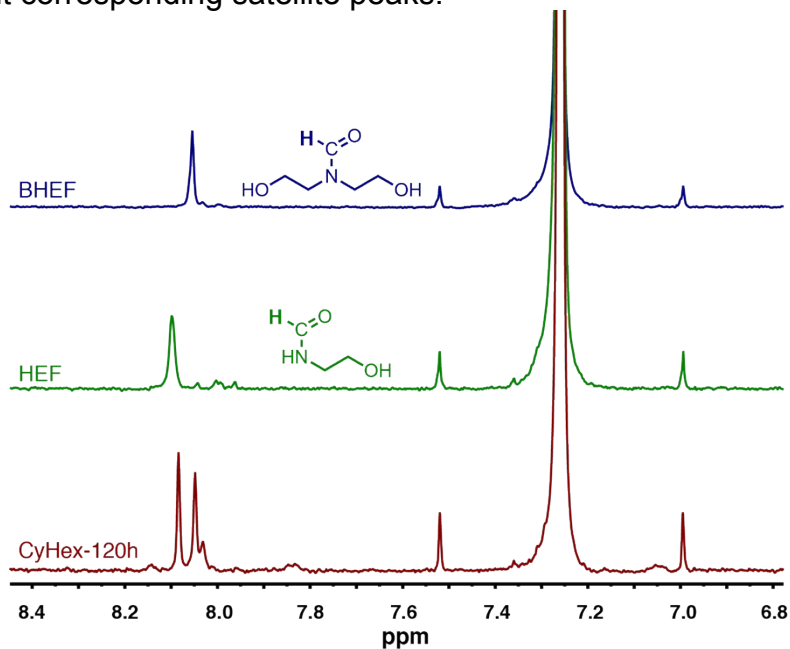


Figure S74. Kinetic plot of CO_2 -photoreduced products using MIL-125- NH_2 .

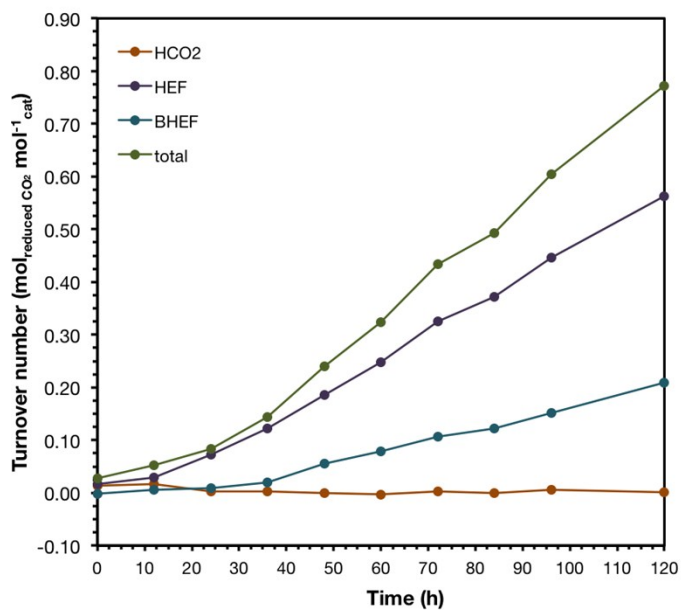


Figure S75. Kinetic plot of CO₂-photoreduced products using MIL-125-NHMe.

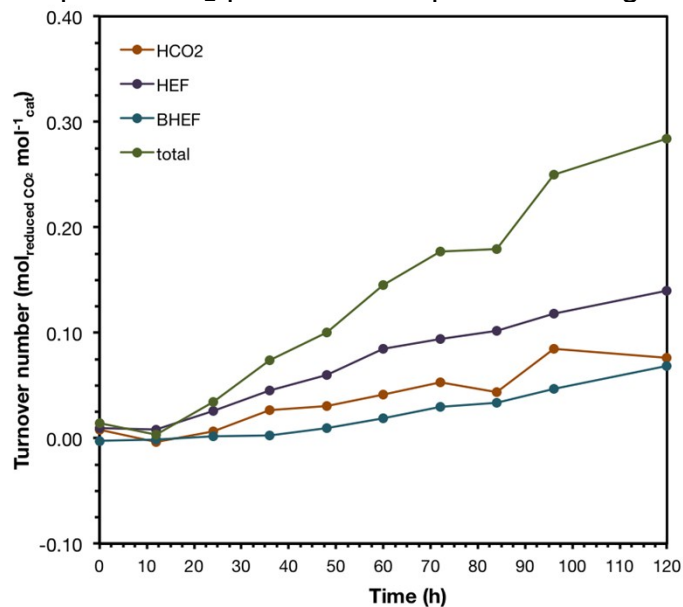


Figure S76. Kinetic plot of CO₂-photoreduced products using MIL-125-NHET.

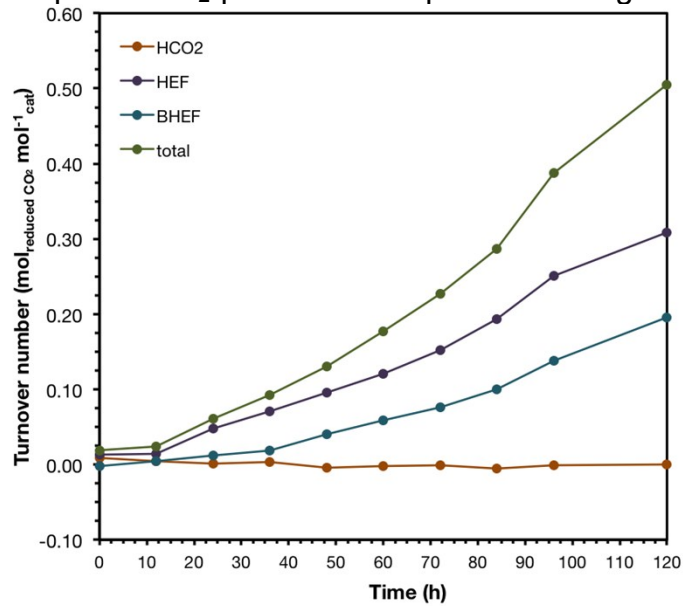


Figure S77. Kinetic plot of CO₂-photoreduced products using MIL-125-NHⁱPr.

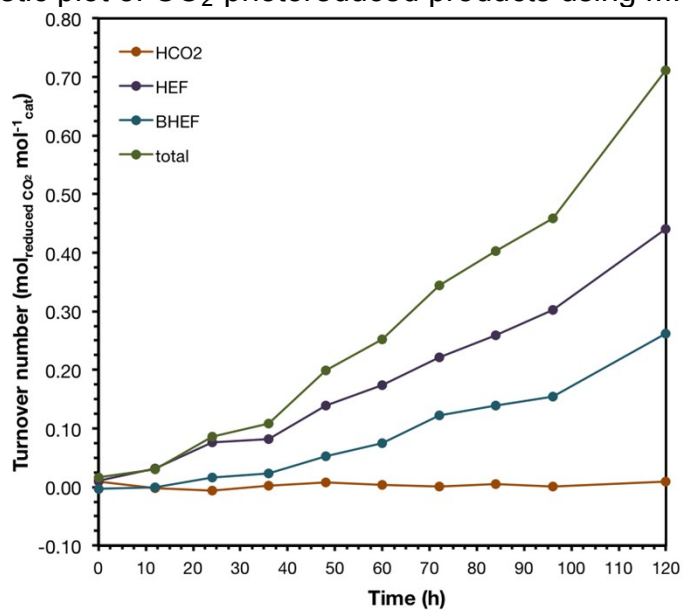


Figure S78. Kinetic plot of CO₂-photoreduced products using MIL-125-NHBu.

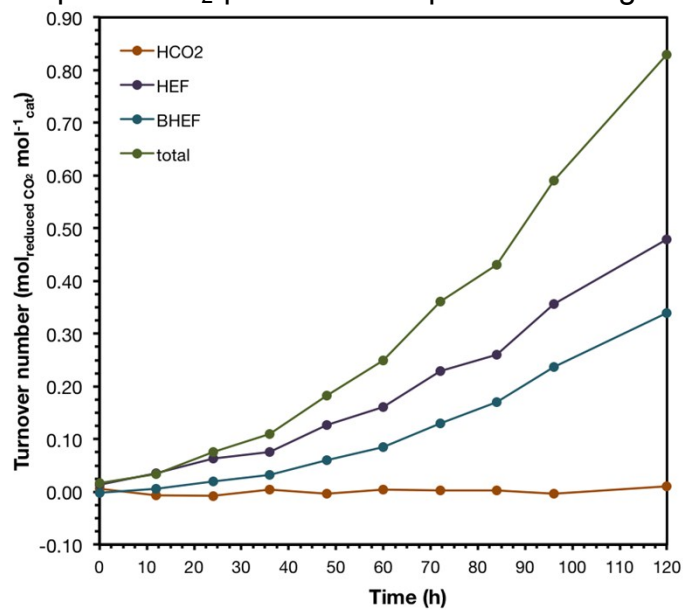


Figure S79. Kinetic plot of CO₂-photoreduced products using MIL-125-NHCyp.

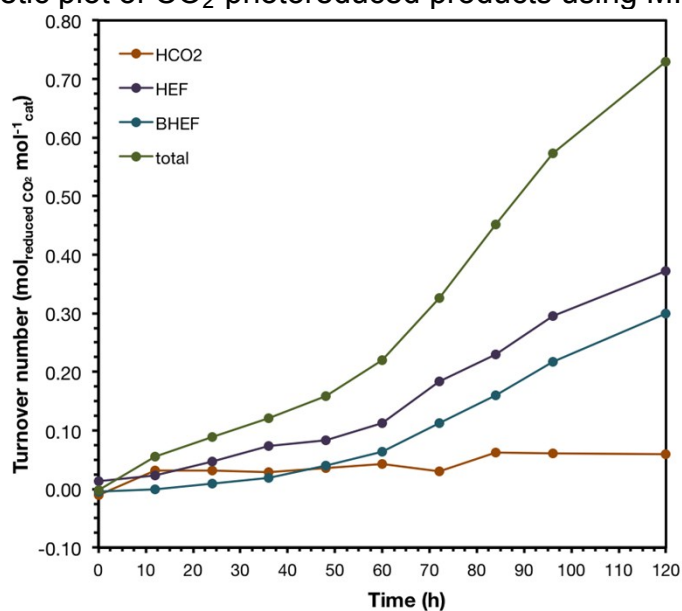


Figure S80. Kinetic plot of CO₂-photoreduced products using MIL-125-NHCy.

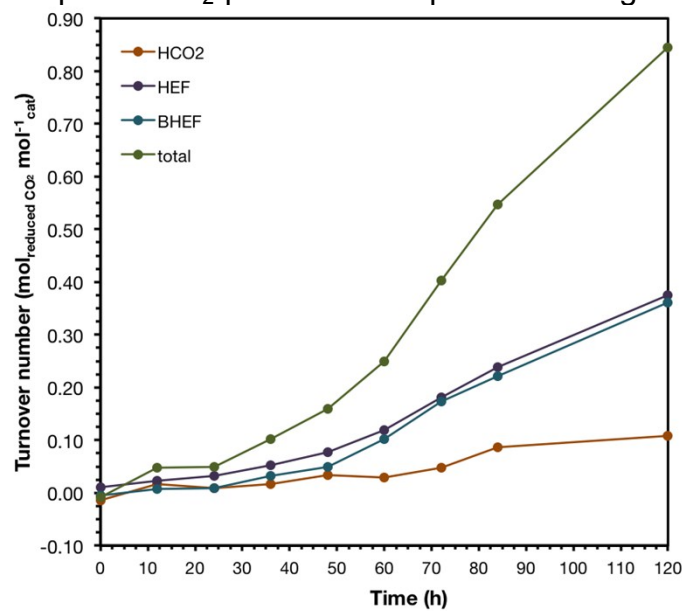


Figure S81. Kinetic plot of CO₂-photoreduced products using MIL-125-NHhep.

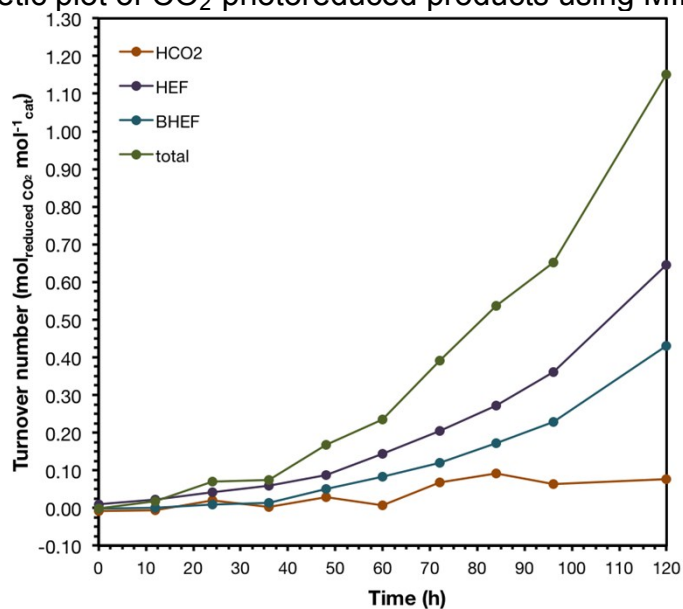


Figure S82. Control experiments at 120 h blue LED exposure showing the concentration in mol L⁻¹, compared to MIL-125-NHhept MOF.

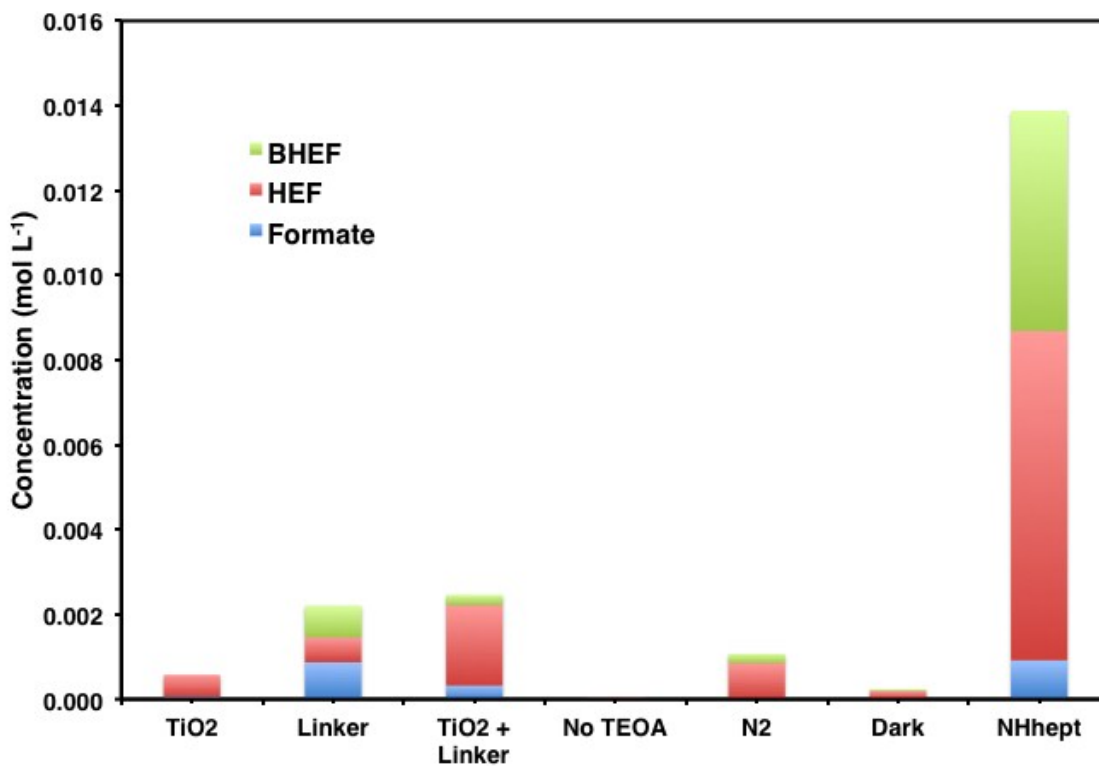


Figure S83. Plot showing the concentration in mol L⁻¹ of CO₂ reduced species from re-utilized MIL-125-NHCyp after an additional 120 h exposure under blue LED compared to the pristine MOF photocatalyst.

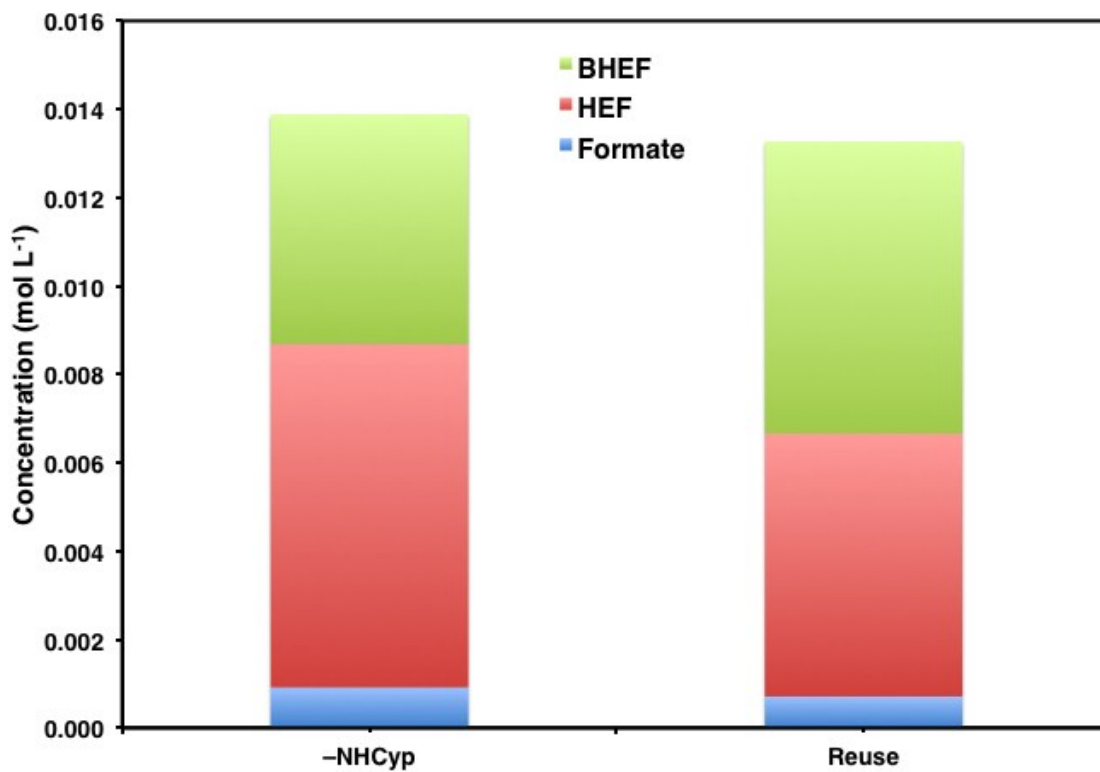


Table S8. Initial rate of reaction and apparent quantum yield. Initial rate of reaction obtained from evaluation at $t = 0$ of the first derivative of the 3rd order polynomial fit. Apparent quantum yield obtained according to eq. (2)

MIL-125-NHR	R^{in} (mol L⁻¹ h⁻¹)	Apparent quantum yield (Φ_{app})
MIL-125-NH ₂	5.97×10^{-6}	0.31%
MIL-125-NHMe	7.52×10^{-6}	0.39%
MIL-125-NHEt	6.42×10^{-6}	0.33%
MIL-125-NH ⁱ Pr	3.00×10^{-5}	1.56%
MIL-125-NHBu	5.71×10^{-6}	0.30%
MIL-125-NHCyp	3.41×10^{-5}	1.78%
MIL-125-NHCy	2.95×10^{-5}	1.54%
MIL-125-NHhep	1.33×10^{-5}	0.69%

Section S9. NMR Spectra

Figure S84. ^1H NMR spectra (400 MHz, CDCl_3 , 25 $^\circ\text{C}$) of compound **1a**.

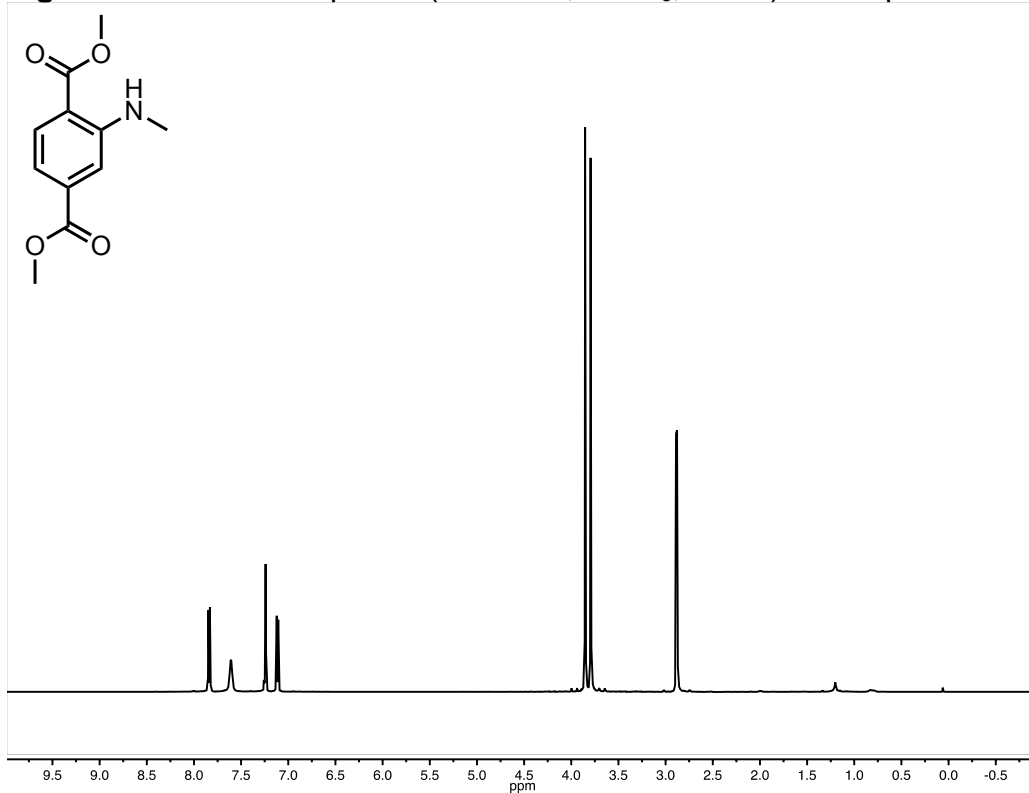


Figure S85. ^{13}C NMR spectra (100 MHz, CDCl_3 , 25 $^\circ\text{C}$) of compound **1a**.

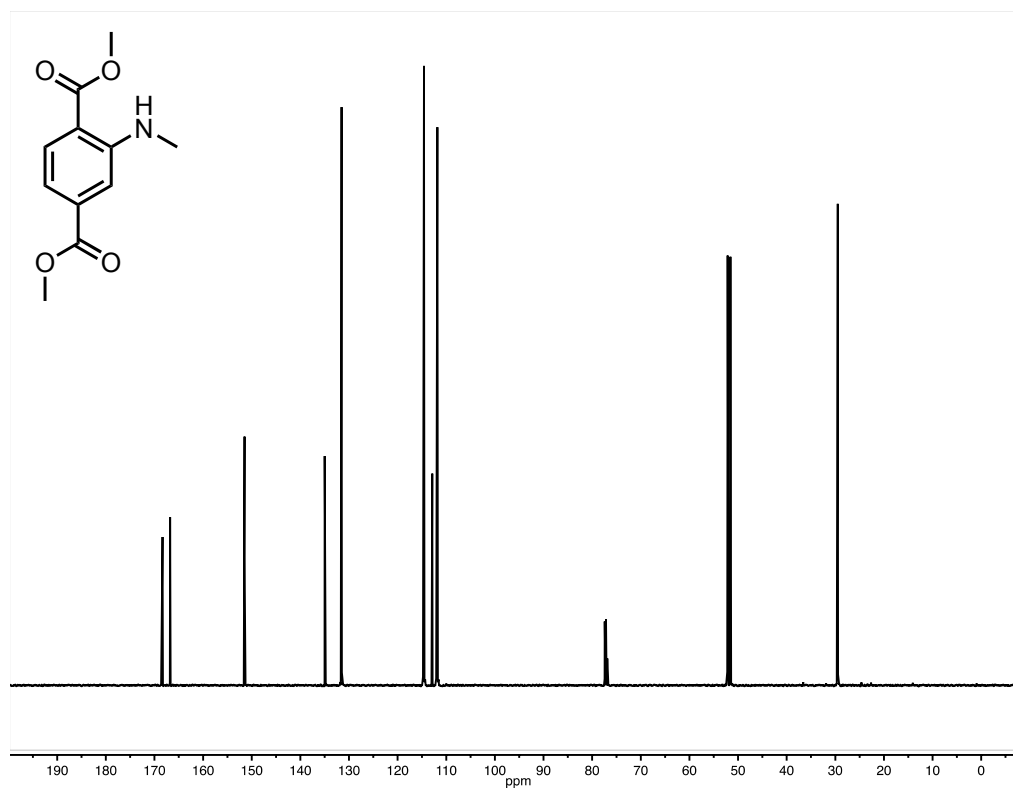


Figure S86. ^1H NMR spectra (400 MHz, CDCl_3 , 25 $^\circ\text{C}$) of compound **1b**.

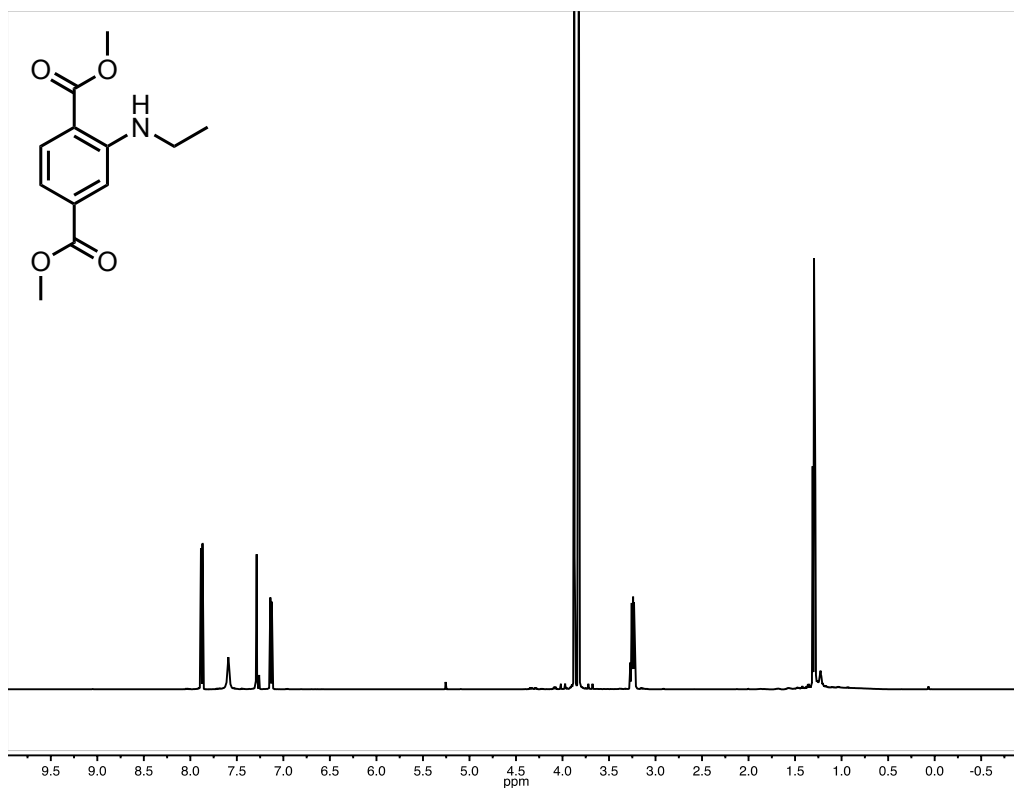


Figure S87. ^{13}C NMR spectra (100 MHz, CDCl_3 , 25 $^\circ\text{C}$) of compound **1b**.

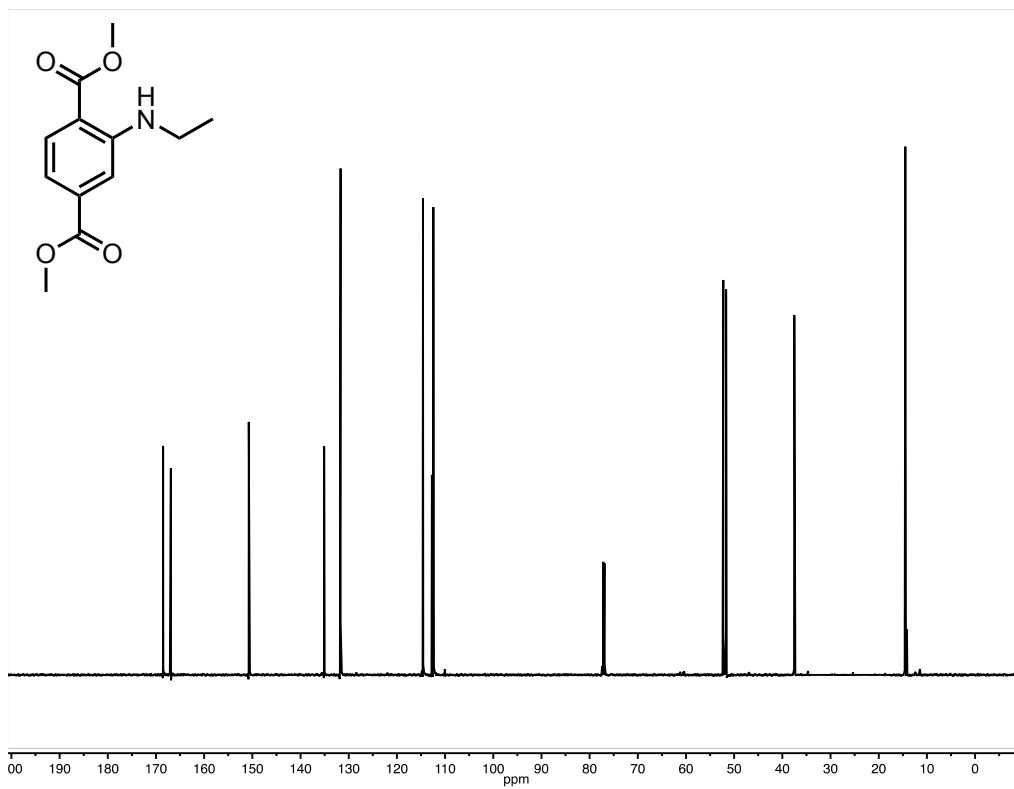


Figure S88. ^1H NMR spectra (400 MHz, CDCl_3 , 25 $^\circ\text{C}$) of compound **1c**.

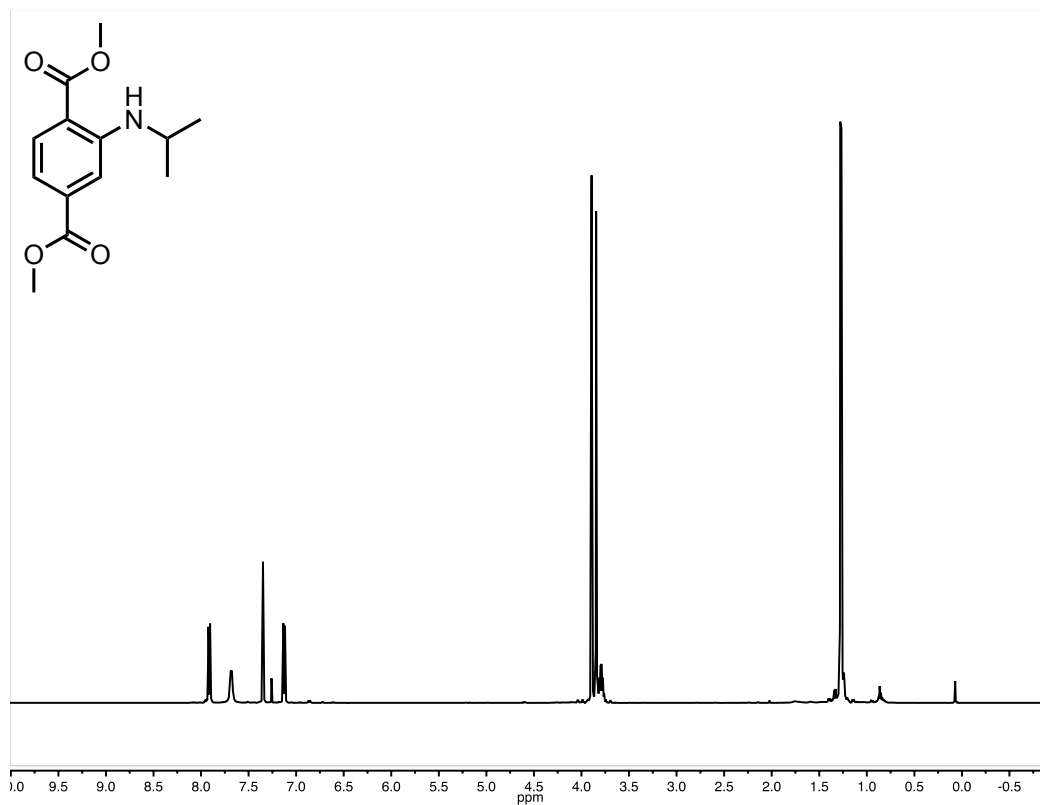


Figure S89. ^{13}C NMR spectra (100 MHz, CDCl_3 , 25 $^\circ\text{C}$) of compound **1c**.

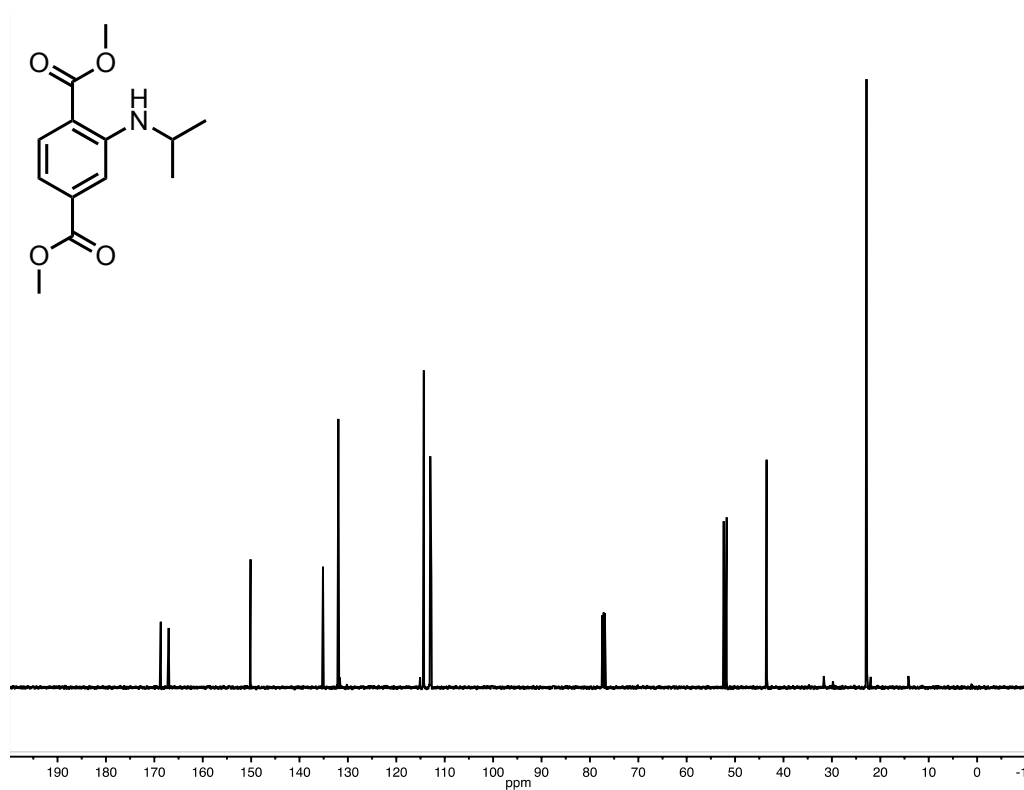


Figure S90. ^1H NMR spectra (400 MHz, CDCl_3 , 25 $^\circ\text{C}$) of compound **1d**.

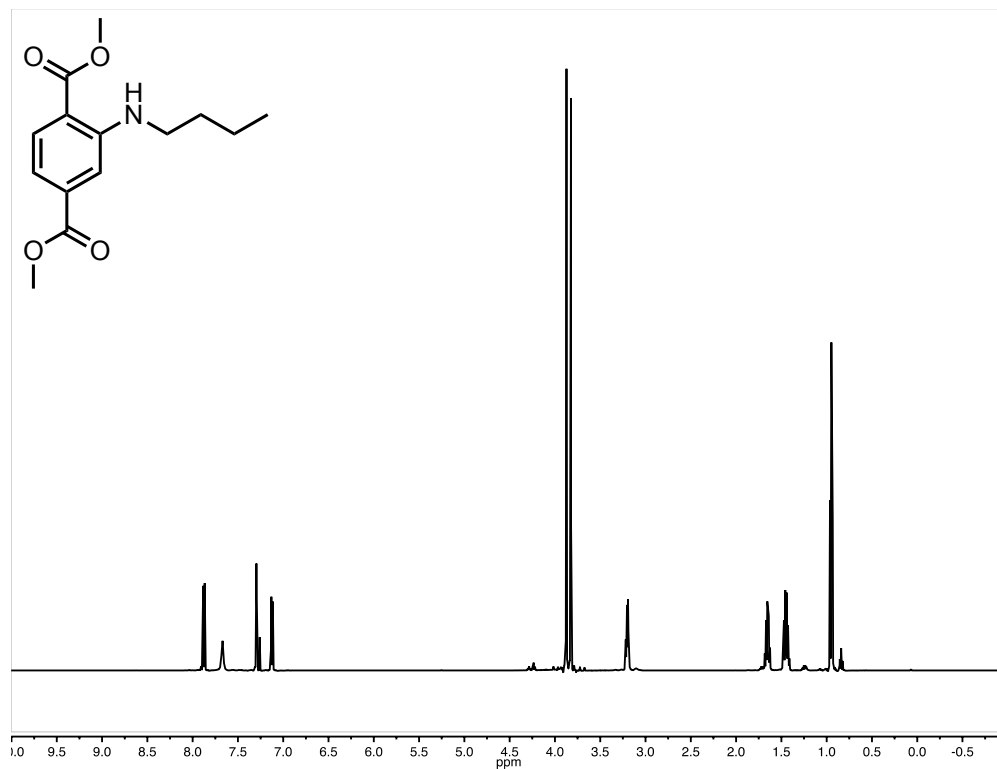


Figure S91. ^{13}C NMR spectra (100 MHz, CDCl_3 , 25 $^\circ\text{C}$) of compound **1d**.

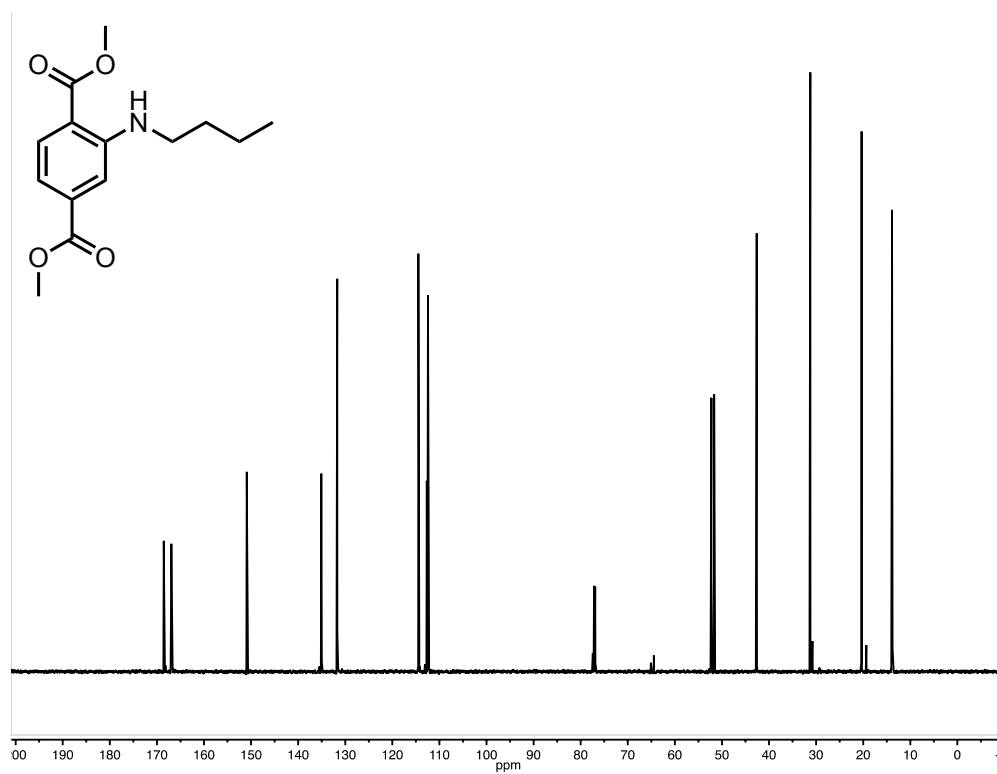


Figure S92. ^1H NMR spectra (400 MHz, CDCl_3 , 25 °C) of compound **1e**.

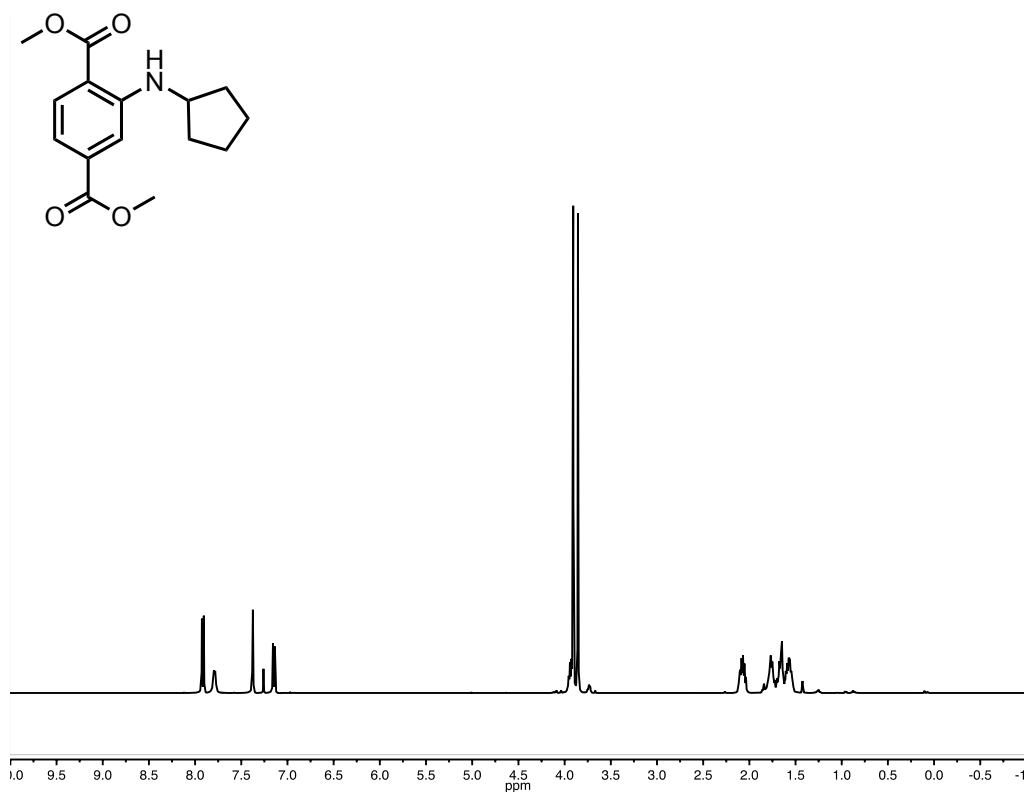


Figure S93. ^{13}C NMR spectra (100 MHz, CDCl_3 , 25 °C) of compound **1e**.

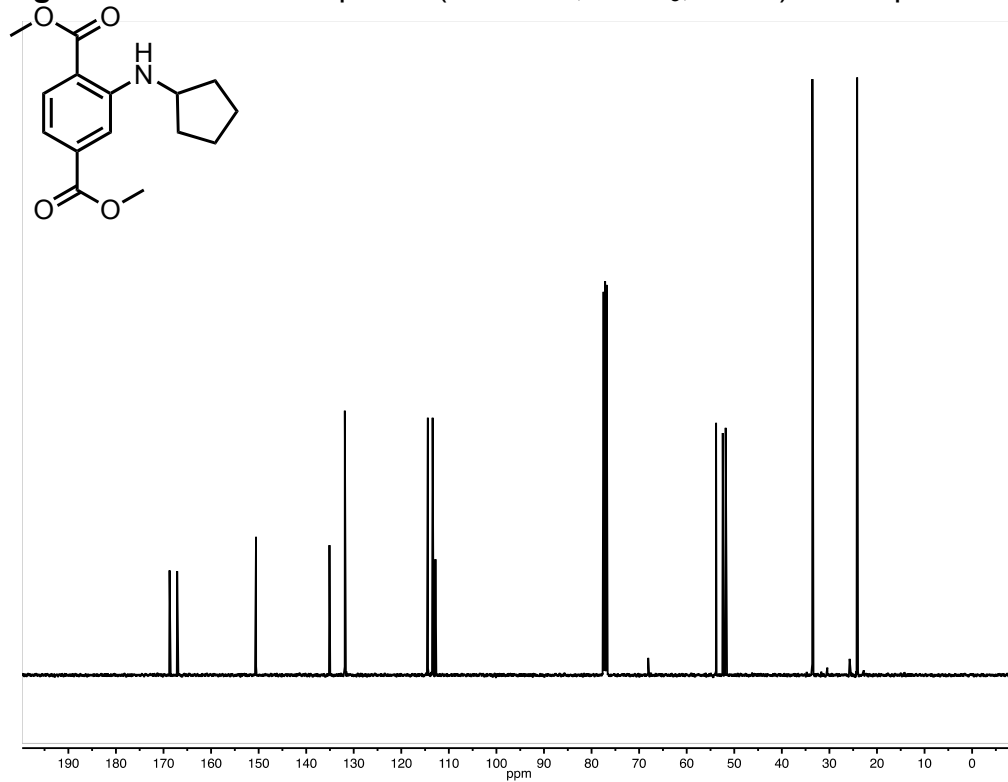


Figure S94. ^1H NMR spectra (400 MHz, CDCl_3 , 25 °C) of compound **1f**.

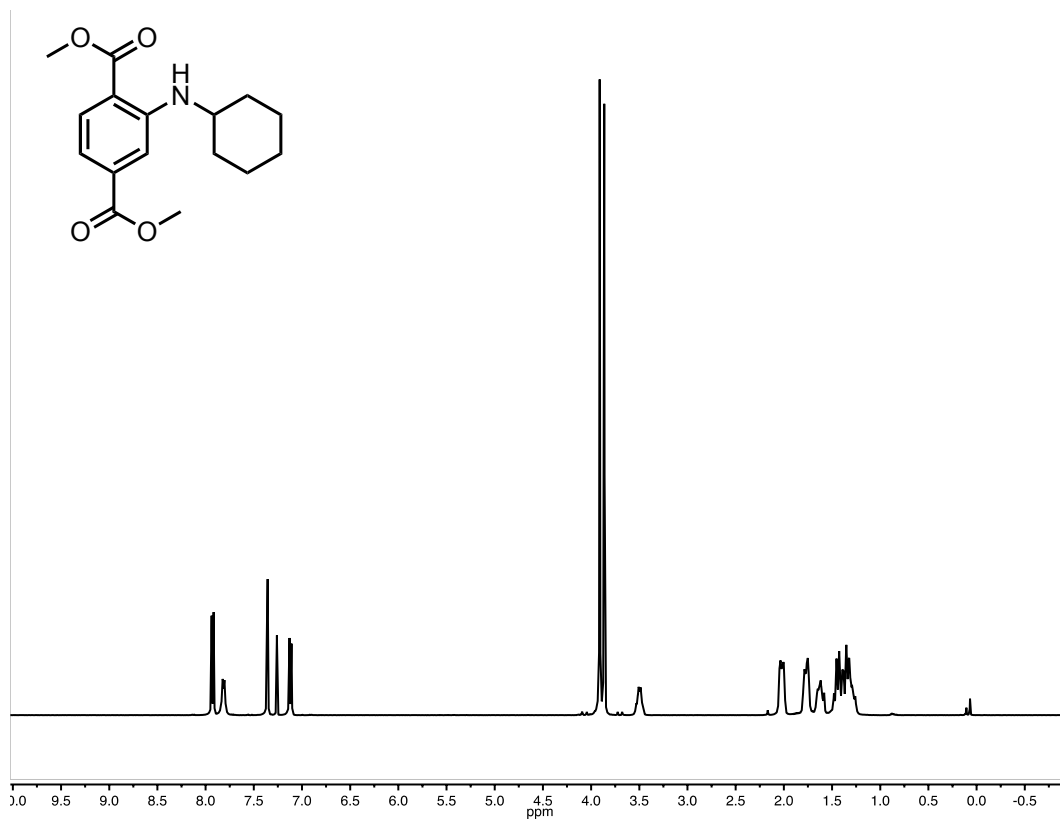


Figure S95. ¹³C NMR spectra (100 MHz, CDCl₃, 25 °C) of compound **1f**.

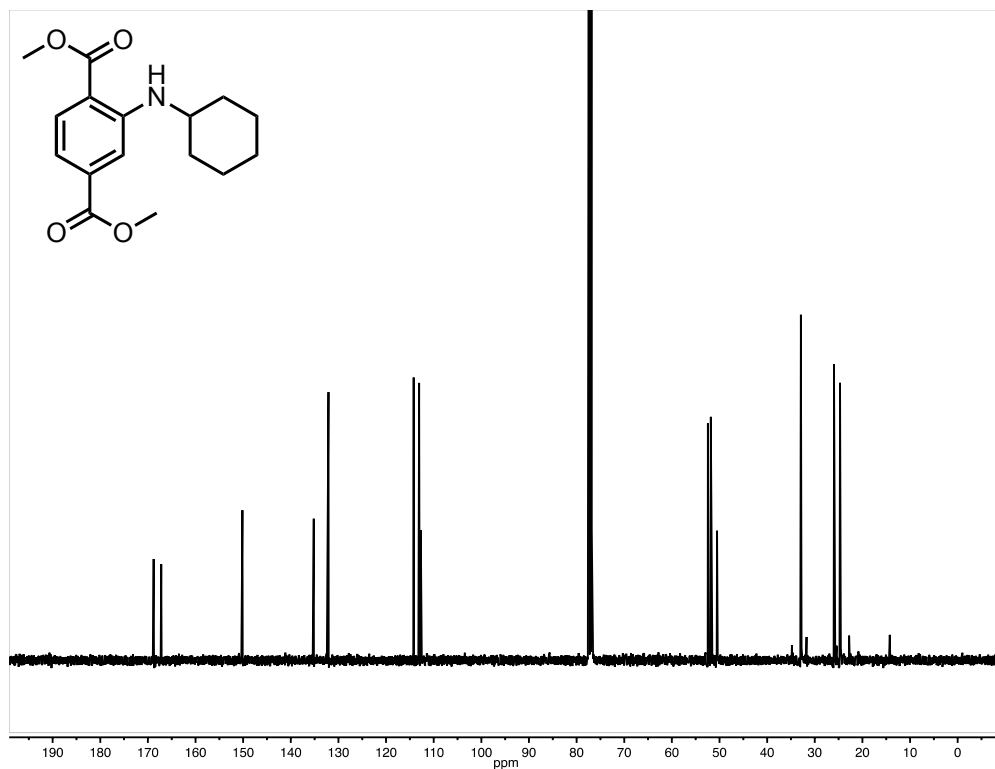


Figure S96. ¹H NMR spectra (400 MHz, CDCl₃, 25 °C) of compound **1g**.

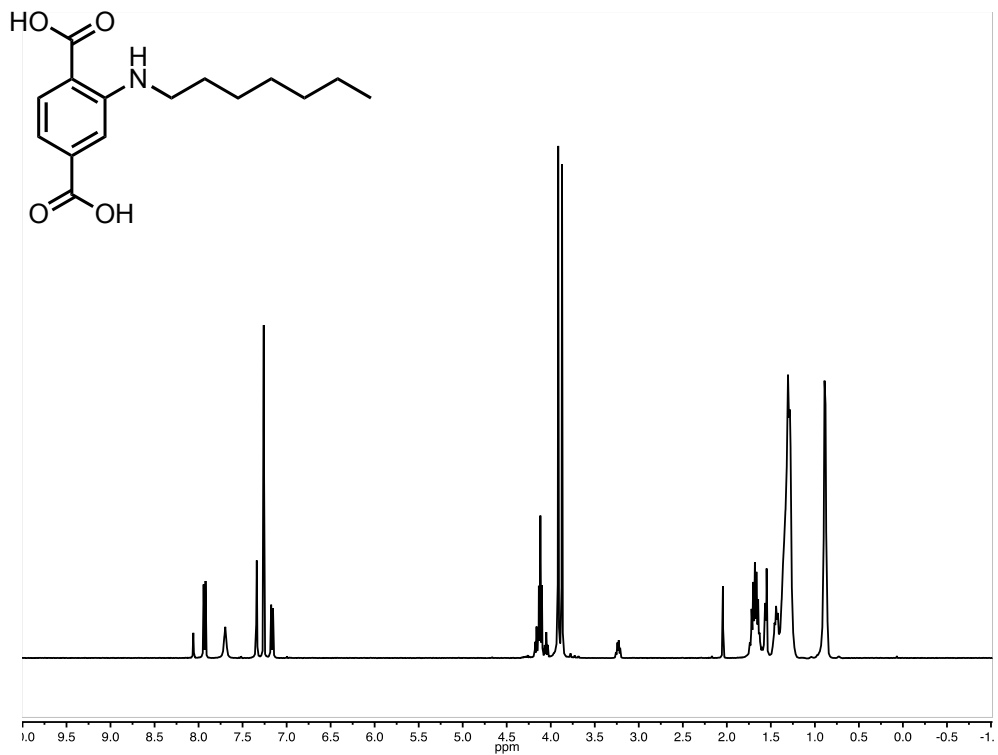


Figure S97. ¹³C NMR spectra (100 MHz, CDCl₃, 25 °C) of compound **1g**.

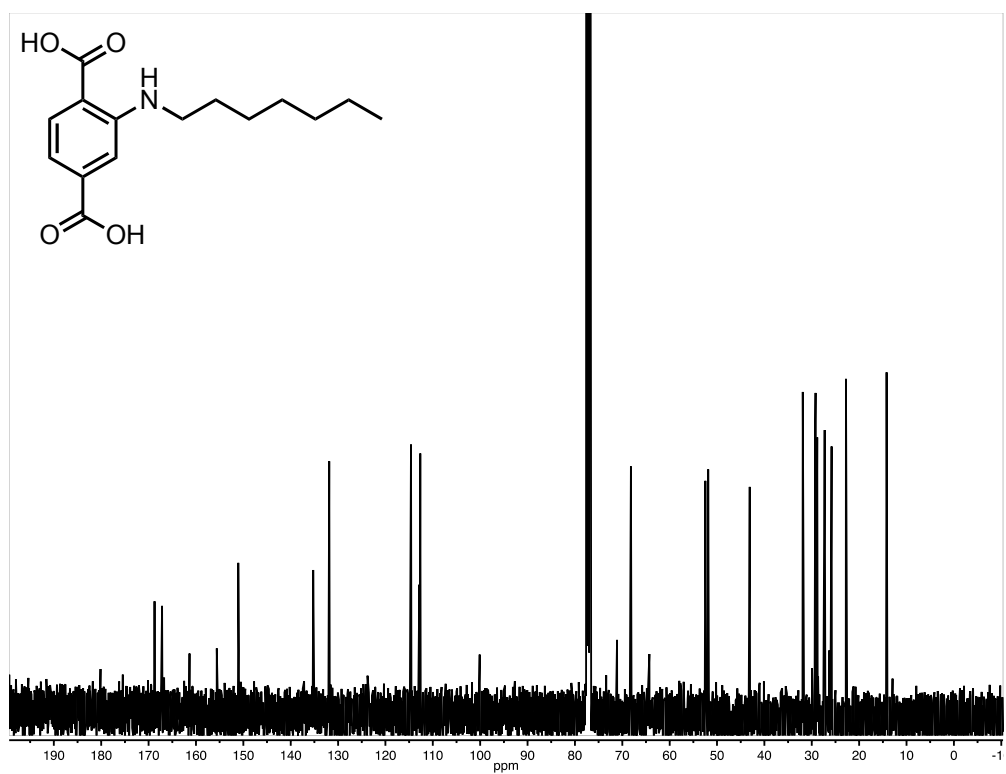


Figure S98. ¹H NMR spectra (400 MHz, DMSO-*d*₆, 25 °C) of compound **2a**.

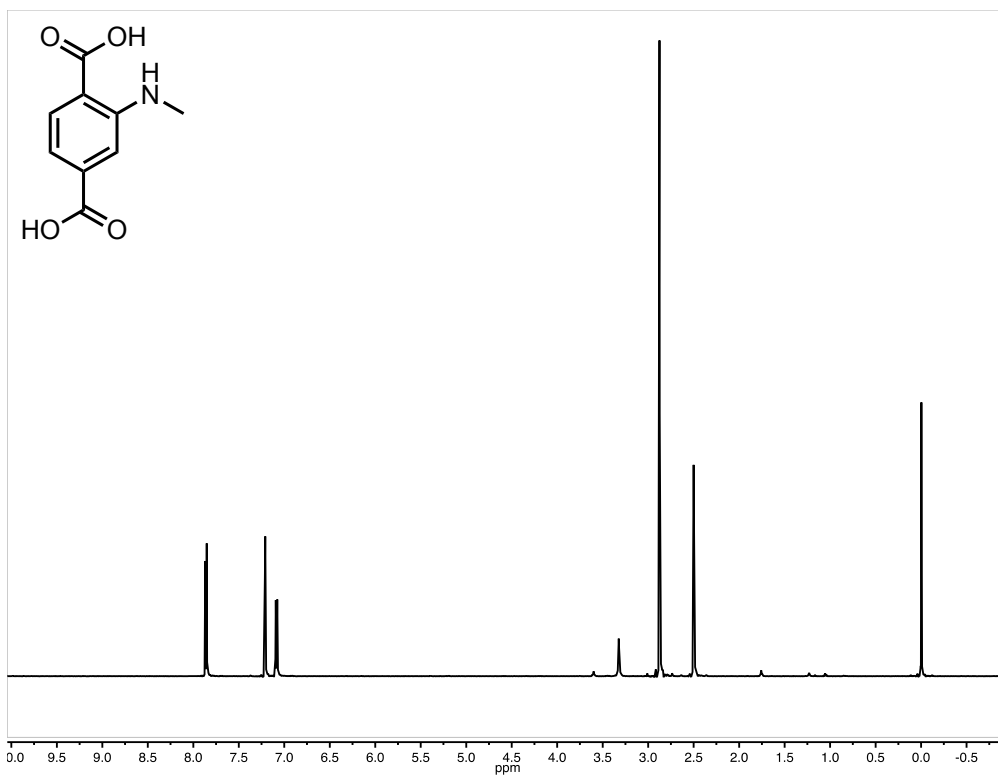


Figure S99. ¹³C NMR spectra (100 MHz, DMSO-*d*₆, 25 °C) of compound **2a**.

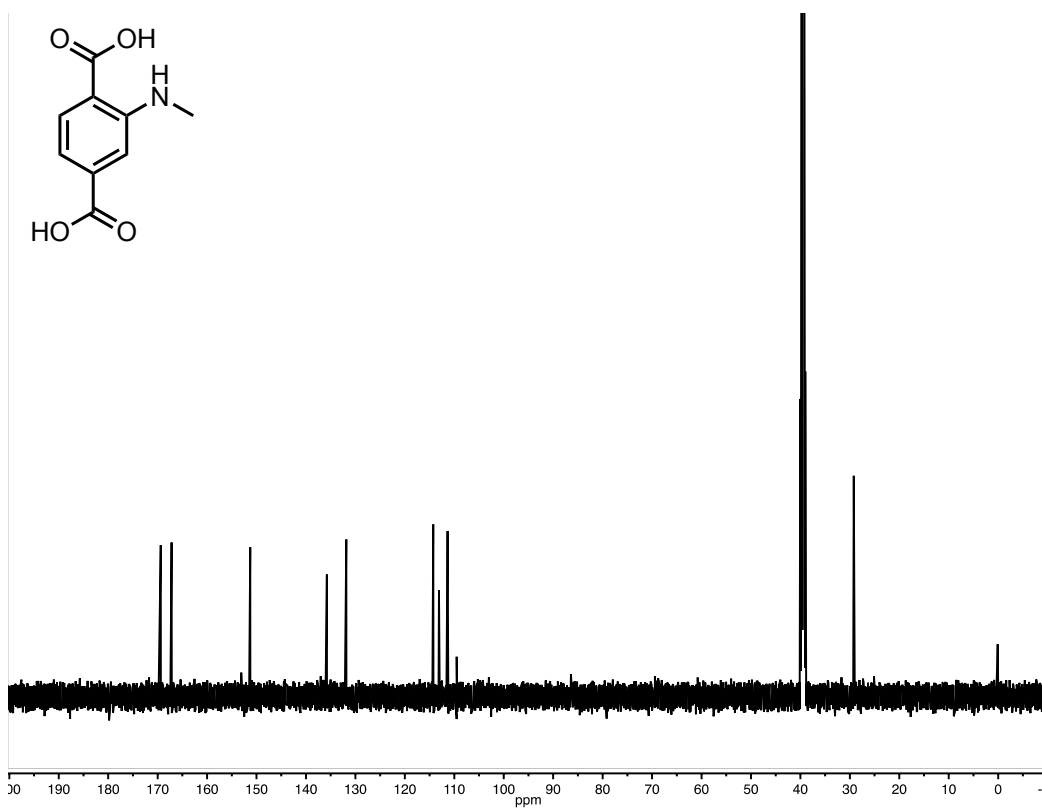


Figure S100. ¹H NMR spectra (400 MHz, DMSO-*d*₆, 25 °C) of compound **2b**.

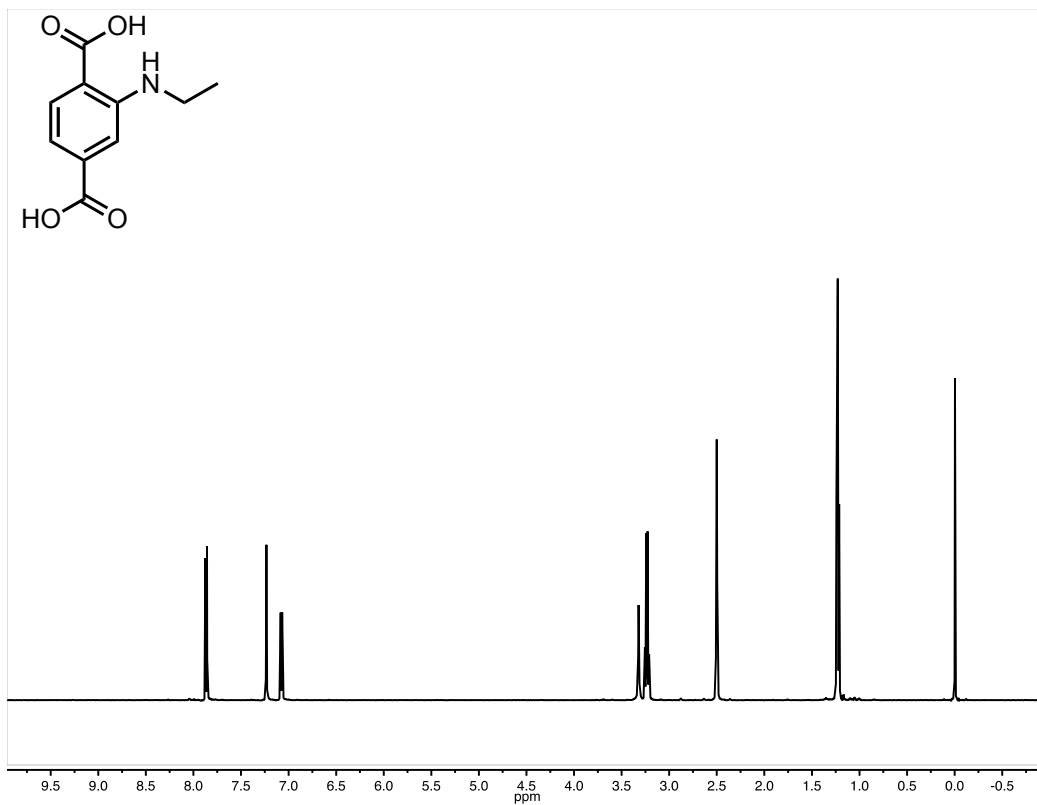


Figure S101. ¹³C NMR spectra (100 MHz, DMSO-*d*₆, 25 °C) of compound **2b**.

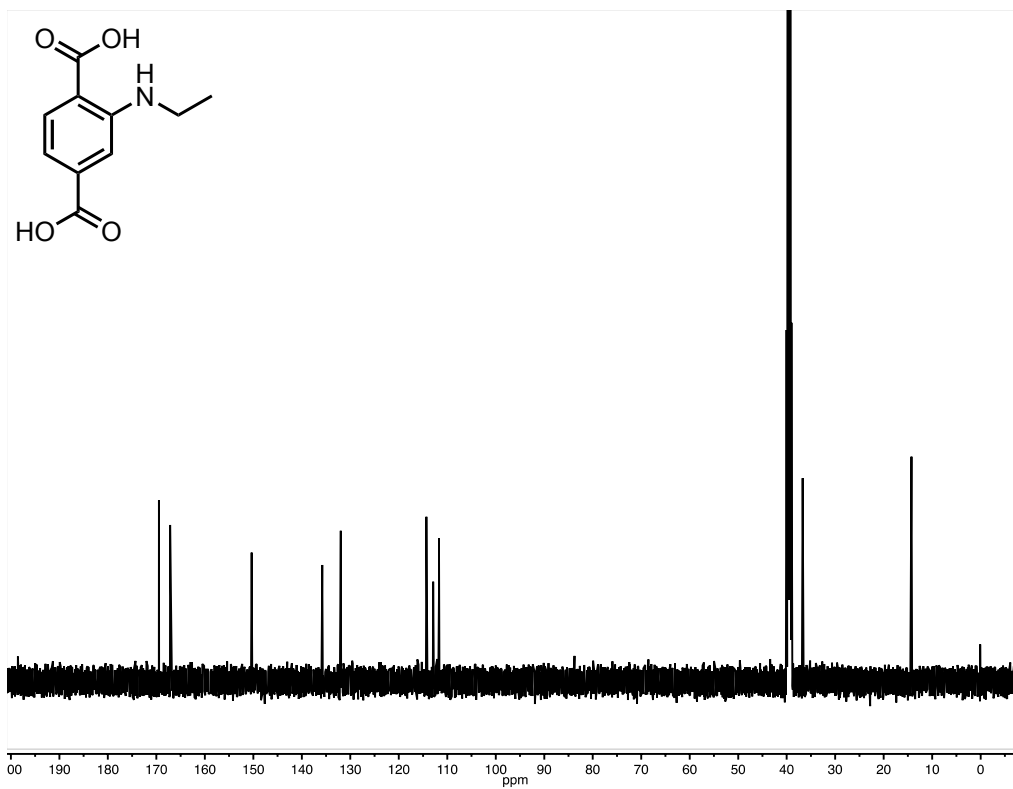


Figure S102. ¹H NMR spectra (400 MHz, DMSO-*d*₆, 25 °C) of compound **2c**.

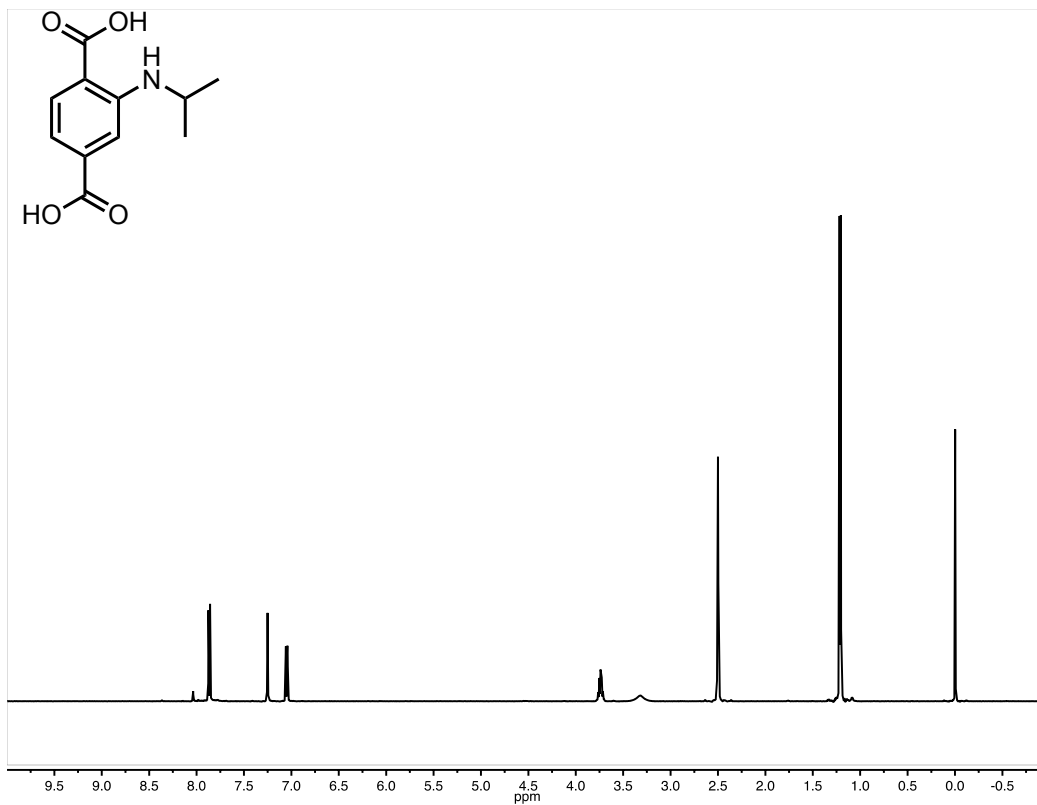


Figure S103. ^{13}C NMR spectra (100 MHz, $\text{DMSO-}d_6$, 25 °C) of compound 2c.

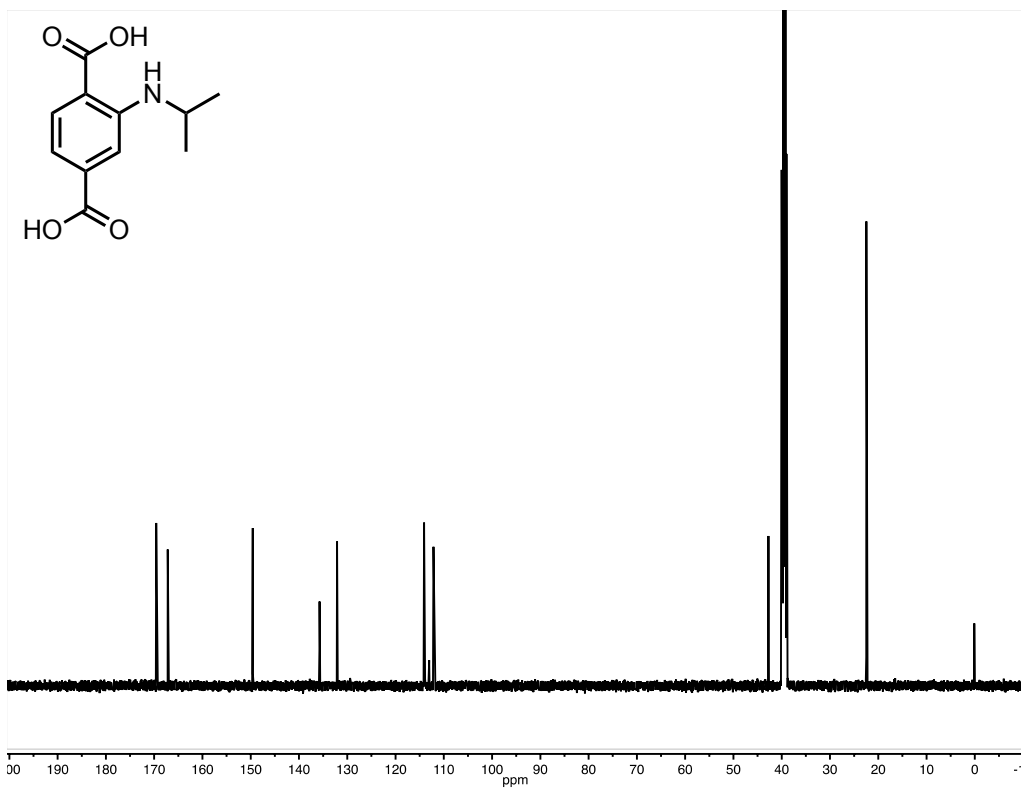


Figure S104. ^1H NMR spectra (400 MHz, $\text{DMSO-}d_6$, 25 °C) of compound **2d**.

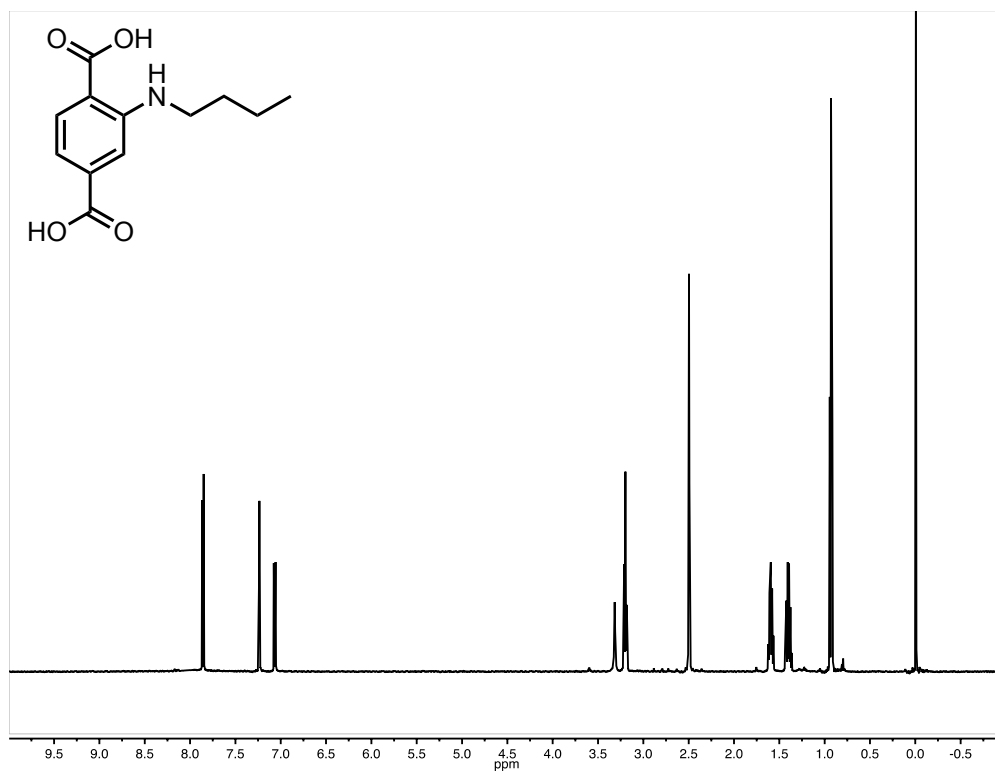


Figure S105. ^{13}C NMR spectra (100 MHz, $\text{DMSO-}d_6$, 25 °C) of compound **2d**.

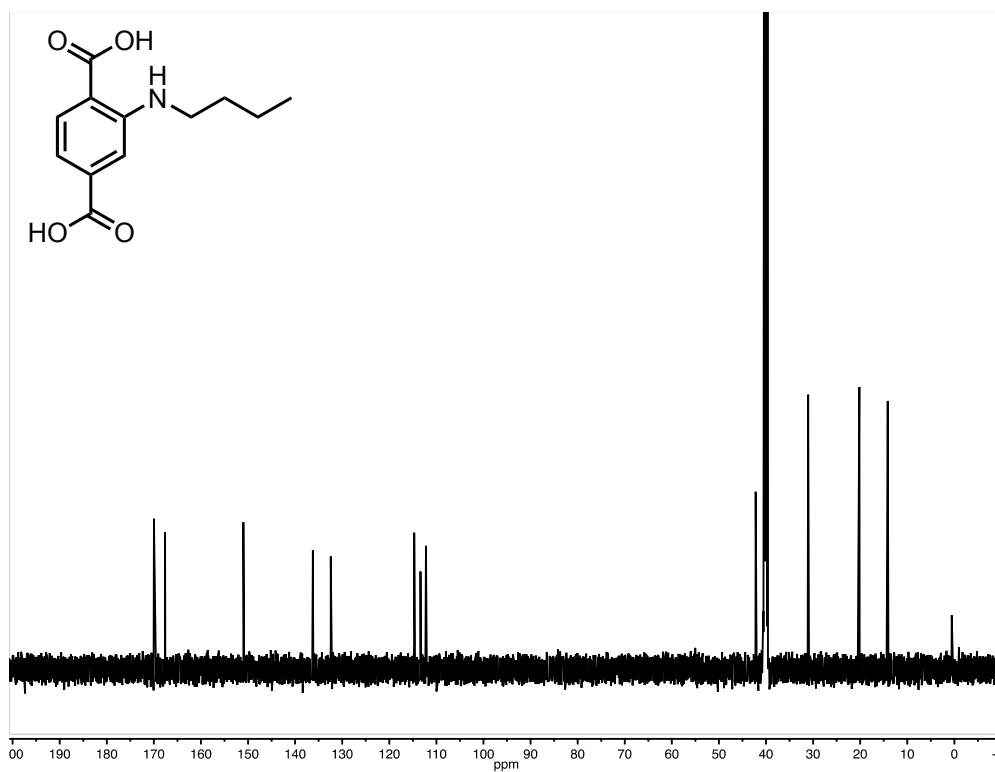


Figure S106. ^1H NMR spectra (400 MHz, $\text{DMSO-}d_6$, 25 °C) of compound **2e**. Broad signal at 3.3 ppm corresponds to residual water.

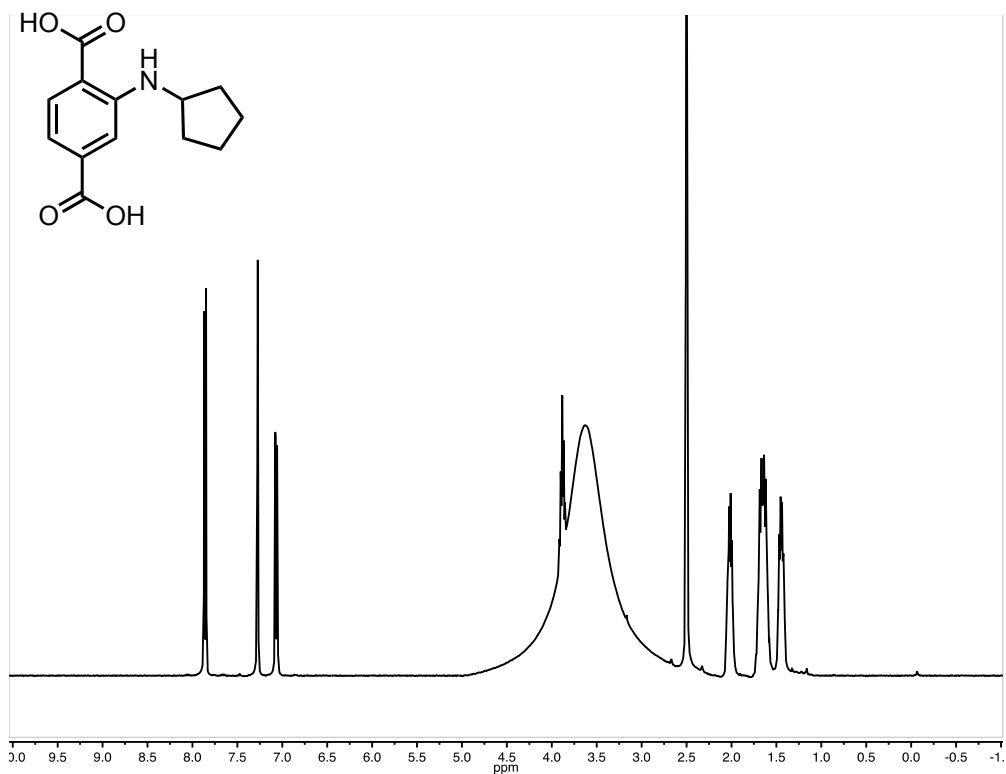


Figure S107. ^{13}C NMR spectra (100 MHz, $\text{DMSO-}d_6$, 25 °C) of compound **2e**.

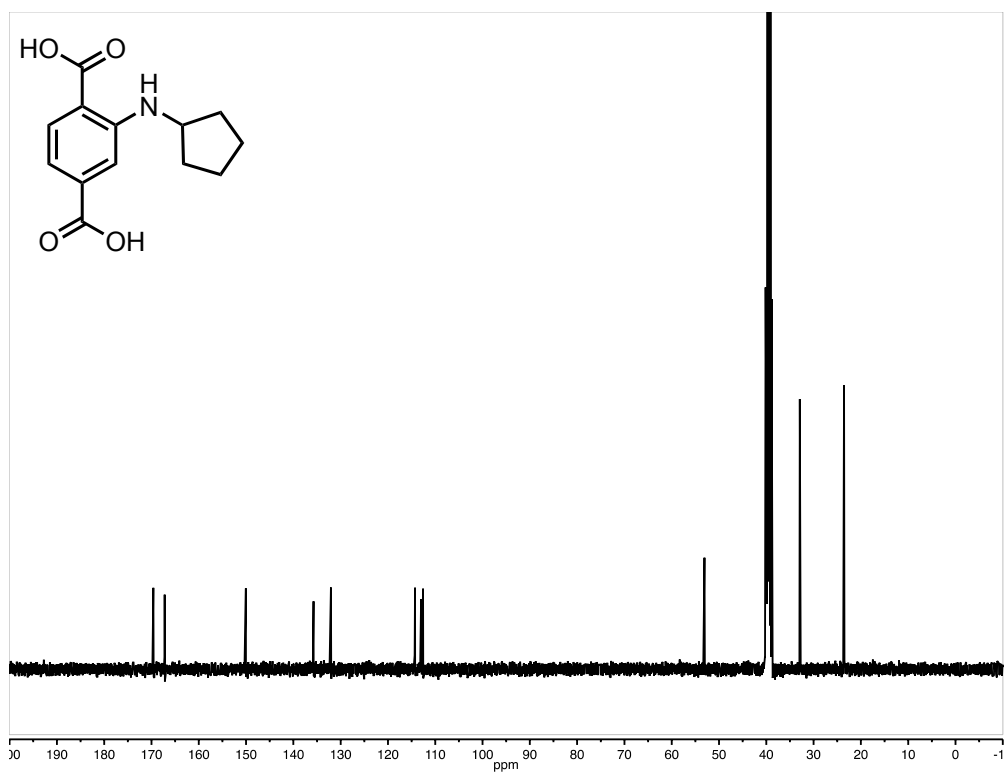


Figure S108. ^1H NMR spectra (400 MHz, $\text{DMSO-}d_6$, 25 °C) of compound **2f**. Broad signal at 3.3 ppm corresponds to residual water.

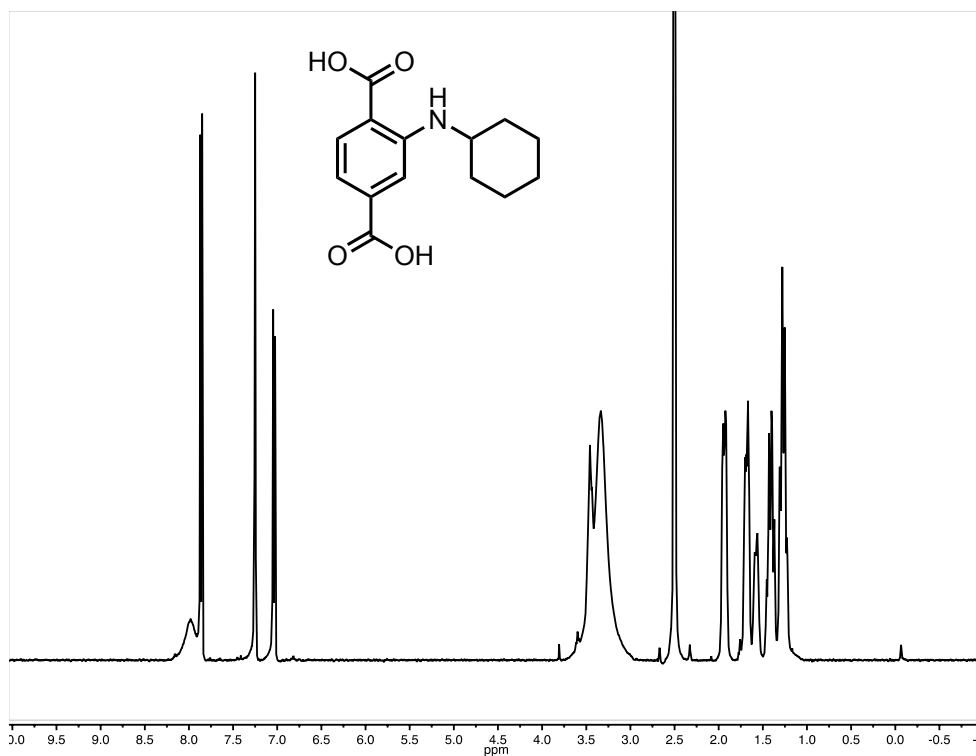


Figure S109. ^{13}C NMR spectra (100 MHz, $\text{DMSO-}d_6$, 25 °C) of compound **2f**.

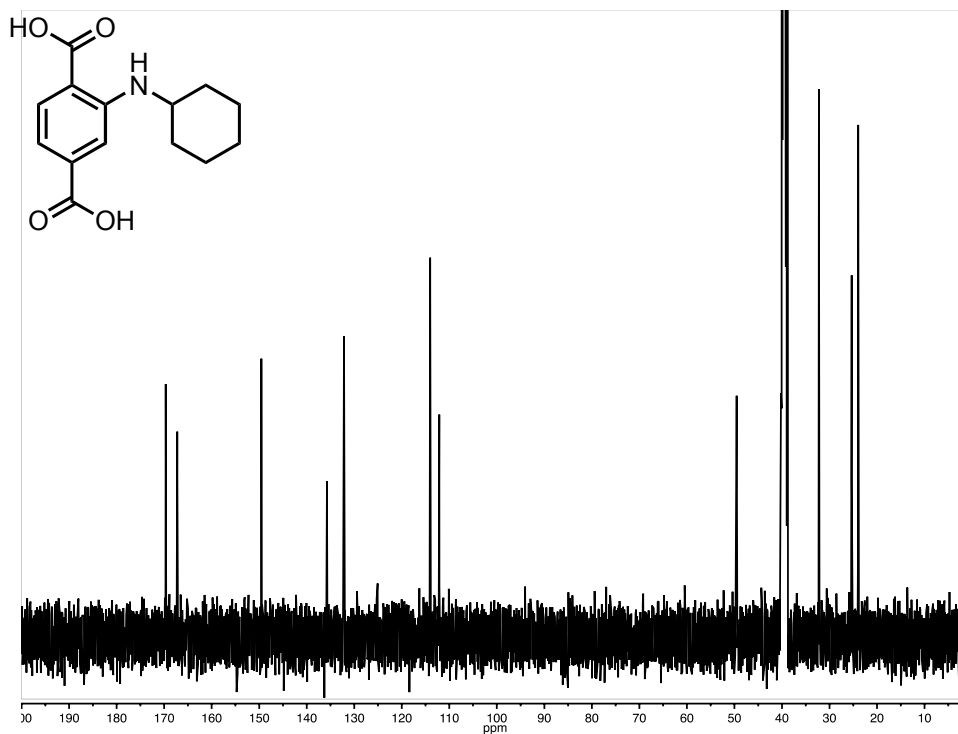


Figure S110. ^1H NMR spectra (400 MHz, $\text{DMSO-}d_6$, 25 °C) of compound **2g**.

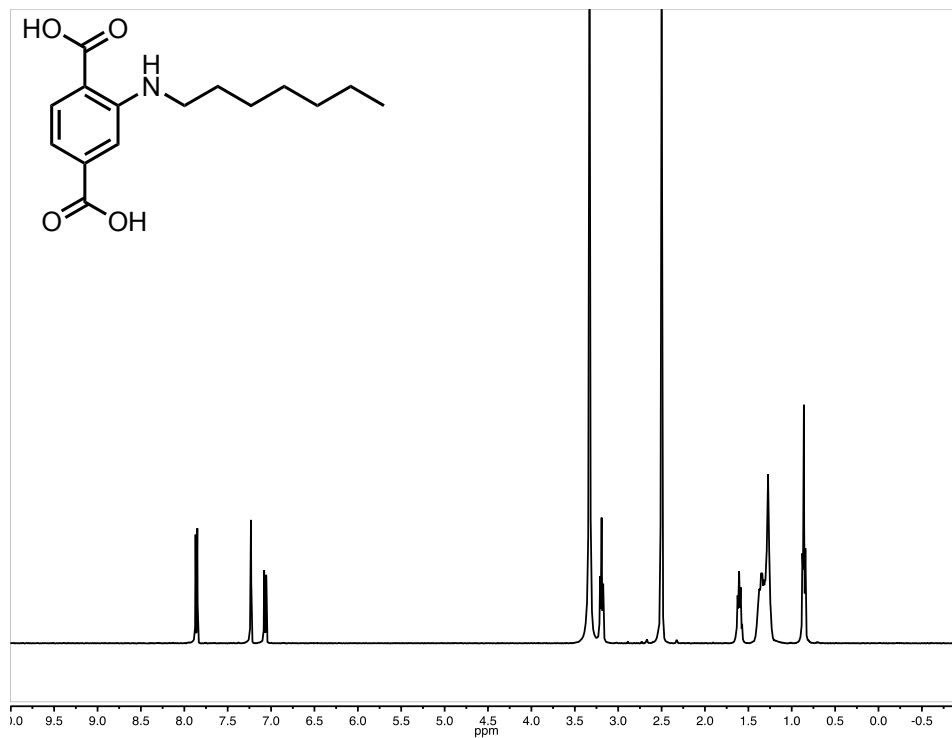


Figure S111. ^{13}C NMR spectra (100 MHz, $\text{DMSO-}d_6$, 25 °C) of compound **2g**.

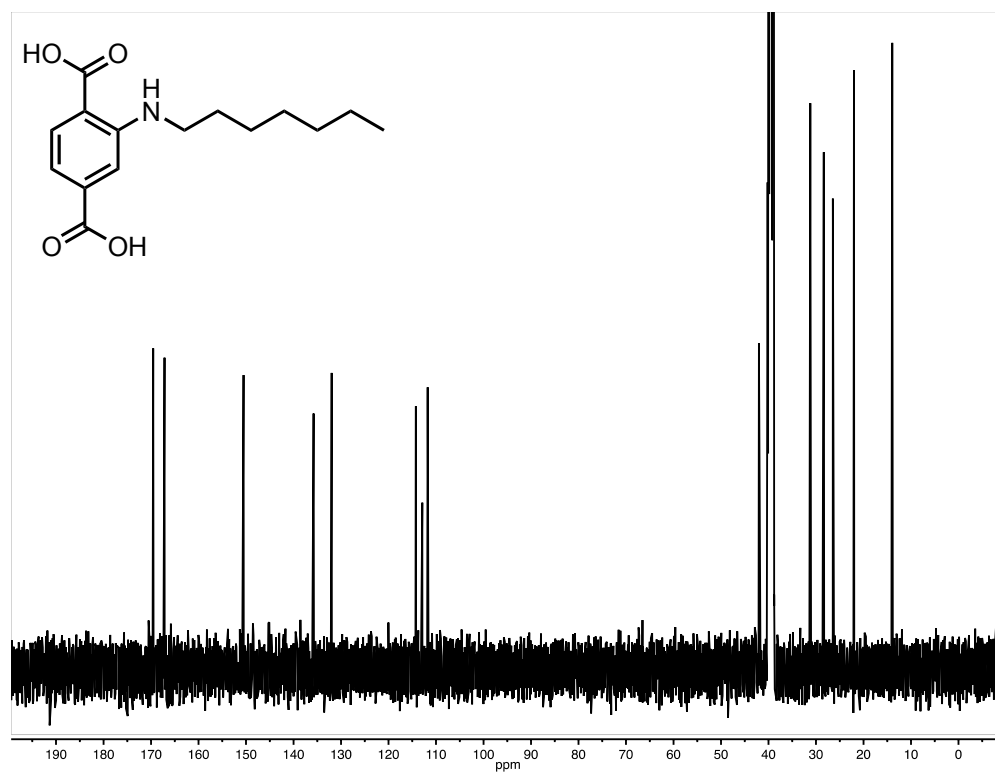


Figure S112. ^1H NMR spectra (400 MHz, CDCl_3 , 25 $^\circ\text{C}$) of compound **S1**.

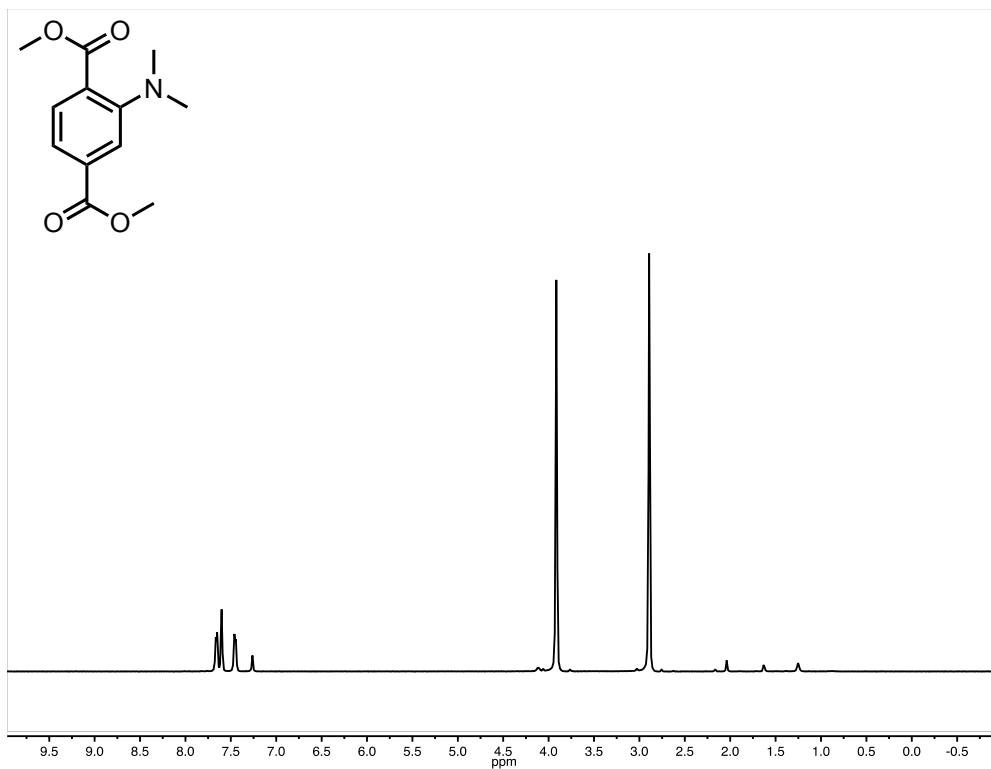


Figure S113. ^{13}C NMR spectra (100 MHz, CDCl_3 , 25 $^\circ\text{C}$) of compound **S1**.

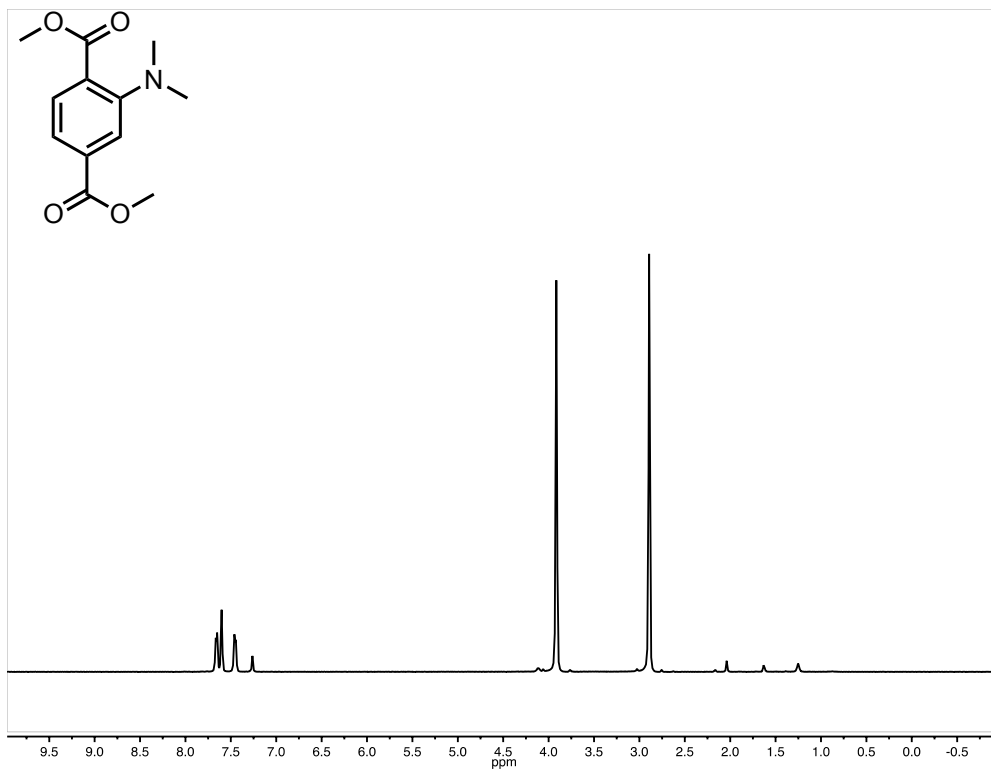


Figure S114. ^1H NMR spectra (400 MHz, $\text{DMSO-}d_6$, 25 $^\circ\text{C}$) of compound **3**.

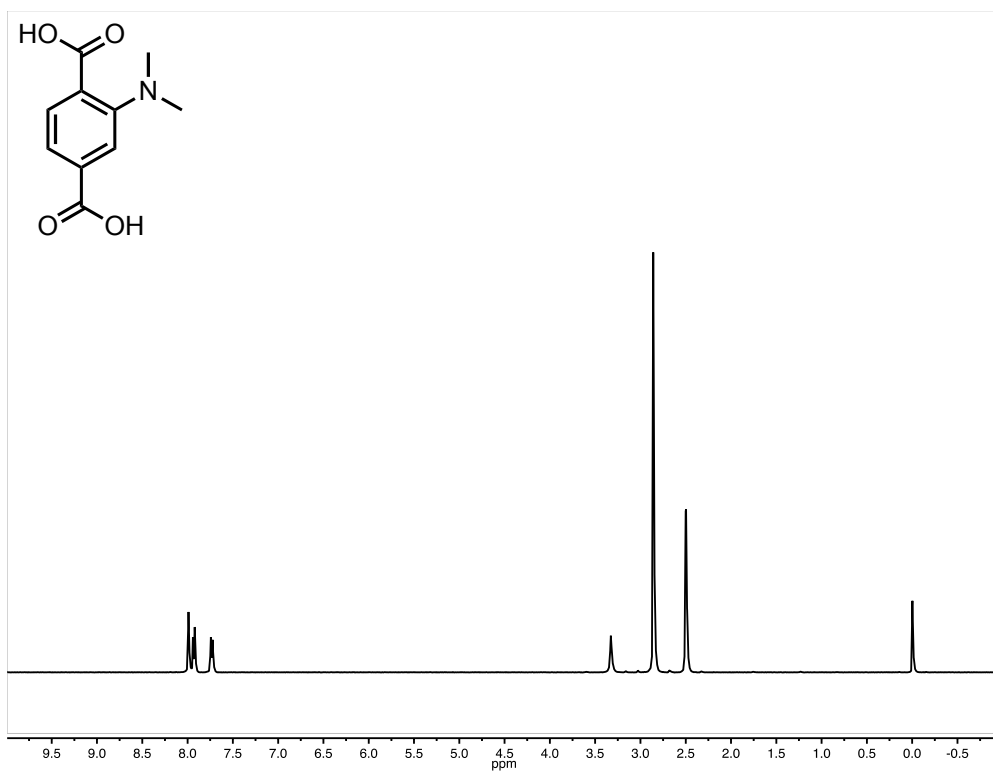


Figure S115. ^{13}C NMR spectra (100 MHz, $\text{DMSO-}d_6$, 25 $^\circ\text{C}$) of compound **3**.

